MODELING AND SIMULATION OF INTERACTION BETWEEN LIGHT SOURCES AND LIVING BIOLOGICAL TISSUES

by

Ahmet Yasin Çitkaya

B.S., Electrical and Electronics Engineering, Boğaziçi University, 2002

M.S., Electrical and Electronics Engineering, Boğaziçi University, 2006

Submitted to the Institute for Graduate Studies in
Science and Engineering in partial fulfillment of
the requirements for the degree of
Doctor of Philosophy

Graduate Program in Electrical and Electronics Engineering
Boğaziçi University
2013

ACKNOWLEDGMENTS

I would like to thank everybody for their support throughout this thesis study, which enabled my Ph.D. degree.

I want to express my sincere gratitude to Prof. Ş. Selim Şeker from the Electrical and Electronic Engineering Department of Boğaziçi University, for his efforts, motivation, technical information, support, supervision and guidance.

My special thanks are also directed to the evaluation committee members, Prof. Oğuzhan Çiçekoğlu, Prof. Naci İnci, Assist Prof. Hamdi Torun for their advice and provision. I would also like to present my appreciation to all the thesis committee members for their valuable comments and suggestions at various steps of the study.

I am also grateful to Prof. Osman Çerezci, who has never wavered his support, for his invaluable contribution throughout the study of my thesis to put in a better shape towards its aim.

My special thanks go to the department staff, Emre Arslan, Cem Çakır, Uğur Çini, Umut Yazkurt, for their innumerable help, friendship and accompaniment.

I express my heartfelt gratitude to my dear friends, Mustafa Aktan and İpek Şen for their motivation, support and always being there.

Last, but not least, I would like to express the warmest thanks to my parents and dear sister for always backing me up and encouraging me to keep struggling for the best execution of my work.

This thesis was supported by Boğaziçi University Research Fund under Project Code: *10A02D9*.

ABSTRACT

MODELING AND SIMULATION OF INTERACTION BETWEEN LIGHT SOURCES AND LIVING BIOLOGICAL TISSUES

The assessment of exposure level due to commonly used light sources needs specific attention in today's technology of lighting. The main reason behind this concern is that if exposure levels are not known, the biological implications and necessary safety limits cannot be determined accurately. In this regard, this thesis study has aimed to design, implement, analyze and solve partial differential equations related to thermal response of biological tissue which is subject to optical radiation. This thesis, however, is not limited to the numerical models for analysis of tissue thermal response under different light sources. The validation of the implemented mathematical algorithm is obtained via in-vitro experiments. Examining the most powerful factors in light-tissue interaction has made it possible to investigate each parameter by variations and their induced outputs. Accompanying the theoretical and numerical validation, this dissertation has enlarged its scope with in-vivo experiments for providing reference data to scientific research in the literature and medical application development for safer lighting designs.

ÖZET

IŞIK KAYNAKLARI İLE BİYOLOJİK CANLI DOKU ETKİLEŞİMİNİN MODELLENMESİ VE SİMÜLASYONU

Günümüz aydınlatma teknolojisinde, yaygınlıkla kullanılan ışık kaynakları altında oluşan maruziyet seviyelerinin ölçümlenmesi ve değerlendirilmesine özen göstermek gerekmektedir. Bunun temel sebebi ise, maruziyet seviyelerinin bilinmediği durumlarda oluşacak olan biyolojik etki ve gerekli olan güvenlik limitlerinin doğrulukla belirlenemeyecek olmasıdır. Bu bakımdan, yapılan bu tez çalışması optik radyasyona maruz kalan biyolojik dokulardaki ısısal tepkinin incelenmesi, ilgili kısmi diferansiyel denklemlerin çözümü ve bunlar için gerekli olan tasarımların ve uygulamaların gerçekleştirilmesini hedeflemiştir. Bu tez farklı ışık kaynakları altındaki dokuda oluşan ısıl tepkinin incelenmesi için sayısal metotlar ile sınırlı kalmamıştır. Cansız doku örnekleri üzerinde yapılan deneysel çalışmalar ile de kullanılan sayısal algoritmanın geçerliliği onaylanmıştır. Yapılan simülasyon ve cansız doku deneylerde, ışık-doku etkilenmesinin en kuvvetli faktörleri incelenerek, her bir parametrede yapılan değişiklikler ile ortaya çıkan sonuçlar gözlenmiştir. Teori ve sayısal modellemenin doğrulanmasının beraberinde, bu bilimsel çalışmanın vizyonu yapılan canlı doku deneyleri ile de genişletilmiştir. Bu deneysel çalışmalar ile daha güvenli ışık kaynaklarının geliştirilmesi konusunda yapılan bilimsel araştırmalara kaynak sağlayacak veriler elde edilmesi amaçlanmıştır.

TABLE OF CONTENTS

LIST OF FIGURES

LIST OF TABLES

LIST OF SYMBOLS

c_b	Specific heat of blood
C	Specific heat capacity
E	Young's modulus
E_{eff}	Effective Irradiance
$\vec{E}$	Electric field strength
g	Asymmetry factor
h	Local heat convection coefficient
I	Transmitted intensity
I_0	Incident intensity
k	Thermal conductivity
k_{dis}	Dissipation constant
l	Distance
q	Heat flow or maximum heat flux
Q	Heat sources
Q_{met}	Metabolic heat source
Q_{ext}	Spatial heat source
$\hat{s}$	Unit solid angle along
t	Time
T_b	Temperature of arterial blood
T_{inf}	External bulk temperature
T_s	Tissue temperature
T_∞	Environmental temperature
ν	Poisson's ratio or speed of light
w_b	Volumetric perfusion rate
α	Thermal expansion coefficeint
δ_{ts}	Time-scaling coefficient
$\varepsilon(\vec{r},\hat{s},t)$	Emitted source power
λ	Thermal conductivity

μ_a	Absorption coefficient;
μ_s	Scattering coefficient
μ_s'	Reduced scattering coefficient
ρ	Density
σ	Stefan-Boltzmann constant or conductivity
$\Phi(\vec{r},t)$	Fluence rate

LIST OF ACRONYMS / ABBREVIATIONS

ACGIH	American Conference of Governmental Industrial Hygienists
ANSI	American National Standards Institute
ArF	Argon Fluoride
ASTM	American Standard Testing Method
CCT	Correlated Color Temperature
CFD	Computational Fluid Dynamics
CFL	Compact Fluorescent Lamps
CIE	International Commission on Illumination
CO_2	Carbon dioxide
CPU	Central Processing Unit
CRI	Color Rendering Index
EEC	European Economic Community
EL	Exposure Limits
EM	Electromagnetic
EU	European Union
FDM	Finite Difference Method
FEM	Finite Element Method
FIT	Finite Integration Technique
FVM	Finite Volume Method
GLS	General Lighting Service
GSM	Global System for Mobile Communications
HeNe	Helium-Neon
HID	High Intensity Discharge
HPS	High Pressure Sodium
IEC	International Electrotechnical Commission
IEEE	Institute of Electrical and Electronics Engineers
IR	Infrared
LED	Light Emitting Diode
LPS	Low Pressure Sodium
MoM	Method of Moments

Nd:YAG	Neodymium-Doped Yttrium Aluminum Garnet
NIEHS	National Institute of Environmental Health Sciences
RGB	Red-Green-Blue
PDE	Partial Differential Equation
RF	Radio Frequency
RTE	Radiative Transfer Equation
SAR	Specific Absorption Rate
SCENIHR	Scientific Committee on Emerging and Newly Identified Health Risks
UV	Ultraviolet
UVR	Ultraviolet radiation

1. INTRODUCTION

1.1. Overview

Life on the Earth could not have been possible without the vital source of light, due to its definite interactions with all living organisms. From its definition, light is the only electromagnetic radiation which is visible to the human eye, and which is generated by the oscillation or acceleration of electrons or other electrically charged particles. On the other hand, when describing its interaction with matter, light can also be considered as particles, named as photons, each carrying a specific amount of energy.

Interaction of light with biological tissue is widely investigated in different perspectives: physics of propagation of light through media and its biological effects to the absorbing media. Some of the characteristics have found great applications in life for photo-thermal curing techniques. In these treatments, the most important issue is to control the temperature increase and distribution over the living tissue; otherwise, high temperatures could potentially lead to undesired thermal damages in the surrounding tissue. Especially for medical treatment applications of light, prediction of thermal response of tissue can be realized by utilizing simulation tools so that appropriate selection of dose and exposure time can be made.

Recent studies in literature have aimed to model the physical interaction of light with biological tissue from mainly two different points of concerns: the optical propagation of light, and its thermal distribution in biological tissue [1, 2]. While different approaches for optical propagation have been developed; thermal modeling part has always been given the special attention with the usage of most widely known approach: the bio-heat equation by Pennes [3]. Although various alternative models exist for investigation of temperature distribution in tissue, advancements in computation technology have enabled the mathematical modeling for investigation of Bioheat equation to become the prevalent, most common two of which are finite difference and finite element methods.

Optical radiation from artificial sources is used in a wide variety of applications, including consumer, scientific, industrial and medical purposes; which directly or indirectly affect living species, especially humans. In most instances light and energy emitted is thought to be non-hazardous; and if there is a potential of reaching hazardous levels, excessive light and radiation is often filtered to reduce discomfort. Additionally, in cases where total irradiance is sufficiently high, thermal discomfort sensed by skin and eye will produce an aversion response [4]. Never though, certain exposures remain potentially hazardous and require specific attention in terms of safety standards.

Despite the abundance of studies in literature focusing on utilizing light sources for medical treatment, there is a crucial need in literature for investigation about the negative health effects humans are exposed to, so that awareness can give birth to protective limits establishment by international organizations.

1.2. Overall Objective of the Study

Because of the rapid growth in usage of new types of special-purpose light sources in medicine, science and consumer applications, there is no doubt that importance on optical radiation exposure limits (EL) will increase day by day. This brings the growing need for codes of practice for all potentially hazardous optical sources [4]. The first step to be taken in this respect should indefinitely be the determination of light sources together with potential adverse health effects.

In the light of the foregoing discussion, the following scientific goals are identified for this study in order to investigate the interaction between light sources and tissue,

- Utilizing Finite Element Method (FEM) numerical algorithm, which provides more accuracy and allows more complex geometries in simulation.
- Developing a numerical model to analyze opto-thermal response of skin tissue under various light sources.
- Determination of the thermal distribution over tissue which is exposed to different kinds of light sources, via a simulated model.

- Determination of the temperature rise caused on biological tissue, via in-vitro experiments.
- Determination of the temperature elevation on human skin caused by daily usage light applications, via in-vivo experiments.
- Evaluation of the parameters and their effects on the variation of thermal effects.

1.3. Organization of the dissertation

This study mainly focuses on construction, evaluation and implementation of numerical methods for investigating thermal responses of biological tissue under exposure to commonly used light sources.

Chapter 2 provides theoretical information on light and tissue parameters, as well as international standards and safety limits for light-tissue interaction. In chapter 3, detailed aspects of light-tissue interaction are discussed with the fundamental physical and physiological background. Having focused on theoretical data on previous chapters, modeling and simulation methods are presented in chapter 4, with introduction on FEM numerical algorithm and details on mathematical models developed for simulations. Chapter 5 follows with experimental studies done both in-vitro and in-vivo, together with validations of mathematical modeling. Much of the scientific work provided in chapter 4 and 5 are also prepared for publication each as an independent journal paper. Finally chapter 6 summarizes whole study and its findings, and recommends not only various directions for future research, but also improvements for safety standards.

2. THEORETICAL BACKGROUND

2.1. Electromagnetic Spectrum and Common Light Sources

The term light generally relates to the electromagnetic radiation which is visible to human eye. Electromagnetic radiation, which is generated by the oscillation or acceleration of electrons or other electrically charged particles, extends from gamma rays (γ) through to long radio waves. This is often referred to as "the electromagnetic spectrum", depicted as in Figure 2.1 [5]. Electromagnetic waves are characterized by their wavelength and by their intensity (or amplitude). The energy of a wave depends on its wavelength: the longer the wavelength, the lower the energy. On the other hand, light can also be considered particles when describing how it interacts with matter. These particles, called photons, each carry a specific amount of energy; and light intensity increases with the number of photons.

In the electromagnetic spectrum, gamma rays have the highest energy, and long radio waves the lowest. The sun emits visible light, but also infrared (IR) and ultraviolet (UV) radiation. The visible part of the electromagnetic spectrum only covers a small range of wavelengths, from 380 nm to 750 nm. In the electromagnetic spectrum, shorter wavelengths (from 10 nm to 380 nm) are UV and longer wavelengths (from 750 nm to 1 mm) are IR radiation. UV radiation carries more energy and IR radiation less energy than visible light [6].

According to the wavelengths, the UV portion of the spectrum is further divided into: UVA (315 – 400 nm), UVB (280 – 315 nm) and UVC (100 – 280 nm), as summarized in Table 2.1 [7]. All radiation from the sun with a wavelength below 290 nm, that is most high-energy UV-radiation, is filtered out by the atmosphere before reaching the Earth's surface.

The way electromagnetic radiation interacts with matter depends on its wavelength and therefore its energy. Radiation of short wavelength has high energy and can set off damaging chemical processes in living cells. Many indoor lighting sources in general use,

such as fluorescent, quartz halogen and even tungsten filament incandescent lamps, emit UVA, UVB and sometimes even UVC wavelengths. Intensities of some emissions are of similar magnitude to those in sunlight [8]. Findings in literature show that chronic exposure may pose risks through cumulative UV exposure to skin and eyes, especially for photosensitive patients.

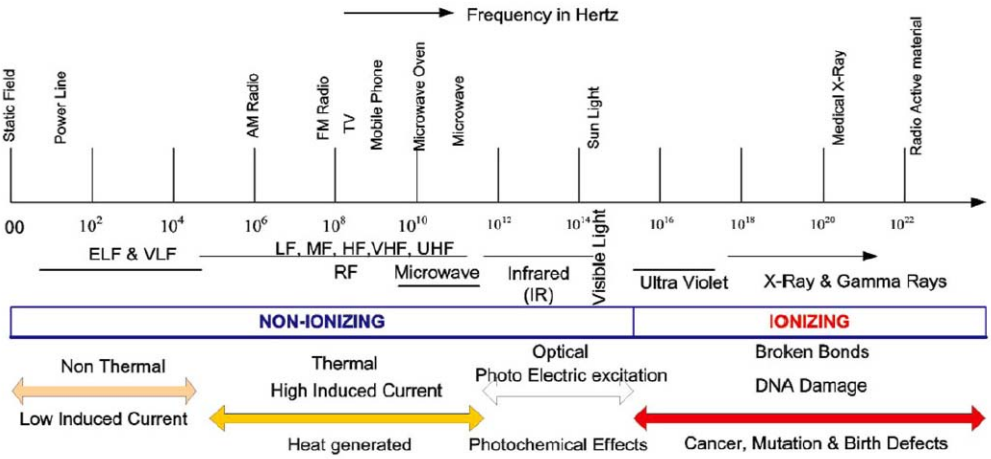

Figure 2.1. The Electromagnetic Spectrum.

Table 2.1. Division of the Optical Spectrum.

Band	***Wavelength***	***Description***
UVC	100 nm to 280 nm	Far ultraviolet
UVB	280 nm to 315 nm	Middle ultraviolet
UVA	315 nm to 400 nm	Near ultraviolet
Light	400 nm to 780 nm	Visible
IRA	780 nm to 1400 nm	Near infrared
IRB	1.4 μm to 3 μm	Middle infrared
IRC	3 μm to 10^3 μm	Far infrared

Light source designs are undergoing a continuous evolution, utilizing newer and more powerful sources of optical radiation; and there is a rapid growth in usage of new types of special-purpose light sources in medicine, science and consumer applications.

Incandescent, fluorescent, compact fluorescent lamps (CFL), High Intensity Discharge (HID) sources including mercury vapor, metal halide, High Pressure Sodium (HPS), Low Pressure Sodium (LPS) are the common light source types and their spectral power distribution curves are given in Figure 2.2 [9].

To look more deeply for working topology of light sources, incandescent lamp creates light by heating a thin filament in a glass cover filled with an inert gas or vacuum to a high temperature above 2500°C, and then turns the heat to the visible light. Hence, over 90% for the energy is transferred to the invisible IR light or heat [10]. Construction wise, a halogen lamp is like an incandescent lamp with the addition of a small amount of halogen gas, such as iodine or bromine, along with an inert gas [11]. To let the fluorescent lamp and the halogen lamp glow up, firstly the energy is used to produce UV light and then the electricity is passed across the tube through the mercury vapor to make the phosphor coating glow or fluorescent. Hence, the efficiency for the fluorescent lamp will be decreased during the process of the generation of the UV light, and converting the UV light to the visible light [10]. For HID - high intensity discharge lamp, the light is emitted from the arc discharge between two closed spaced electrodes hermetically sealed inside a small quartz glass tubular envelope capsule [10]. The working topology for light emitting diode (LED) is much simpler. It is a semiconductor light source. Like in other diodes, when charge-carrier electrons meet holes, they fall into a lower energy band, where energy is released in the form a photon. The band gap energy determines the wavelength and hence the color of light emitted. LEDs present many advantages over incandescent light sources including lower energy consumption, longer lifetime, improved physical robustness and smaller size. The simplest topology is to use a current limit resistor to control the current passing through the LEDs [10].

Regarding the efficiency of lighting devices, most compared with the others, LEDs do not provide UV radiation and IR radiation, the only loss for LED is the heat loss. From the Table 2.2, which shows the losses for the common used lighting device; the efficiency for the incandescent lamp is 8-14%, for the fluorescent lamp is 24-26%, for the HID (mercury) is 13-22%, for HID (metal halide) is 6-36%, for HID (sodium) is 13.7-42.7%, and for LED is 11.8-20% [10].

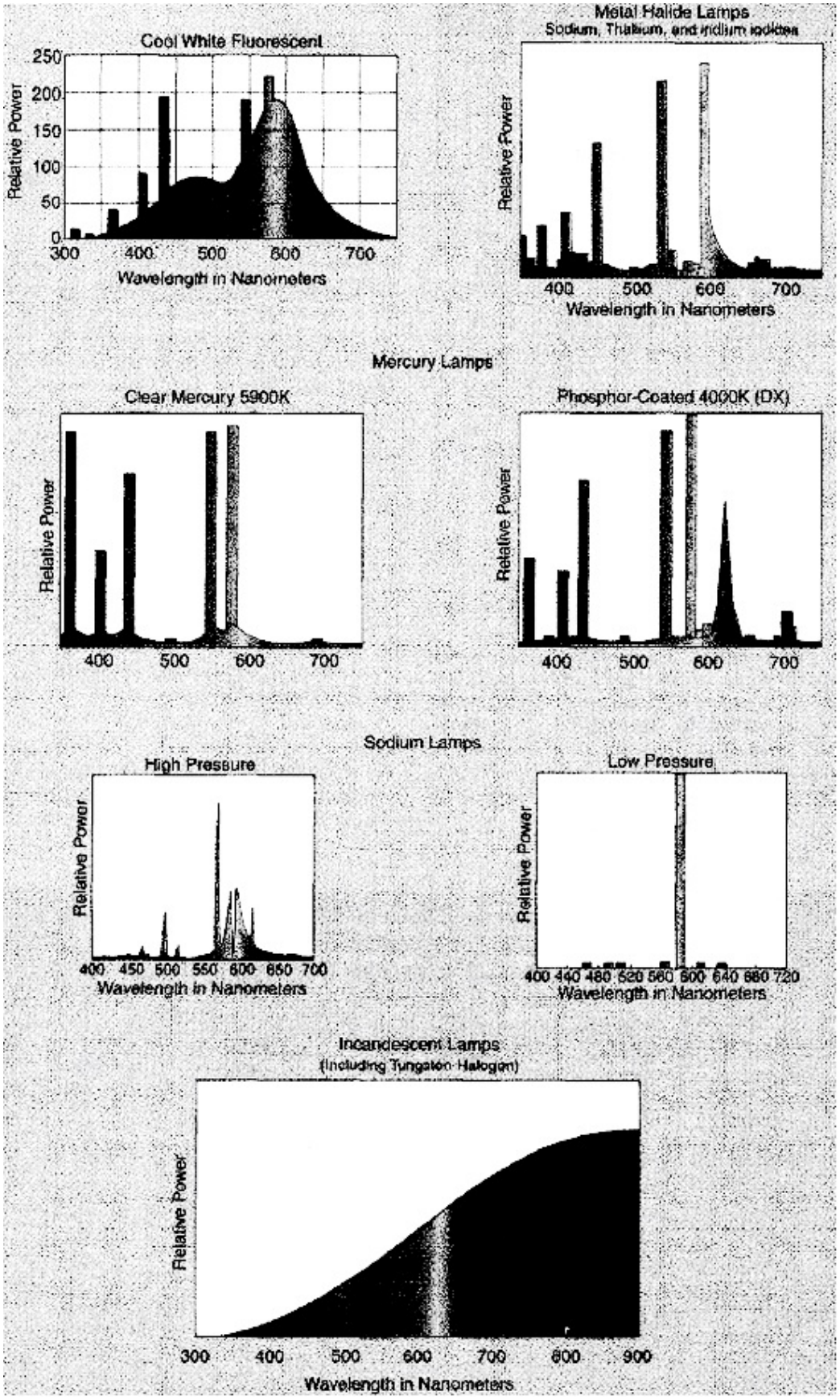

Figure 2.2. Spectral power distribution curves for various light sources.

Table 2.2. Losses for different lighting devices.

Light Source	***Loss in Radiation [%]***	***Heat Loss [%]***
Incandescent Lamp	81 – 86	5 – 6
Flourescent Lamp	30 – 32	44
HID (mercury)	62 – 65	16 – 22
HID (metal halide)	54 – 74	7 – 20
HID (sodium)	47.3 – 63.3	10 – 23
LED	0 – 0.2	80 – 88

The color rendering index rating from 0 to 100 which is used to describe how the light source makes the color appears to human eyes and the higher color rendering index (CRI) rating is the better. Table 2.3 shows the CRI index for different kind of devices. Color temperature is the index to indicate how warm the light source is. The lower the color temperature, the warmer the light source is. For a 40W incandescent lamp, the correlated color temperature (CCT) is 2800K. Halogen Lamp: 3200K, compact fluorescent Lamp is around 2700K-6000K. HID's car headlight CCT index is 3900K-4200K and the daylight white is 5000K-5500K. For the LED cold white 6500K and warm white is 3300K and for the red-green-blue (RGB) package can produce the CCT index from 1000K-10000K depending to the color mixing for red, green and blue value [10].

Table 2.3. CRI index for lighting device.

Light Source	***CRI Index***
Flourescent Lamp	52 – 95
Incandescent Lamp	~100
HID (mercury)	15 – 55
HID (metal halide)	65 – 80
HID (low pressure sodium)	0 (monochromatic light)
HID (high pressure sodium)	22 – 75
LED	0 (mono-color LED) – 80 (high flux LED)

The spectra of unshielded compact fluorescent bulbs and 4 ft T-8 fluorescent tubes (including specimens with daylight or cool-white phosphors) shown in Figure 2.3 and 2.4 are similar to those reported earlier [12]. Fluorescent tube lamps, installed without plastic sleeves or diffusing panels, are frequently encountered in commercial venue lighting, presenting numerous opportunities for unwelcome indoor UV exposure. Shorter T-8 fluorescent tubes and compact fluorescent bulbs used in desk lamps or other types of unshielded close task lighting clearly support the rationale for non - general lighting service (GLS) evaluation for realistic hazard assessment.

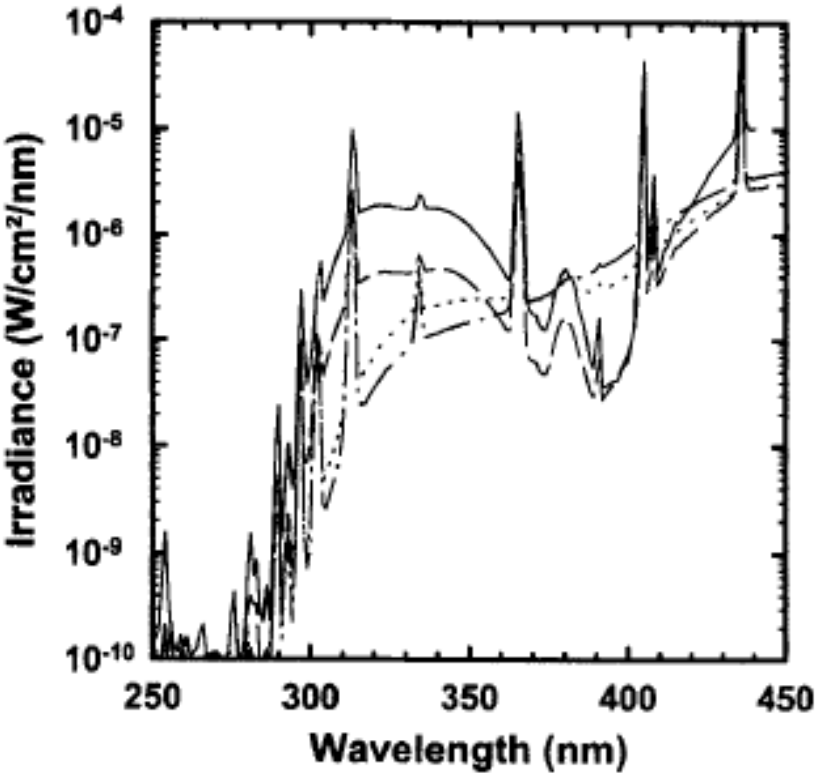

Various fluorescent tube lamps. Lamps shown are all T-8 format and include (—) Philips UNIVERSAL/HI-VISION Alto F32T8/TL741; (– –) GE Starcoat F32T8-SP41; (···) Damar F32T8 Truetone 741 75CRI VV; and (– · –) Damar F32T8 Truetone 750 75CRI VVV. Mercury lines are detectable above the instrumental background at wavelengths well below 300 nm.

Figure 2.3. Irradiance of various fluorescent tube lamps.

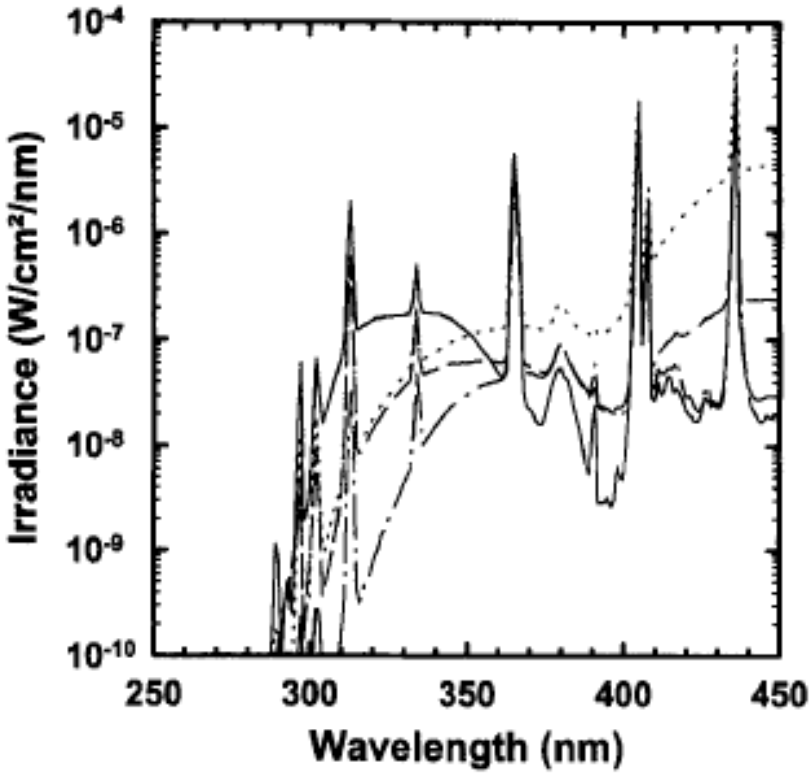

Various compact fluorescent lamps. Constructed with standard medium lamp bases, these compact fluorescent are intended to replace tungsten filament incandescent bulbs. Lamps shown include, (—) Lights of America 2127 (517); FDL27LE.Y 120V 27W; (– –) Commercial Electric Mini Spiral EDSO-14, 120V 14W; (···) Damar Energy Saving Daylight 6400 K; and (– · –) Philips Marathon Household BC-EL/A 120 V 20 W.

Figure 2.4. Irradiance of various compact fluorescent lamps.

Comparison of a reference solar spectrum, American Standard Testing Method (ASTM) air mass 1.5 [13], with those emitted by a specimen of quartz halogen, incandescent, and both compact and T-8 fluorescent sources (Figure. 2.5) shows that all these lamps emit readily detectable amounts of carcinogenic UV wavelengths shorter than those present in sunlight. Unlike sunlight, several emit at least to 280 nm, and some fluorescent sources may even emit the 254 nm mercury line. Although possible roles for UVA and visible radiation in development of melanoma have been invoked, the potential importance of such non-solar shorter wavelengths in the development of melanoma has not been widely considered.

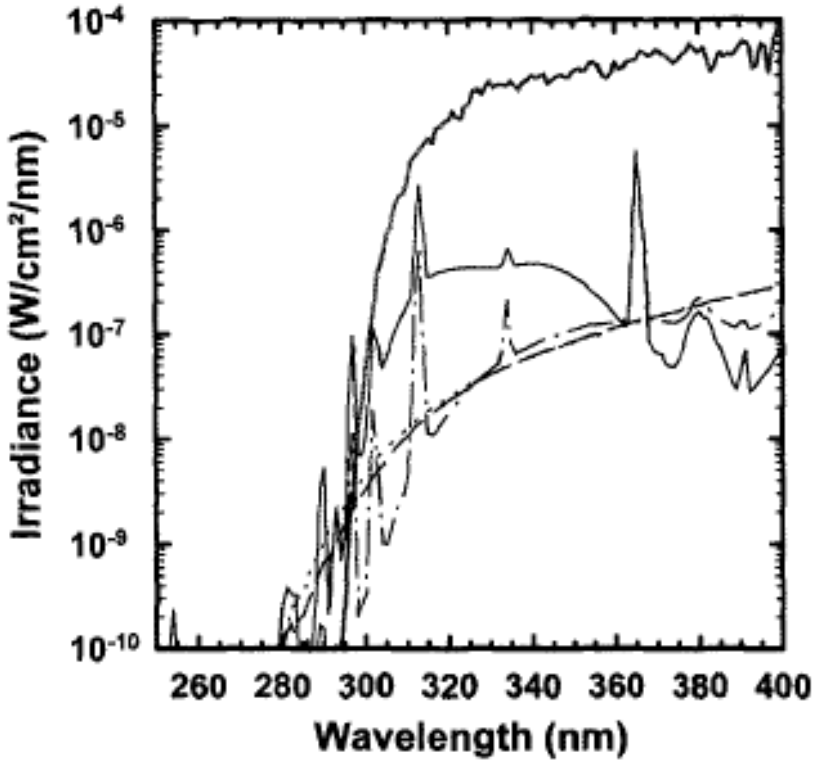

Comparison of sunlight with selected lamps. Reference solar spectral irradiance (thick grey line), ASTM G173-03 air mass 1.5, drops below 1×10^{-10} W at ~295 nm, whereas these representative lamps, measured at 20 cm, clearly demonstrate detectable UV radiation as short as 280 nm. Lamps shown above are (—) Philips T8 F32T8/TL741 fluorescent tube at 4318 lux, showing 254 nm mercury line detected; (– –) Philips Halogena Classic 60 W at 1708 lux; (···) GE Crystal 60 tungsten incandescent at 1670 lux; and (– · –) Damar Energy Saving Daylight 6400 K compact fluorescent at 3374 lux. The illuminance of the reference solar spectrum is 97 140 lux.

Figure 2.5. Irradiance comparison of sun light with selected lamps.

Although UVA hazards from sunlight, indoor tanning devices, or fluorescent interior lighting have been recognized, UVA risk from incandescent lighting was considered negligible.

If wavelengths shorter than those in sunlight, or intensities of UVA approaching those in sunlight are present, exposed skin may accumulate adverse effects over time that are of concern not only for photosensitive individuals but also for the general population.

2.2. Characteristics of Biological Tissues

It is a common practice to study the behavior of electromagnetic waves in homogeneous media. It is well known that the homogeneous media is characterized by the constant values of permittivity, permeability and conductivity throughout the medium. On the other hand, non-homogenous media is a medium for which the above fundamental parameters are not constant and are different from point to point in the media. It has been possible to find out relative electromagnetic energy absorption characteristics from the data on fundamental constants of the tissues [14].

Skin is the largest organ as an integrated structure in human body which serves critical functions for body's unique needs, among which the most crucial one can be named as the first line of defense from the environmental insults. Thermoregulation is another vital process that skin is thermally responsible for through heat generation, absorption, transmission, conduction, radiation, and vaporization. An exact representation of light propagation in skin requires a model that characterizes the spatial distribution and the size distribution of tissue structures, their absorbing qualities and their refractive indices [15]. However, skin is an inhomogeneous organ with complex optical properties, comprehensive study of thermal behavior in real skin tissue is rather complicated, almost impossible and multidisciplinary; which sometimes necessitates a number of assumptions and simplifications to be made.

The skin models consist of three layers, the epidermis, dermis and subcutis (hypodermis), as depicted in Figure 2.6 [16]. Two primary layers, namely epidermis and dermis, which resides on the subcutaneous fat layer or hypodermis constitutes the human skin morphology, as illustrated in Figure 2.7 [17]. All these layers have distinct characteristics in terms of both dimensions and optical properties. This fact sheds light on the importance of parameters for different tissue layers used in the simulations for light interactions. Obviously, it is not practical to assume a one-layer model for the skin for thermal simulatory purposes, because quite important effect of dermal blood flow cannot be underestimated.

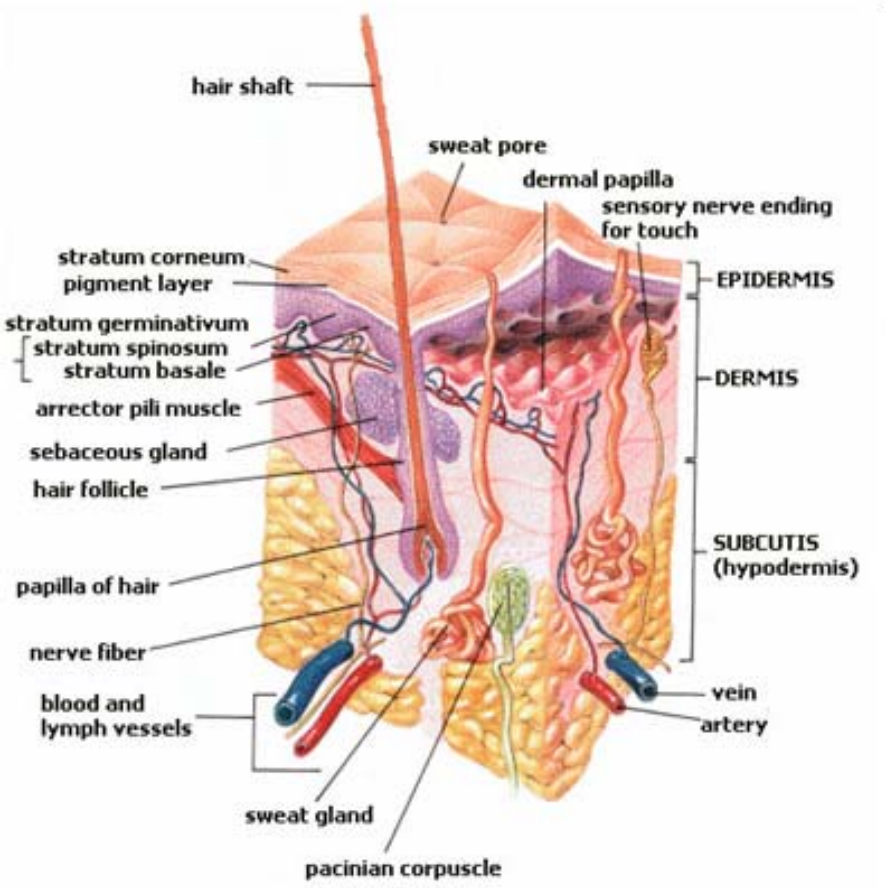

Figure 2.6. Layers of skin tissue.

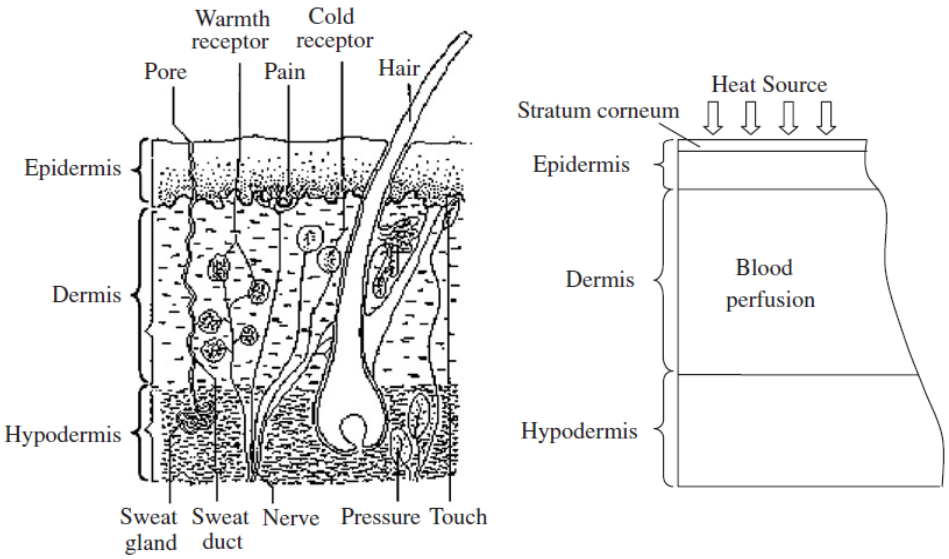

Figure 2.7. Three layer composition of skin.

Some of the thermal and mechanical properties of three skin layers used in FEM are summarized in Table 2.4.

Analysis of interaction of skin tissue with commonly used light sources necessitates the documentation of skin parameters at different wavelengths. Figure 2.8 [18] illustrates the absorption spectra of skin and skin components: water (75%), epidermis, melanosome, vessel wall, and whole blood. Diagnostic/therapeutic lasers and their wavelengths as well as diagnostic/therapeutic window and wavelength ranges suitable for superficial and deep spectroscopy or treatment are also shown in the same figure.

Table 2.4. Thermal and Mechanical properties of skin layers used in FEM.

	Epidermis	***Dermis***	***Subcutaneous Fat***
Density (gmm^{-3})	1.2×10^{-3}	1.2×10^{-3}	1.0×10^{-3}
Specific Heat (c) ($Jg^{-1}K^{-1}$)	3.590	3.300	1.900
Thermal Conductivity (k) ($Wmm^{-1}K^{-1}$)	2.4×10^{-4}	4.5×10^{-4}	1.9×10^{-4}
Young's Modulus (E) (Pa)	1.36×10^{3}	8.0×10^{4}	3.4×10^{4}
Poisson's Ratio (ν)	0.499	0.499	0.499
Thermal Exp'n coeff (α) (K^{-1})	3.0×10^{-4}	3.0×10^{-4}	9.2×10^{-4}

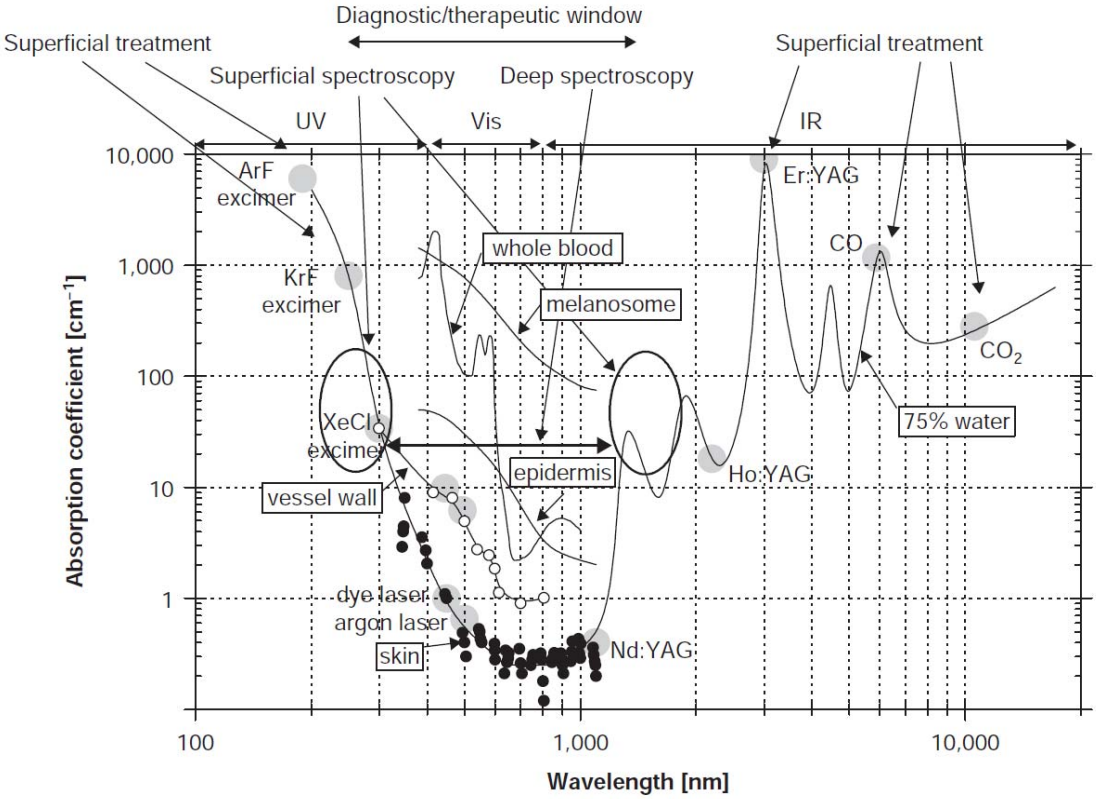

Figure 2.8. Absorption spectra of skin and skin components.

2.3. Safety Standards and Exposure Limits

The principles used in toxicological risk assessment, are: (i) hazard identification, (ii) dose-response, and (iii) exposure. In considering the hazard identification for laser devices, the mechanism or mode of action is particularly important. Specifically, by knowing the mode/mechanism of action and information around dose-responsivity, the adverse event profile can be predicted.

On the minimum health and safety requirements, the European Parliament and the Council of European Union has published a directive (19th individual Directive within the meaning of Article 16(1) of Directive 89/391/EEC) to specify the exposure of workers to risks arising from physical agents, in other words artificial optical radiation. This well-organized directive [19] provides both exposure determination and risk assessments, together with provisions aimed at avoiding or reducing risks.

Ultraviolet radiation (UVR) is used in a wide variety of medical and industrial processes, which includes photo curing of inks and plastics, photo resist processes, solar simulation, cosmetic tanning, fade testing, dermatology, and dentistry. Even though the principal operating wavelengths for most of these processes are in the UVA, almost always some shorter wavelength (UVB and UVC) radiation and violet light are emitted as well. While it is generally agreed that some low level exposure to UVR benefits health [20], there are adverse effects that necessitate the development and use of EL for UVR. However, the development of UVR EL poses a real challenge to achieve a realistic balance between beneficial and adverse health effects. While it is kind of a challenge in terms of UVR, more special attention should be paid to safety concerns about general lighting sources, to which every human without an exception is subject with different doses.

In discussing UVR biological effects, the International Commission on Illumination (CIE) has divided the UV spectrum into three bands as defined in Table 2.1. Wavelengths below 180 nm (vacuum UV) are of little practical biologic significance since they are readily absorbed in air. UVR is used in a wide variety of medical and industrial processes and for cosmetic purposes. These include photocuring of inks and plastics (UVA and UVB), photoresist processes (all UV), solar simulation (all UV), cosmetic tanning (UVA and UVB), fade testing (UVA and UVB), dermatology (all UV), and dentistry (UVA). Even though the principal operating wavelengths for most of these processes are in the UVA, almost always some shorter wavelength (UVB and UVC) radiation and violet light are emitted as well. Many industrial applications employ arc sources for heat or light (e.g., welding), which also produce UVR as an unwanted admixture for which control measures may be necessary. Until 1980, it was generally thought that the most significant adverse UVR health effects resulted from exposures at wavelengths below 315 nm; but today these effects are recognized to be produced at longer wavelengths (UVA) at substantially higher doses. At one time, wavelengths below 315 nm were collectively known as “actinic radiation” [20], when it was thought that these effects occurred only in the UVB and UVC. This guideline has been limited to wavelengths greater than 180 nm where UVR is transmitted through air. The most restrictive limits are for exposure to radiation having those wavelengths less than 315 nm.

For the UV-A spectral region 315 to 400 nm, the total radiant exposure on the unprotected eye must not exceed 10 $kJ.m^{-2}$ within an 8 hour period and the total 8 hour radiant exposure incident on the unprotected skin must not exceed the values given in Table 2.5 [20]. Values for the relative spectral effectiveness are given up to 400 nm to expand the action spectrum into the UV-A for determining the EL for skin exposure.

In addition, the UV radiant exposure in the actinic UV spectral region (UVB and UVC from 180 to 315 nm) incident upon the unprotected skin and unprotected eye(s) within an 8 hour period must not exceed the values given in Table 2.5.

Permissible exposure time in seconds for exposure to actinic UVR incident upon the unprotected skin or eye may be computed by dividing 30 $J.m^{-2}$ by E_{eff} in $W.m^{-2}$. The maximum exposure duration may also be determined using Table 2.6 [20] of this schedule which provides representative exposure durations corresponding to effective irradiances in $W.m^{-2}$ (and $\mu W.cm^{-2}$).

For the EL for both general and occupational exposure to UVR incident upon the skin or eye within an 8 hour period, the following applies:

- *Exposure of the eyes:* UV radiant exposure in the spectral region 180 to 400 nm incident upon the unprotected eye(s) should not exceed 30 $J\ m^{-2}$ effective spectrally weighted using the spectral weighting factors contained in Table 2.5, and the total (unweighted) UV radiant exposure in the spectral region 315 to 400 nm should not exceed $10^4 J\ m^{-2}$ [20].

- *Exposure of the skin:* For the most sensitive, non-pathologic, skin phototypes (known as “melano-compromised”), UV radiant exposure in the spectral region 180 to 400 nm upon the unprotected skin should not exceed 30 $J\ m^{-2}$ effective spectrally weighted using the spectral weighting factors contained in Table 2.5. This limit should be considered a desirable goal for skin exposure to minimize the long-term risk, but it must be recognized that this limit is difficult to achieve in sunlight and judgment must be used in its practical application. It has a very substantial safety factor for dark skin phototypes (known as “melano-competent”) and more generally

for individuals who have been conditioned by previous, repeated exposures (known as "melano-adapted," i.e., tanned) [20].

Table 2.5. UV radiation EL and Relative Spectral Effectiveness.

λ (nm)	EL ($J\ m^{-2}$)	EL ($mJ\ cm^{-2}$)	$S(\lambda)$	λ (nm)	EL ($J\ m^{-2}$)	EL ($mJ\ cm^{-2}$)	$S(\lambda)$
180	2,500	250	0.012	310	2,000	200	0.015
190	1,600	160	0.019	313[c]	5,000	500	0.006
200	1,000	100	0.030	315	1.0×10^4	1.0×10^3	0.003
205	590	59	0.051	316	1.3×10^4	1.3×10^3	0.0024
210	400	40	0.075	317	1.5×10^4	1.5×10^3	0.0020
215	320	32	0.095	318	1.9×10^4	1.9×10^3	0.0016
220	250	25	0.120	319	2.5×10^4	2.5×10^3	0.0012
225	200	20	0.150	320	2.9×10^4	2.9×10^3	0.0010
230	160	16	0.190	322	4.5×10^4	4.5×10^3	0.00067
235	130	13	0.240	323	5.6×10^4	5.6×10^3	0.00054
240	100	10	0.300	325	6.0×10^4	6.0×10^3	0.00050
245	83	8.3	0.360	328	6.8×10^4	6.8×10^3	0.00044
250	70	7	0.430	330	7.3×10^4	7.3×10^3	0.00041
254[c]	60	6	0.500	333	8.1×10^4	8.1×10^3	0.00037
255	58	5.8	0.520	335	8.8×10^4	8.8×10^3	0.00034
260	46	4.6	0.650	340	1.1×10^5	1.1×10^4	0.00028
265	37	3.7	0.810	345	1.3×10^5	1.3×10^4	0.00024
270	30	3.0	1.000	350	1.5×10^5	1.5×10^4	0.00020
275	31	3.1	0.960	355	1.9×10^5	1.9×10^4	0.00016
280[c]	34	3.4	0.880	360	2.3×10^5	2.3×10^4	0.00013
285	39	3.9	0.770	365[c]	2.7×10^5	2.7×10^4	0.00011
290	47	4.7	0.640	370	3.2×10^5	3.2×10^4	0.000093
295	56	5.6	0.540	375	3.9×10^5	3.9×10^4	0.000077
297[c]	65	6.5	0.460	380	4.7×10^5	4.7×10^4	0.000064
300	100	10	0.300	385	5.7×10^5	5.7×10^4	0.000053
303[c]	250	25	0.120	390	6.8×10^5	6.8×10^4	0.000044
305	500	50	0.060	395	8.3×10^5	8.3×10^4	0.000036
308	1,200	120	0.026	400	1.0×10^6	1.0×10^5	0.000030

Table 2.6. Limiting UV exposure durations based on EL.

Duration of exposure per day	Effective irradiance	
	E_{eff} ($W\ m^{-2}$)	E_{eff} ($\mu W\ cm^{-2}$)
8 h	0.001	0.1
4 h	0.002	0.2
2 h	0.004	0.4
1 h	0.008	0.8
30 min	0.017	1.7
15 min	0.033	3.3
10 min	0.05	5
5 min	0.1	10
1 min	0.5	50
30 s	1.0	100
10 s	3.0	300
1 s	30	3,000
0.5 s	60	6,000
0.1 s	300	30,000

Standards for photobiological safety classification [21, 22] divide lamps into two broad categories, GLS and non-GLS. The primary deciding factor between GLS and non-GLS evaluation is intended use, with GLS sources defined as those intended for lighting spaces that are occupied or viewed by people. GLS sources are spectrally evaluated at a variable distance where the illuminance produced by the lamp is 500 lux, whereas non-GLS lamps are measured at a standard 20 cm. GLS categorization does not consider dermatological risk potential for photosensitive individuals.

However, the safety standards give priority to a non-GLS evaluation in circumstances where a reasonable expectation that the source emits UVB or UVC exists or when intended use distance may actually be closer and potentially hazardous, where illuminance may significantly exceed *500* lux.

Table 2.7 [23] below gives a summary for EL under various spectral regions for both human eye and skin tissue.

Table 2.7. Limiting apertures for applying the EL.

Spectral region	Exposure duration, t (s)	Eye exposure (mm)	Skin exposure (mm)
180–400 nm	<10 s	1.0	3.5
	≥10 s	3.5	3.5
400–1,400 nm	1 ns to 30 ks	7.0	3.5
1,401–10^5 nm	1 ns to 0.3 s	1.0	3.5
	0.3 to 10 s	$1.5t^{3/8}$	3.5
	10 s to 30 ks	3.5	3.5
10^5–10^6 nm	1 ns to 30 ks	11.0	11.0

3. OPTO THERMAL INTERACTION OF LIGHT WITH TISSUE

Interaction of light with tissue is widely investigated in different perspectives: physics of propagation of light through media and its biological effects to the absorbing media. Some of the characteristics have found great applications in life for photo-thermal curing techniques.

Once the light reaches the tissue, part of it is absorbed, part is reflected or scattered, and part is further transmitted, illustrated in Figure 3.1.

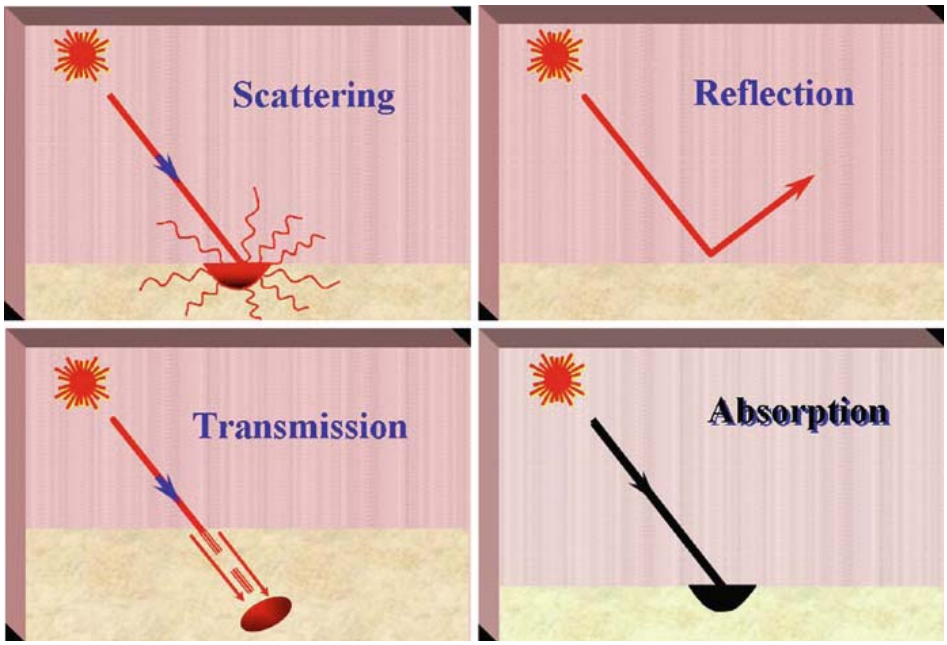

Figure 3.1. Interaction of biological tissue exposed to any kind of light source.

Interaction of biological tissue exposed to any kind of light source is characterized by the light propagation in tissue, and the following mechanisms meanwhile arise: conversion of light to heat, transfer of heat and the tissue reactions has effects ultimately related to temperature and heating time [24]. Understanding the interaction of light with tissue can be realized through the analysis of heat transfer mechanisms in biological tissues.

3.1. Heat Transfer in Tissue

In the context of tissue heat treatment the principal modes of heat transfer are conduction, convection, and radiation. This section briefly describes the different modes. Conduction is an intrinsic property of the medium, whereas evaporation acts as a boundary condition at tissue-air boundaries. Radiation and convection are present to varying degrees both inside the bulk tissue and at surfaces.

- *Conduction:* Thermal conduction is transfer of energy from the more energetic particles in a substrate to the adjacent less energetic ones as a result of interactions between the particles. This mode of tissue heat transfer is described by Fourier's law, which states that the heat flow at a given point in the tissue is proportional to the gradient of the temperature. An energy balance for a volume element gives the following relation for transient conduction:

$$\rho c \frac{\partial T}{\partial t} = \nabla(\lambda \nabla T) \tag{3.1}$$

where ρ (kg m^{-3}) is the density, c (J $kg^{-1}K^{-1}$) is the specific heat capacity, T (K) is the tissue temperature, and λ (W $m^{-1}K^{-1}$) is the thermal conductivity. The ratio $\lambda/(\rho c)$ is called the thermal diffusivity, α (m^2s^{-1}), which describes the dynamic behavior of the thermal process.

The thermal properties depend on the type of tissue. Since most tissues can be considered as being composed of a combination of water, proteins and fat, the magnitude of the conductivity can be estimated with knowledge of the proportions of these components. Table 3.1 shows selected data on the thermo-physical properties of tissue measured at room or body temperature. It can be observed that of the different components constituting tissue, water has the highest values of the thermal conductivity and diffusivity. Therefore, tissues with high water content are the best thermal conductors and respond the fastest to a thermal disturbance.

Table 3.1. Thermophysical properties of human tissue and water.

Material	***Conductivity*** $(Wm^{-1}K^{-1})$	***Density*** $(kg\ m^{-3})\times10^{-3}$	***Specific Heat*** $(kJ\ kg^{-1}K^{-1})$	***Diffusivity*** $(m^2s^{-1})\times10^{7}$
Muscle	0.38 – 0.54	1.01 – 1.05	3.6 – 3.8	0.90 – 1.5
Fat	0.19 – 0.20	0.85 – 0.94	2.2 – 2.4	0.96
Kidney	0.54	1.05	3.9	1.3
Heart	0.59	1.06	3.7	1.4
Liver	0.57	1.05	3.6	1.5
Brain	0.16 – 0.57	1.04 – 1.05	3.6 – 3.7	0.44 – 1.4
Water @37°C	0.63	0.99	4.2	1.5

- *Convection:* Convection is the term applied to heat transfer between a surface and a fluid, e.g., air or blood, moving over the surface. Convection problems involve heat transfer between the surface of the body and the surrounding air and also between blood and the vessel wall. The heat transfer between a conducting solid, which in this context is tissue, and a convecting fluid is usually described using Newton's law of cooling which states that the heat flow q (W m^{-2}) normal to the surface is proportional to the temperature difference between the surface T(K) of the tissue and the bulk temperature of the fluid T_∞:

$$q = h\left(T - T_\infty\right) \tag{3.2}$$

where the proportionality constant, h (W $m^{-2}K^{-1}$), is called the local heat convection coefficient.

At the tissue surface there is no fluid motion and energy transfer occurs only by conduction. The magnitude of the heat convection coefficient therefore depends on the temperature gradient at the surface but also on the conditions in the boundary layer. Equations can be set up to account for the physical processes in the boundary layer but the solutions readily become very complex. Here it is sufficient just to give examples, as in Table 3.2, of the convection coefficient in a few cases;

Table 3.2. Values of the convection coefficient for a few cases.

Mode	***h (W/m^2/K)***
Free convection (tissue – air)	5 – 25
Forced convection (tissue – air, i.e. a windy day)	50 – 20000
Convection with phase change (boiling)	2500 – 100000

- *Radiation:* Every body emits electromagnetic radiation proportional to the fourth power of the absolute temperature. The maximum heat flux, q (W m^{-2}) emitted from a black body is expressed by:

$$q = \varepsilon\sigma\left(T_s^4 - T_\infty^4\right) \tag{3.3}$$

where σ (W m^{-2}K^{-4}) is the Stefan-Boltzmann constant, T_s and T_∞ (K) are the tissue surface and environmental temperature, respectively and ε is the emissivity. Since tissue is not a perfect black body the emissivity is less than one. For human skin, the value of the emissivity is in the range 0.98-0.99. When modeling internal biological tissue, intrinsic radiative heat transfer processes constitute a negligible contribution and the process of radiation is often considered only a boundary effect.

3.1.1. Diffusion Equation

The balance of energy for light propagation through a volume element of an absorbing and scattering medium is represented by an integro-differential equation, called the Radiative Transfer Equation (RTE). The fact that retrieval of solutions for the equation is an extremely expensive computational process has made scientists seek simpler approximate models, such as the diffusion approximation, parabolic-type partial differential equation [19]. Obtained from the Radiative Transfer Equation, the Diffusion equation, where optical properties of the biological tissue dominate, can be written as:

$$\left[\frac{1}{v}\frac{\partial}{\partial t} - \nabla.(D\nabla) + \mu_a\right]\Phi(\vec{r},t) = q_0(\vec{r},t) \tag{3.4}$$

where

$$q_0(\vec{r},t) = \int_{4\pi} \varepsilon(\vec{r},\hat{s},t)d\Omega - 3\nabla.\left[D\int_{4\pi} \varepsilon(\vec{r},\hat{s},t)\hat{s}d\Omega\right] \tag{3.5}$$

is the source term.

Nomenclaturation of the terms in the equation:

v is the speed of light; μ_a is the absorption coefficient; $\Phi(\vec{r},t)$ is the fluence rate (or irradiance or simply fluence); $\varepsilon(\vec{r},\hat{s},t)$ is the source term that is power emitted at time t per unit volume and unit solid angle along $\hat{s}$.

D is the diffusion coefficient, defined as

$$D = \frac{1}{3(\mu_a + \mu_s')} \tag{3.6}$$

where, $\mu_s' = \mu_s$ (1-g) is the reduced scattering coefficient for scattering coefficient μ_s and asymmetry factor g.

3.1.2. Bioheat Equation

The absorption of light in tissue causes a local elevation in temperature. Tissue heat transfer due to the deposited light is described by the Bioheat transfer equation taking into account conduction, convection by blood and possible heat sources (Q). The Bioheat transfer equation was first introduced by Pennes in 1948 [3] to model heat transfer in perfused tissue such that

$$\delta_{ts}\rho C\frac{\partial T}{\partial t} + \nabla\cdot(-k\nabla T) = \rho_b C_b \omega_b (T_b - T) + Q_{met} + Q_{ext} \tag{3.7}$$

where δ_{ts} is a time-scaling coefficient (dimensionless), T = temperature (°C), ρ = density of tissue (kg cm^{-3}), *C* = specific heat of tissue (J kg^{-1} $°C^{-1}$), k = thermal conductivity of tissue (W cm^{-1} $°C^{-1}$), T_b = temperature of arterial blood (°C), w_b = volumetric perfusion rate (kg s^{-1} cm^{-3}), c_b = specific heat of blood (J kg^{-1} $°C^{-1}$), Q_{met} is the metabolic heat source (W cm^{-3}), Q_{ext} is the spatial heat source (W cm^{-3}).

On the left hand side of the equation, second term describes the thermal conduction; whereas the first term on the right hand side describes the convective effects of blood flow represented as a heat sink proportional to tissue perfusion (Pennes 1948) excluding effects of large blood vessels [26]. Note that for a phantom with no perfusion, w_b would be set to 0 [27].

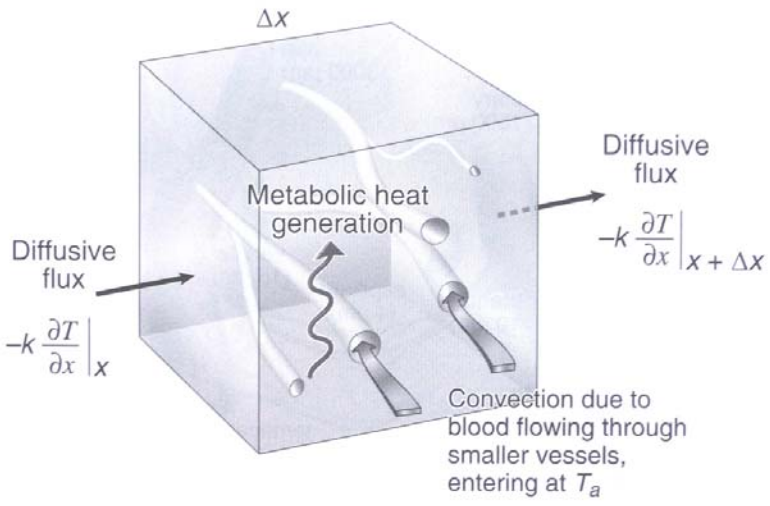

Figure 3.2. Idealized heat transfer in a tissue showing metabolic heat generation Q and a convective heat transfer due to the passage of blood.

Figure 3.2 [28] illustrates the idealized heat transfer in a biological tissue as described by Pennes' Bioheat equation, taking the effects of metabolic heat generation and convective heat transfer due to blood perfusion into account.

Convection between tissue surface and surrounding air, radiation and evaporation are processes that have to be modeled as appropriate boundary conditions. Boundary

conditions for the Bioheat transfer equation is described by the following equations and the related parameters:

- *Heat Flux:*

$$-n\cdot(-k\nabla T)=q_0+h(T_{\text{inf}}-T) \tag{3.8}$$

Here in this equation, q_0 represents a heat source or heat sink on the boundary, for example an electrical heater or a known inflow of energy, such as radiation with specified intensity. The term $h(T_{inf} - T)$ models convective heat transfer with the surrounding environment, where h is the heat transfer coefficient and T_{inf} is the external bulk temperature. The value of h depends on the geometry and the ambient flow conditions.

- *Insulation or Symmetry:*

$$-n\cdot(-k\nabla T)=0 \tag{3.9}$$

This condition applies to boundaries where the domain is well insulated; or it can be utilized to reduce model size by taking advantage of symmetry.

- *Prescribed temperature:*

$$T=T_0 \tag{3.10}$$

This condition prescribes the temperature value to T_0.

- *Axial symmetry:*

$$r=0 \tag{3.11}$$

This boundary condition is available only for ax symmetric heat transfer models, and used on the symmetry axis r=0. Note that from the mathematical point of view, this condition is identical to thermal insulation.

The boundary conditions for interior boundaries of tissue are determined by the heat flux equation in two ways: heat flux discontinuity and the continuity.

- *Heat Flux Discontinuity:*

$$n \cdot (k_u \nabla T_u - k_d \nabla T_d) = q_0 + h(T_{\text{inf}} - T) \tag{3.12}$$

On interior boundaries, a heat flux discontinuity can be specified, which is same as a heat source or heat sink. In the equation for this boundary condition, the terms on the left are sub indexed with "u" for upside and "d" for downside. The equation states that the difference between the heat flux on the left and the right is equal to the heat source (q_0) on the interior boundary. The second term, $h(T_{inf} - T)$, models heat exchanged with a fluid flowing in a network of thin channels embedded in the boundary, in this study blood vessels. An appropriate value for h can for example be found from a local analysis of a unit cell.

- *Continuity:*

$$n \cdot (k_u \nabla T_u - k_d \nabla T_d) = 0 \tag{3.13}$$

The default setting for interior boundaries is Continuity, which is a special case of the above Heat flux discontinuity condition. In the absence of sources or sinks, that condition specifies that the heat flux in the normal direction is continuous across the boundary [29].

3.2. Adverse Health Effects due to Light-Tissue Interaction

Literature dealing with laser–tissue interaction has been basically targeted to main medical applications. It has been inferred that four main effects occur due to laser interaction with biological tissues [30], namely,

- *Photochemical and photobiological smooth effects:* The irradiance could be continuous-wave or pulsed, from 10^{-3} to 1 W/cm^2 or from 10^{-2} to 10^5 J/cm^2, its temporal duration is very variable.

- *Photothermal effects*: The radiation is absorbed by the tissue transforming in internal energy producing a temperature increment, the following process can occur: thermophysical, chemical, and biological. The irradiance could be continuous-wave or pulsed, from 0.1 to 10^5 W/cm^2 or from 0.1 to 10^6 J/cm^2, its temporal duration is from 1 ms to hours.

- *Photochemical hard effects or photoablation*: UV radiation is used because of the photon's high-energy can break molecular links and to ionize atoms. By this way can be affected only focalized atoms and molecules. The exposition times are very short, from 1 to 500 ns and irradiance from 10^5 to 10^9 W/cm^2.

- *Photodisruption*: In this process is used an exposition time very short from ps to ns and high-power laser focused by a lens into the treated tissue. In this way are obtained irradiances in the magnitude of 10^{14} W/cm^2.

A study [8] on contemporary lighting found that both daylight and cool-white fluorescent lamps may emit UVA and UVB radiation as short as 280 nm; 254 nm emission. They concluded that for a general, normally responding population, the UVR risk from these sources remains very low. However, they advised that the condition of photo-sensitive patients may be exacerbated by exposure to selected fluorescent lamps and that further investigation into UV exposure from lamps used at short distances (e.g. desk or task lamps) may be warranted.

In 1990, Diffey [31] suggested that exposures from the following sources accounted for most individual human UV risk: sunlight, cosmetic tanning units, medical and dental phototherapies, industrial photoprocesses, sterilization and disinfection units, research laboratory sources, insect traps and lamps used for office and general lighting. He noted that small quantities of UVA and UVB are emitted by fluorescent lamps but not transmitted through plastic diffuser panels.

Studies of UV risk accumulated from indoor lighting sources have primarily focused on the possible relationship between fluorescent room lighting and increasing prevalence of melanoma [32-41]. Spectral measurements reported by Cole [12] and by Maxwell and Elwood [38, 39], addressing possible risks of UV from indoor lighting, were limited to fluorescent sources.

Several studies in the literature concluded that the UV emissions from a significant percentage of the tested CFLs with single envelopes may result in foreseeable overexposure of the skin when these lamps are used in desk or task lighting applications [42]. CFLs generate UVR from a discharge in mercury vapor. The energy in the ultraviolet photons is converted into visible optical radiation in the phosphor coating inside the glass envelope of the lamp. Ideally, the conversion would be 100% efficient. However, in reality, some UVR is transmitted through defects in the phosphor coating and the glass envelope. A study [43] in the 1990s concluded that, under normal use, the UVR emission from CFLs would not constitute a significant UVR hazard, when assessed at 65 cm. The assessment was made against EL recommended by the American Conference of Governmental Industrial Hygienists (ACGIH) and against a minimum erythemal dose of 300 J m^{-2} effective [44].

The National Institute of Environmental Health Sciences (NIEHS) in USA warns that solar UVR and exposure to sunlamps and tanning beds are carcinogenic. It has been also suggested that artificial UVR is linked to melanoma development [45, 46].

In the short exposure period of time, the Scientific Committee on Emerging and Newly Identified Health Risks (SCENIHR) concluded that [6]:

- The UV and blue light radiation from CFLs is a potential risk factor for the aggravation of symptoms in some light-sensitive patients with such diseases as chronic actinic dermatitis and solar urticaria. Across the European Union (EU), an estimated 250 000 patients could be concerned (preliminary rough estimation of worst case scenario).
- Using some single-envelope CFLs for prolonged periods of time near the body (at distances smaller than 20cm) can result in UV exposures nearing current workplace limits set to protect workers from skin and retinal damage.
- The use of double-envelope energy-saving lamps or similar technology would largely or entirely mitigate risks both of approaching workplace limits on UV emissions in extreme conditions and the risk of aggravating the symptoms of light-sensitive people.

4. MODELLING AND SIMULATIONS FOR RF AND LASER

4.1. FEM as the Computational Technique

Many physical phenomena in engineering and science can be described in terms of partial differential equations. In general, solving these equations by classical analytical methods for arbitrary shapes is almost impossible. Computational techniques and numerical analysis allow the study of complex systems and natural phenomena that would be too costly and time consuming, or even impossible, to study directly by experimentation.

For simulating EM scattering and radiation of waves in biological bodies, a wide variety of numerical methods have been developed. Today, most of the popular EM field simulation software packages are based on: (i) FEM, (ii) Method of Moments (MoM), (iii) Finite Integration Technique (FIT), (iv) Finite Difference Method (FDM). Each method has its own advantages besides some difficulties posing restrictions in applications.

FEM is a numerical approach, developed in early 1950s, by which partial differential equations can be solved approximately. FDM was developed by Yee in 1966, whose idea was to divide the three dimensional region into cubic cells, to take values of points on each cell, and to convert the partial derivatives to difference equations. The idea is coming from Taylor expansions, where the finite differences are used to approximate derivatives. In this method, continuous equations are replaced with their finite difference of values of selected points. Nevertheless, it is difficult to implement for complex objects [47].

On the other hand, the FEM allows for good approximations of complex boundaries. To explain the basic approach of the FEM, consider a plate with a hole as shown in Figure 4.1 for which we wish to find the temperature distribution. It is straightforward to write a heat balance equation for each point in the plate. The basic idea of FEM is to divide the body into finite elements, often just called elements, connected by nodes, and obtains an approximate solution. This is called the finite element mesh and the process of making the mesh is called mesh generation. The FEM provides a systematic methodology by which

the solution, in the case of our example, the temperature field, can be determined by a computer program, which actually is essential since thousands of nodes are usually needed to obtain a reasonably accurate solution. Generally, the accuracy of the solution improves as the number of elements (and nodes) increases; but the computer time, and hence the cost, also increases. The finite element program determines the temperature at each node and the heat flow through each element and then presents the results as computer visualizations, such as contour plots.

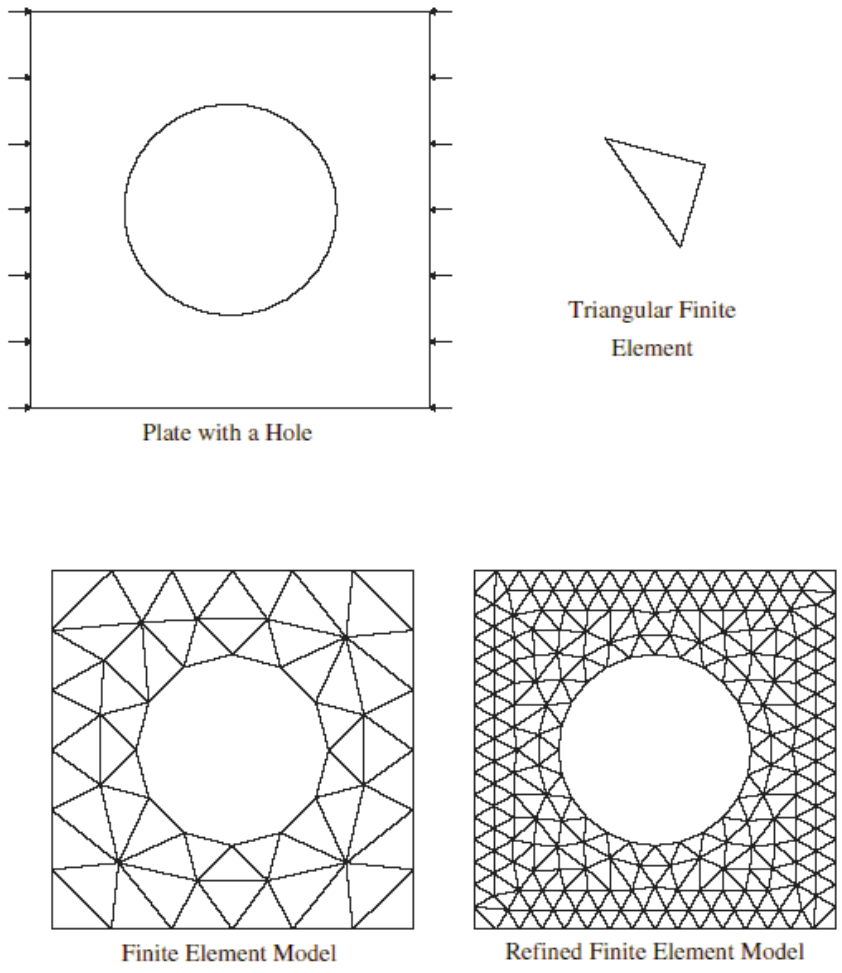

Figure 4.1. Geometry, loads and finite element meshes.

Certain steps in formulating a finite element analysis of a physical problem are common to all such analyses, whether structural, heat transfer, fluid flow, or some other problem. These steps are embodied in commercial finite element software packages The preprocessing step is, quite generally, described as defining the model and includes;

- Define the geometric domain of the problem.
- Define the element type(s) to be used.
- Define the material properties of the elements.
- Define the geometric properties of the elements (length, area, and the like).
- Define the element connectivities (mesh the model).
- Define the physical constraints (boundary conditions).
- Define the loadings.

During the solution phase, finite element software assembles the governing algebraic equations in matrix form and computes the unknown values of the primary field variable(s). The computed values are then used by back substitution to compute additional, derived variables, such as reaction forces, element stresses, and heat flow [47].

- *Comparison to the FDM:* The FDM is an alternative way of approximating solutions of PDEs. The differences between FEM and FDM are:
  (i) The most attractive feature of the FEM is its ability to handle complicated geometries (and boundaries) with relative ease. While FDM in its basic form is restricted to handle rectangular shapes and simple alterations thereof, the handling of geometries in FEM is theoretically straightforward. Please see Figure 4.2 for difference between two methods in simulation.
  (ii) The most attractive feature of finite differences is that it can be very easy to implement.
  (iii) There are several ways one could consider the FDM a special case of the FEM approach. One might choose basis functions as either piecewise constant functions or Dirac delta functions. In both approaches, the approximations are defined on the entire domain, but need not be continuous. Alternatively, one might define the function on a discrete domain, with the result that the continuous differential operator no longer makes sense, however this approach is not FEM.
  (iv) There are reasons to consider the mathematical foundation of the finite element approximation more sound, for instance, because the quality of the approximation between grid points is poor in FDM.

(v) The quality of a FEM approximation is often higher than in the corresponding FDM approach, but this is extremely problem dependent and several examples to the contrary can be provided [48].

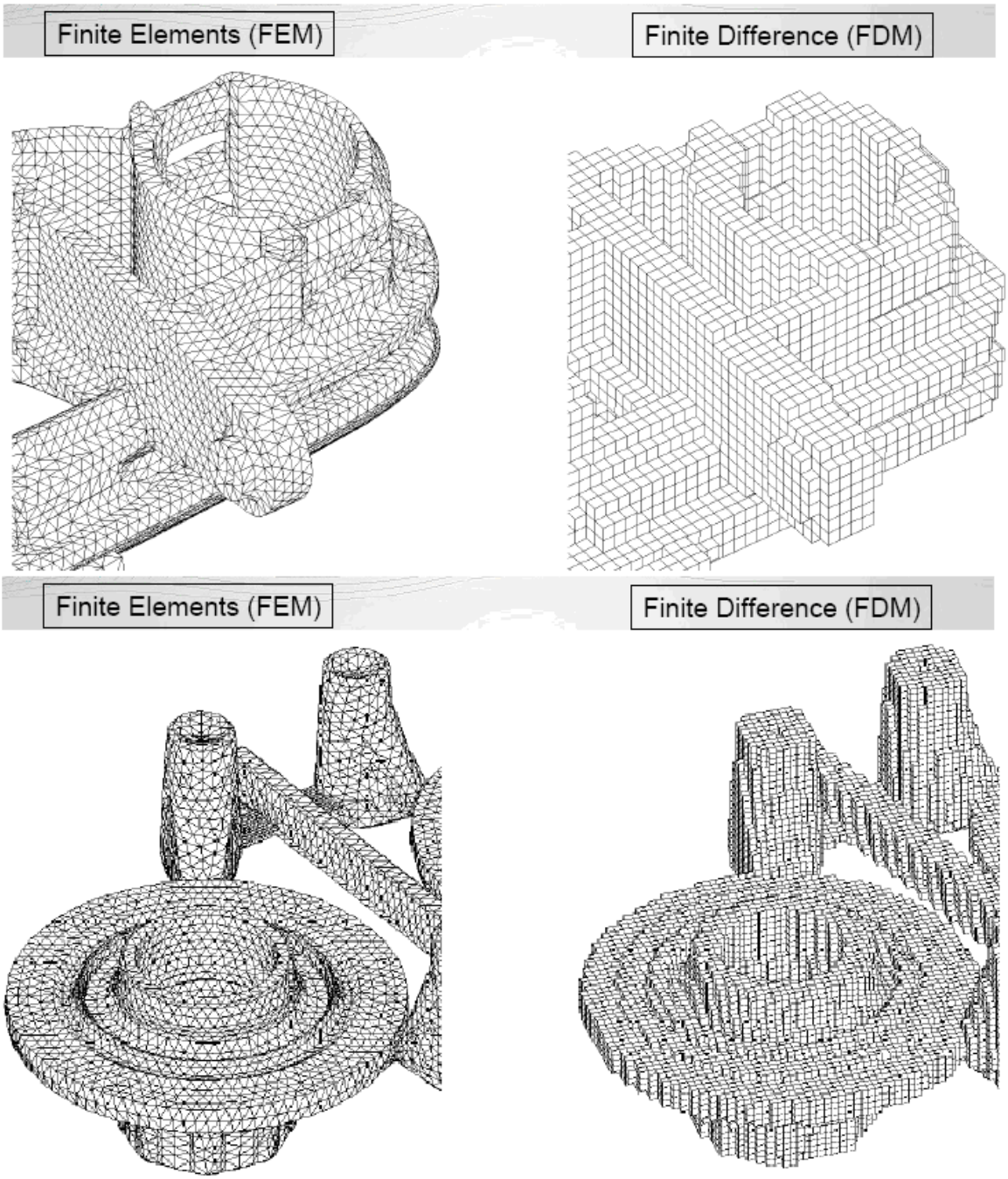

Figure 4.2. Difference between FEM and FDM in simulations.

In the light of the foregoing comparison, FEM in general is the method of choice in all types of analysis in structural mechanics (i.e. solving for deformation and stresses in

solid bodies or dynamics of structures) while computational fluid dynamics (CFD) tends to use FDM or other methods like finite volume method (FVM). CFD problems usually require discretization of the problem into a large number of cells/gridpoints (millions and more), therefore cost of the solution favors simpler, lower order approximation within each cell. This is especially true for 'external flow' problems, like air flow around the car or airplane, or weather simulation in a large area.

In the following sections, numerical studies on thermal response of biological tissue which have taken the foregoing theoretical information as a foundation will be presented each in a detailed way with its methodology, simulation results and the discussion on the obtained results; where it is aimed initially to develop tissue and mathematical models for thermal interaction from radiative exposures so that with the obtained verification on modeling consecutive studies can further expand the scope for various spectrum ranges. First study is the FEM modeling of Specific Absorption Rate (SAR) distribution and related temperature increase in human brain due to Radio Frequency (RF) exposure; in which Bioheat equation and Vector Helmholtz equation is studied for problem solution. Second study focuses on the laser-tissue interaction and displays thermal response results for various laser sources.

4.2. FEM Modeling of SAR Distribution and Temperature Increase in Human Brain from RF Exposure

4.2.1. Methodology of the Study

Dosimetric studies are performed to quantify the interactions of electromagnetic fields with biological tissues. Whether they are numerical or experimental, the SAR distribution has to be determined, based on the fact that the proximity of mobile telephones to the body during their operation leads to highly non-uniform exposure so that it is inappropriate to specify the safety limits based on electric and magnetic fields and power density. For this reason almost all national and international safety guidelines and recommended limits on human exposure to electromagnetic fields are given in terms of SAR [49], and the temperature rise caused by the SAR also serves well for the subject.

SAR, which is the most appropriate metric for determining Electromagnetic (EM) exposure effects in the very near field of a RF source, because of highly non-uniform exposure during the operation of RF sources [50], is defined as the power absorbed by the unit mass of tissue (Watts/kilogram). The SAR is calculated from the electric field strength $\vec{E}$ inside the human body, the conductivity σ and the mass density ρ of the biological tissue, as given in the Equation 4.1, and is averaged out to the mass of 1 or 10g of tissue.

$$SAR = \sigma \frac{\vec{E}^2}{\rho} \tag{4.1}$$

To calculate the SAR distribution values, it is necessary to solve for the Vector Helmholtz equation everywhere in the domain for a certain operating frequency of the RF source. The Vector Helmholtz equation, which comes from the Maxwell's time-dependent curl equations, is given in Equation 4.2.

$$\nabla \times \frac{1}{\mu_r} \nabla \times \vec{E} - k_0^2 \varepsilon_r \vec{E} = 0 \tag{4.2}$$

where μ_r is the relative permittivity, k_0 is the free-space wave vector, and ε_r is the relative permittivity for the material. Solution of this equation provides the required electric field value $\vec{E}$ for SAR calculation.

Following the calculation of SAR, the temperature change due to the induced SAR is obtained by solving the Bioheat Equation. If the effect of blood flow and metabolic heating rate is considered, the Bioheat equation can be written as in Equation 4.3 and 4.4:

$$\rho c \frac{\partial T}{\partial t} = \nabla.(k \nabla T) + \rho Q_{met} + \rho(SAR) - B(T - T_{blood}) \tag{4.3}$$

where the ρ [kg/m^3] is the material density, c [J/(kg°C)] is the specific heat capacity, k [W/(m°C)] is the thermal conductivity, Q_{met} [W/kg] is the metabolic heat generation rate, B [W/(m^3°C)] is the blood perfusion coefficient, w [L/(s*kg)] is the blood perfusion rate, and T_{blood} is blood temperature [51-53].

Specific Anthropomorphic Mannequin (SAM) head model provided by the Institute of Electrical and Electronics Engineers (IEEE) is imported into the numerical solver to be used in this study. Then the microstrip patch antenna is constructed and placed at the left side of head with minimum possible distance. Besides the head and antenna geometries modeled in the study, as depicted in Figure 4.3, surrounding air is also taken into account such that it is also divided into subdomains according to the absorbtions in single or multi directions.

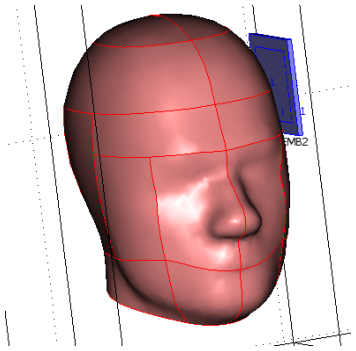

Figure 4.3. SAM Head and Patch Antenna.

In order to make a comparison with the literature and to verify the success of the model used in this study, first simulations are made at 900 MHz, where antenna power is taken to be 600 mW. The simulation parameters for 900 MHz are given in Table 4.1.

Table 4.1. Simulation parameters at 900 MHz.

Name	***Value***	***Description***
epsilonr_pcb	5.23	permittivity for the patch antenna board
epsiolnr0_brain	52.72	permittivity for the brain tissue
sigma0_brain	0.94 [S/m]	conductivity for the brain tissue
rho_brain	1030 [kg/m^3]	density of the brain tissue
rho_blood	1000 [kg/m^3]	density of blood
c_blood	3639 [J/(kg.K)]	heat capacity of blood

4.2.2. Simulation Results and Comparison with Literature

Simulation results for SAR and temperature distribution obtained at 900 MHz frequency are provided in Figures 4.4 and 4.5.

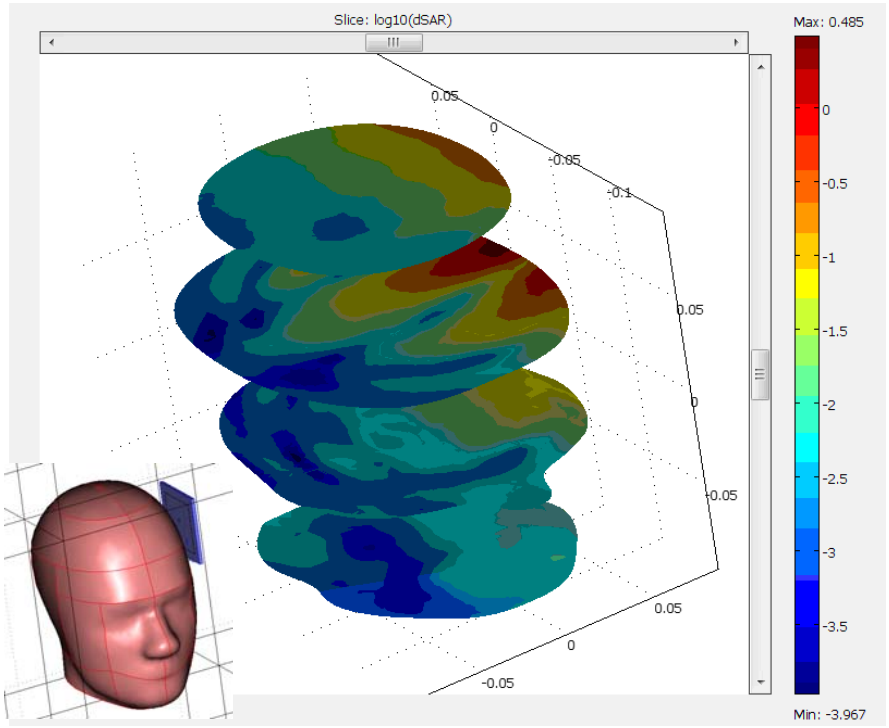

Figure 4.4. Log-scale slice plot of the local SAR value from the front-side of head when it is exposed to antenna from left.

As an initial remark, it should be noted that almost all of the studies available in literature have chosen to use FDTD method [54] as the numerical method to be used in simulations, due to its simplicity. However, already mentioned advantages of FEM become the stimulating factor for the choice on this study. Then in order to make comparisons about the performances of the chosen methods and to verify the models and the methodology of our study, first simulations obtained at 900 MHz are compared with another study (by Yioultsis *et al.* in 2002) [55] which has performed solutions by FDTD method. Additionally that study gives the advantage of comparing the performances of different antenna types.

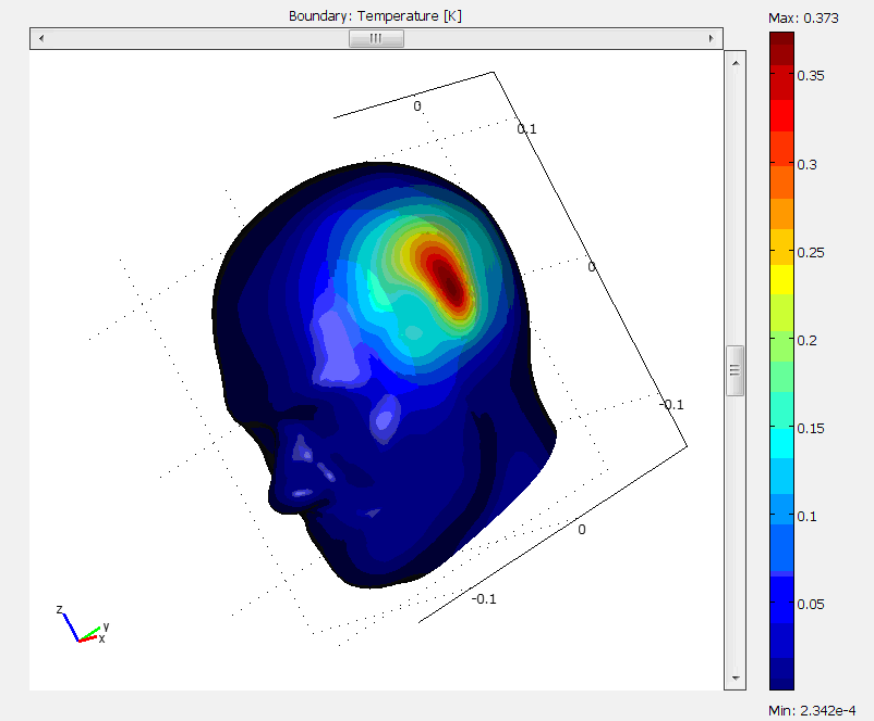

Figure 4.5. The local increase in the temperature at the surface has a maximum right beneath the antenna.

After obtaining the simulation results for SAR and temperature increase at 900 MHz, it is obvious that the results obtained here are in comparable limits with the study from literature made by Yioultsis *et al.* in 2002. The study compared the SAR and temperature values for four different antenna types: monopole, helix, side PIFA and patch antenna. In Table 4.2, the results from that study are summarized and compared with our numerical modeling results.

In literature, although various studies have been made to show the SAR and induced temperature values for RF exposure, almost all of the studies have chosen to use monopole or helical antennas. Having investigated results of those studies, it can be seen that the results vary in an extended range due to the parameters and models chosen. Thus, as the results of Yioultsis provide good reasoning both in terms of SAR and temperature and in terms of antenna types; they are chosen to be compared with our simulation results and to verify our results.

Table 4.2. Comparison of results with literature.

			Max SAR (W/kg) @ 900 MHz	***Max ΔT (℃) @ 900 MHz***
FDTD	Yioultsis, 2002	Monopole	2.072	0.331
		Helix	2.385	0.178
		Side PIFA	2.430	0.139
		Patch	3.105	0.380
FEM	*Citkaya, 2011*	*Patch*	*3.055*	*0.373*

Moreover, it is worth to note that when the studies published in literature are examined, there are some important concerns about the results, because the information provided in literature is not sufficient for us to evaluate and compare them with our results in detail.

To illustrate the fact, first of all, in most of the studies researchers have used different tissue parameters varying up to 40%. This variation must have resulted in different outputs in studies. Moreover, head models and distribution of tissues within head show variation in studies and these different models can possibly affect the SAR distribution and induced temperature increase in head due to RF radiation exposure from cellular phone antenna.

Secondly, most of the papers do not provide their antenna parameters such as power, dimension, etc. Although they explicitly state their choice for the antenna type, they commonly do not specifically mention about the dimensions and antenna parameters. More specific example will be the power of the antennas in different frequencies. In most of the studies for 900 MHz Global System for Mobile Communications (GSM) frequency, researchers have chosen 600 mW output power for antenna. In other studies, they either do not mention the antenna power or choose to use 1 W. This type of ambiguity creates great differences in published results and makes it more difficult to reach a general conclusion.

Thirdly, in almost all of the studies found in literature, there does not exist a clear identification of the distance between head and the antenna. As it will be further discussed in the next section, distance between head and antenna is an important parameter to which

special attention should be paid. The differences in the outputs of published studies may also come from this factor. The mutual positions between the device and head have a considerable amount of effect, as well.

Additionally, these studies found in literature are based on the FDTD method and there will be certain differences between those results and our outputs obtained via FEM due to the performance variations of the methods based on the domains where the partial differential equations (PDE)s are to be solved. FDTD's poor performance on highly curved surfaces is also reflected on the simulation results. In addition to the performance of the methods, mesh sizes used in studies are not specified explicitly; there is no doubt that for coarser meshes solutions will be less accurate with respect to the finer meshes. On contrary, these finer meshes result in longer central processing unit (CPU) times so the optimal point is important for accurate results in achievable limits.

4.2.3. Contributions of the Study

Having verified the simulation model and its results by comparing it with previous studies from literature, it is now necessary to extend the scope of the study by producing extended results. Analyzing possible range of variations of the induced field strengths in various tissues requires an extensive effort, since local field strengths strongly depend on various parameters. Among the others, operational frequency and antenna power, mutual positions of the device and head size and the shape of human head [56], distribution of tissues within the head, electrical properties of the tissues can be listed as important parameters which strongly affect SAR distribution.

In order to make more and meaningful contributions with this study, some of the above listed parameters can be varied, and the results can be compared to induce a general idea. For this purpose, first of all, the frequency of operation is changed from 900 MHz to 1800 MHz, meanwhile notice that tissue parameters are affected as well. Then the effects of variation of distance between head and antenna are investigated. Notice that the results for these variations have undeniable importance in terms of safety levels and health hazards due to RF exposures.

4.2.3.1. Effects of Frequency Variation. Here, geometrical placement of head and antenna is initially left unchanged. Only the operating frequency of patch antenna is increased to 1800 MHz, and consequently antenna power is reduced to 150 mW. The tissue parameters at 1800 MHz are summarized in Table 4.3.

Table 4.3. Parameters used for simulation at 1800 MHz.

Name	Value	Description
epsilonr_pcb	5.23	permittivity for the patch antenna board
epsiolnr0_brain	50.08	permittivity for the brain tissue
sigma0_brain	1.39 [S/m]	conductivity for the brain tissue
rho_brain	1030 [kg/m^3]	density of the brain tissue
rho_blood	1000 [kg/m^3]	density of blood
c_blood	3639 [J/(kg.K)]	heat capacity of blood

By making simulations for 1800 MHz, the effect of frequency difference is observed, as in Figure 4.6 and 4.7. On the other hand, in order to realize these simulation outputs, we had to decrease the mesh sizes because for previous large mesh sizes the numerical analysis did not converge to any solution, it showed continuous oscillating characteristics. This somewhat obligatory reduction in mesh size has brought an important hardness for the study, because finer mesh sizes resulted in larger memory requirements and longer CPU times for the outputs.

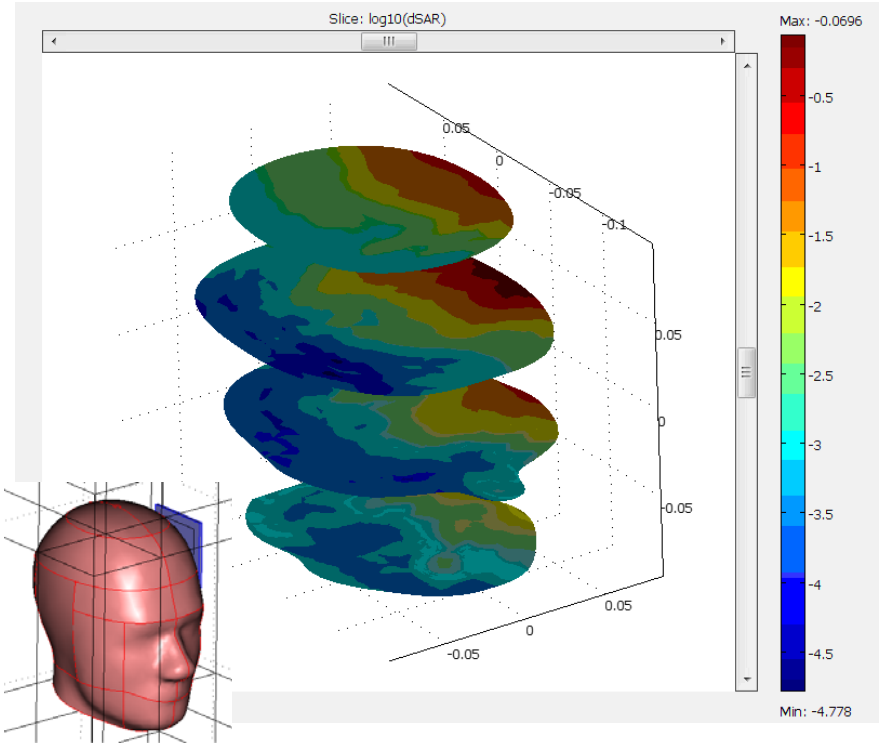

Figure 4.6. Log-scale slice plot of the local SAR value from the front-side of head when it is exposed to antenna from left at 1800 MHz.

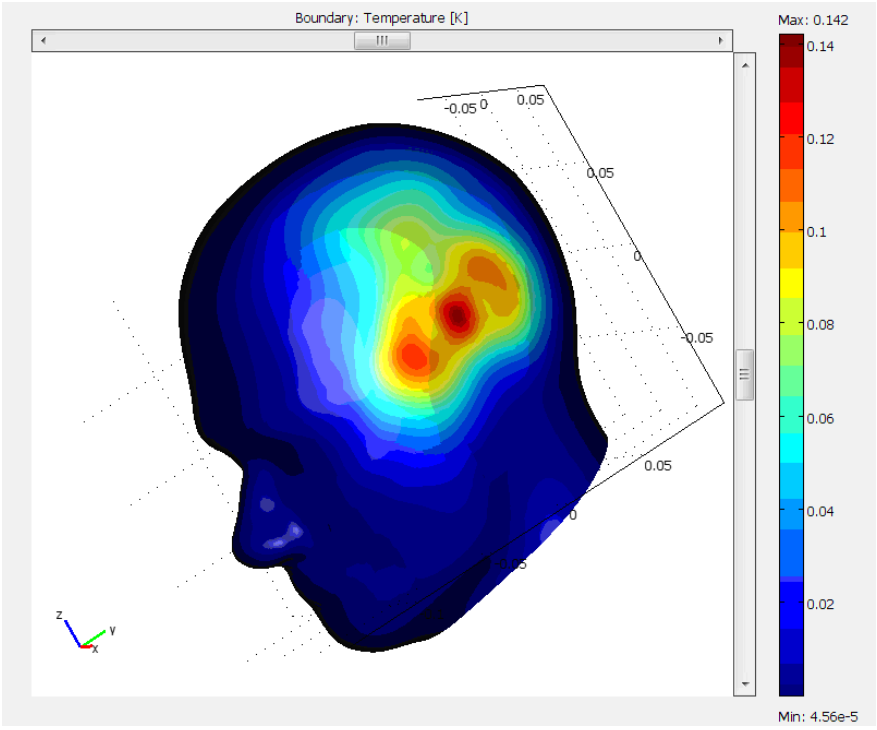

Figure 4.7. The local increase in the temperature at the surface has a maximum right beneath the antenna at 1800 MHz.

4.2.3.2. Effects of Distance Variation between Head and Antenna. Previously obtained simulation outputs were for the case where the antenna is closest to head. Now, in order to see the effect of distance on SAR and temperature increase values, two more simulations are obtained for each of the frequencies: 900 MHz and 1800 MHz. In the first simulation, distance is increased by 2mm; then in the second simulation the distance is increased by 2mm more, hence total of 4mm distance increase is obtained. Figures 4.8 through 4.13 illustrate the simulation outputs.

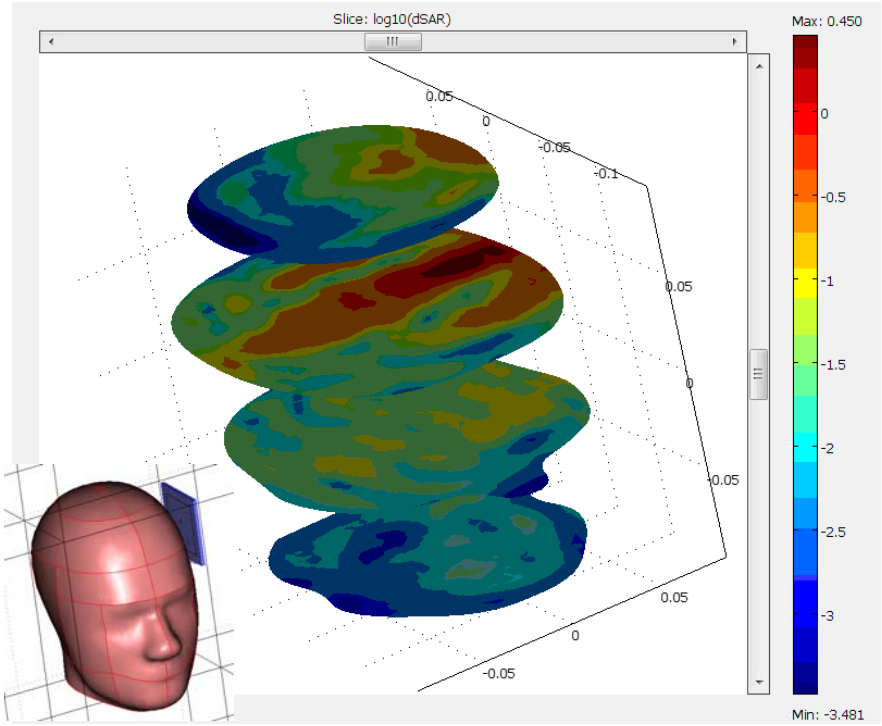

Figure 4.8. Log-scale slice plot of the local SAR value @ 900 MHz when distance is increased by 2mm.

As it can be clearly seen from Table 4.4 and chart in Figure 4.14 which are summarizing the simulation results for different frequencies and distances that as frequency increases, max SAR and max ΔT decrease. Furthermore, as the distance between head and the antenna is increased, max SAR and max ΔT also decrease.

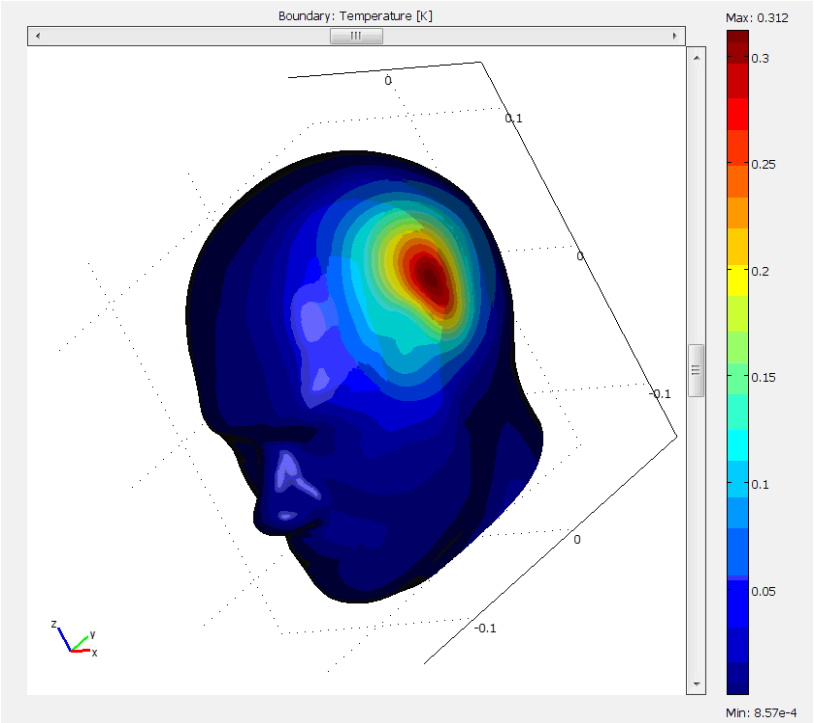

Figure 4.9. The local increase in the temperature at the surface@ 900 MHz when distance is increased by 2mm.

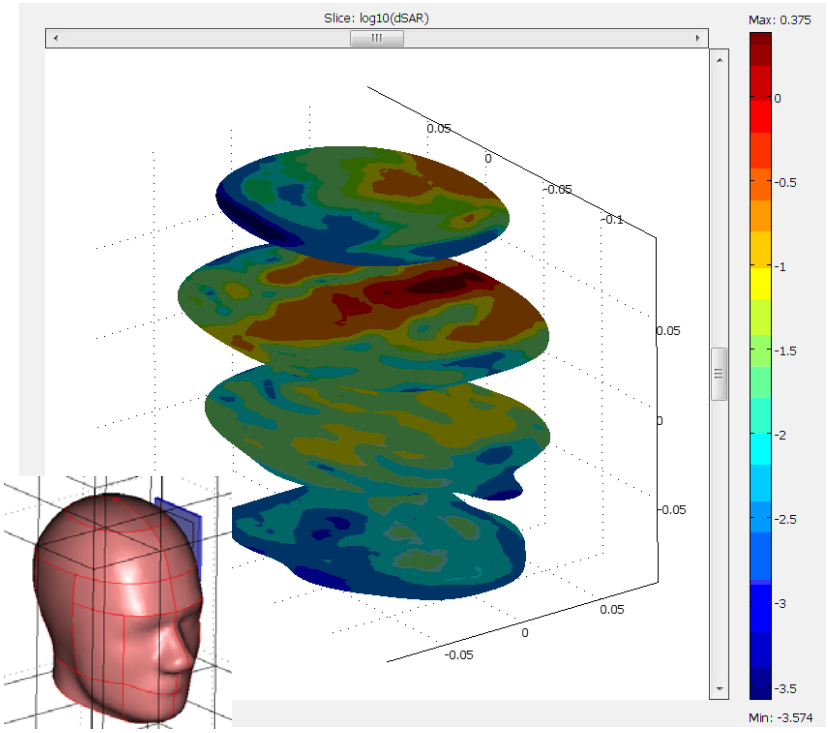

Figure 4.10. Log-scale slice plot of the local SAR value @ 900 MHz when distance is increased by 4mm.

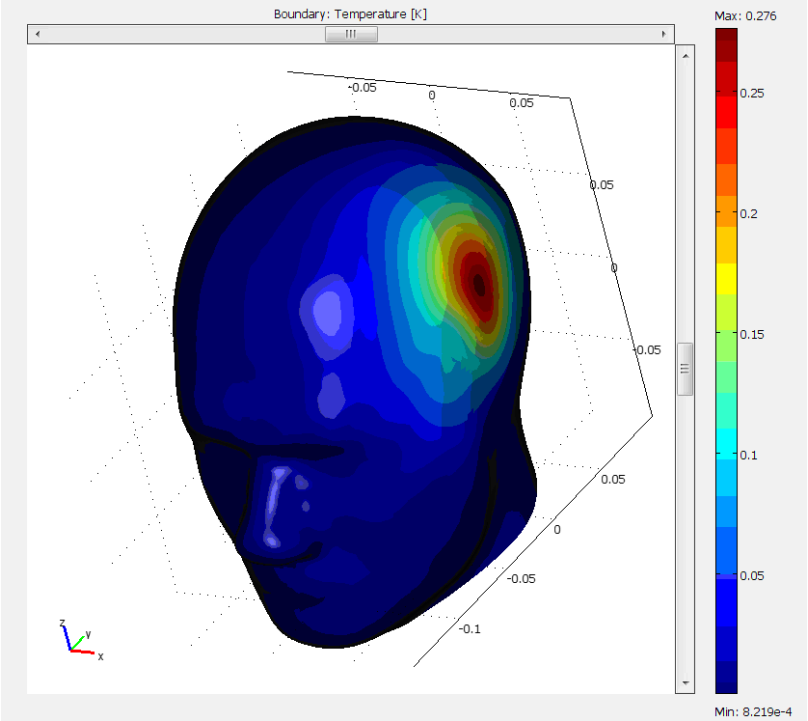

Figure 4.11. The local increase in the temperature at the surface@ 900 MHz when distance is increased by 4mm.

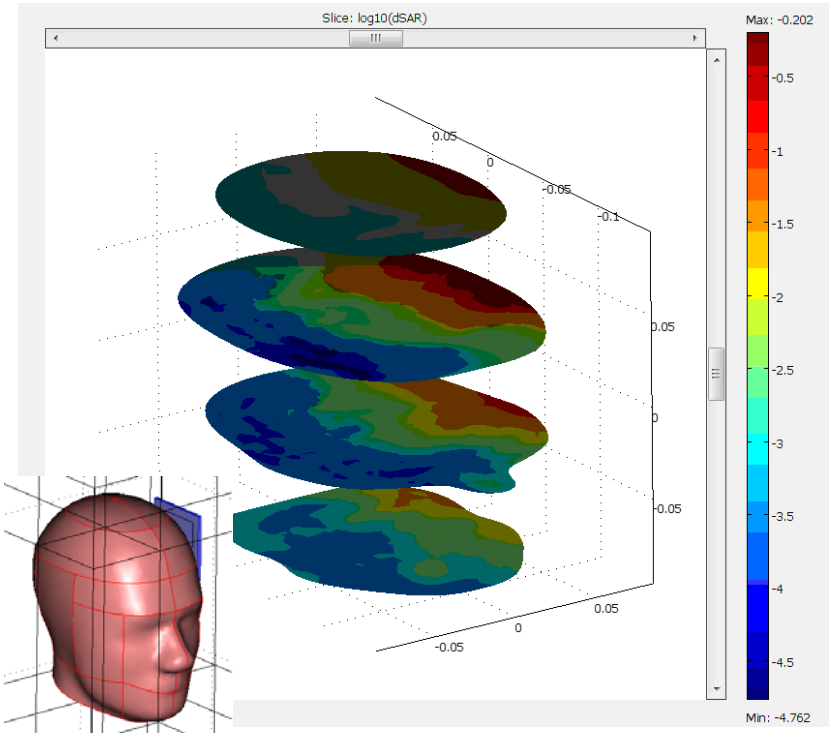

Figure 4.12. Log-scale slice plot of the local SAR value @ 1800 MHz when distance is increased by 2mm.

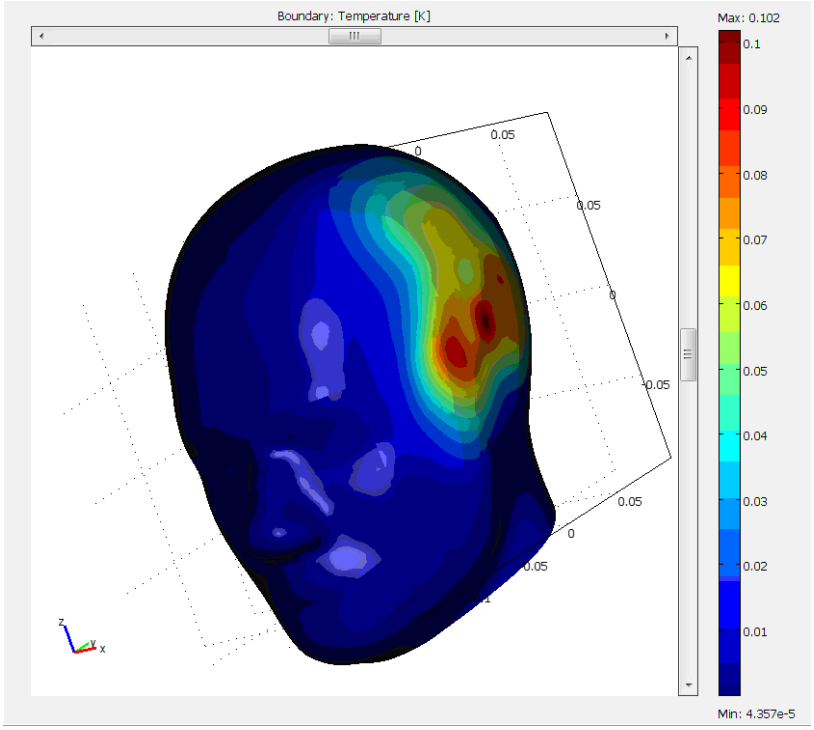

Figure 4.13. The local increase in the temperature at the surface@ 1800 MHz when distance is increased by 2mm.

Table 4.4. Summary of the simulation results.

		Δd = 0	**Δd = +2mm**	**Δd = +4mm**
900 MHz (600 mW)	Max SAR (W/kg)	3.242	2.818	2.371
	Max ΔT (°C)	0.362	0.312	0.276
1800 MHz (150 mW)	Max SAR (W/kg)	0.867	0.640	~0
	Max ΔT (°C)	0.142	0.102	~0

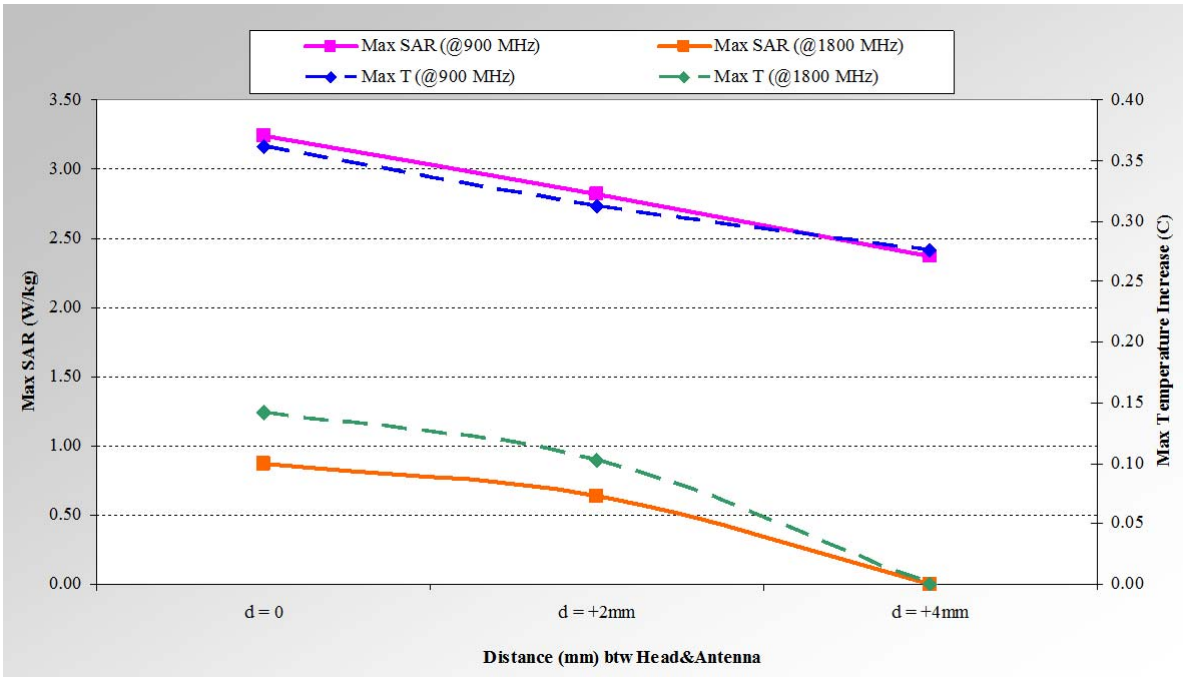

Figure 4.14. Effects of distance and frequency variation on local increase of SAR and temperature.

These results are in line with our expectations because it is natural that as you hold your cellular phone farther away from your head, even with an increase in millimeters range, the exposure from RF radiation is reduced, and consequently the induced temperature increase is also lowered. The only striking result among our simulation outputs is that for Δd=+4mm the max SAR is found to be zero. When you want to obtain the general pattern between distance increase and SAR decrease, data for 900 MHz may suggest almost a linear relation. However, when you look at the data for 1800 MHz, this suggested pattern will not be verified. There may be some underlying reasons for the zero SAR and temperature increase at Δd=+4mm for 1800 MHz. For example, it may be stemming from the insufficient mesh size. As mesh sizes become finer, more accurate results can be obtained, but this brings the increased computational memory and time loads.

It can be clearly stated that by holding your mobile phones away from your body as much as possible, you will be exposed to minimum radiation, and this radiation will be in the predetermined safety limits. Nevertheless, the duration and intensity of exposure and

distance are the most important factors for the exposure to be within the safety standards. To minimize the health effects, better designed antennas can be used in industry, as well.

Depending on the results of the simulations, if the safety limits are exceeded by electromagnetic radiation from the mobile phones, the result should draw the attention of the public. Hence, it may bring a social impact on the public concern of health effects of electromagnetic radiation. Meanwhile, redetermination of the safety standards may be put on the agenda by health organizations. Accordingly, with changing standards, telecommunication companies producing mobile phones will need to take the new standards into account, and even may need to consider redesigning their products.

4.3. Study of Temperature Distribution for Laser-Skin Tissue Interaction

4.3.1. Methodology of the Study

In certain medical treatment applications laser light sources are used to generate opto-thermal effects in tissue. In these treatments, the most important issue is to control the temperature increase and distribution over the living tissue; otherwise, high temperatures could potentially lead to undesired thermal damages in the surrounding tissue. The temperature distribution in the tissue, which is in thermal interaction with laser light, is mainly dependent on opto-thermal properties of both the tissue and the light source, such as exposure duration, wavelength of the beam, energy of the beam, the area and type of tissue exposed to the beam.

For the solution of the proposed problem, the opto-thermal model, which employs the Beer–Lambert law for optical propagation and the Pennes equation for the spatial-temporal temperature distribution, will be used.

The mathematical expression for the absorption of light is defined by Beer-Lambert law, which is described in Equation 4.4.

$$I = I_0 e^{-\mu_a l} \tag{4.4}$$

where I, transmitted intensity, is dependent upon the incident intensity I_0, the distance l and the absorption coefficient μ_a. The absorption coefficient μ_a can thus be interpreted as the probability that a photon will be absorbed by the medium per unit length. In other words, the reciprocal of the absorption coefficient, known as the absorption length, is the distance required for the intensity of the beam to fall to e^{-1} of the initial intensity.

The laser energy radiated at each end of a fiber acts as a spatial heat source defined by Equation 4.5.

$$Q_{laser} = aI_0 e^{-k_{dis} A} \tag{4.5}$$

In this equation, I_0, the intensity of the laser, is calculated by assuming an area of tissue and an output power of the laser. The variable k_{dis} is the dissipation constant, and describes the loss of energy over time in tissue. The variable A is the normal distance between the end point of the fiber and points in the laser beam.

Lastly, for the Pennes Bioheat equation, as given in Equation 3.7, convection process between the tissue surface and the surrounding air should be modeled as appropriate boundary conditions, as in Equation 4.6:

$$q_{conv} = h_{amb}\left(T_s - T_{amb}\right) \tag{4.6}$$

where q_{conv} is the heat flux due to convection and T_s is the skin surface temperature. Assuming that the average temperature at the surface of skin is 34°C, and using values of h_{amb}=10 and T_{amb}=25°C, q_{conv} is calculated to be 90Wm^{-2} [57].

4.3.2. Simulation Results

4.3.2.1. Single Layer Tissue Model. The computational model is simulated for a dimension of 5×5×3mm single layer tissue. The bottom surface of the tissue is assumed to be located within the body core. We applied several laser light sources including carbon dioxide (CO_2), Neodymium-doped yttrium aluminum garnet (Nd:YAG) and argon fluoride (ArF) excimer laser. For the first simulation, 10600 nm CO_2 laser in IR region is used, where the laser beam spot size is 0,3 mm and power is 0,2 W/mm^2 , and absorbivity value of 79200 m^{-1} is used for skin. Additional simulation results are given for 1064nm Nd:YAg laser, whose beam spot size is 1 mm and power 0,2 W/mm^2 in NIR region again for skin, and 1000 m^{-1} absorbivity coefficient is used. Finally in UV region, 193 nm ArF excimer laser, for which laser beam spot of 0,1 mm and power of 8 W/mm^2 is used, and absorbivity value of 255800 m^{-1} is accepted for human eye lens. Penetration depths and temperature distributions obtained from the simulations [14] for the three types of laser sources are given in the Figures 4.15 through 4.17.

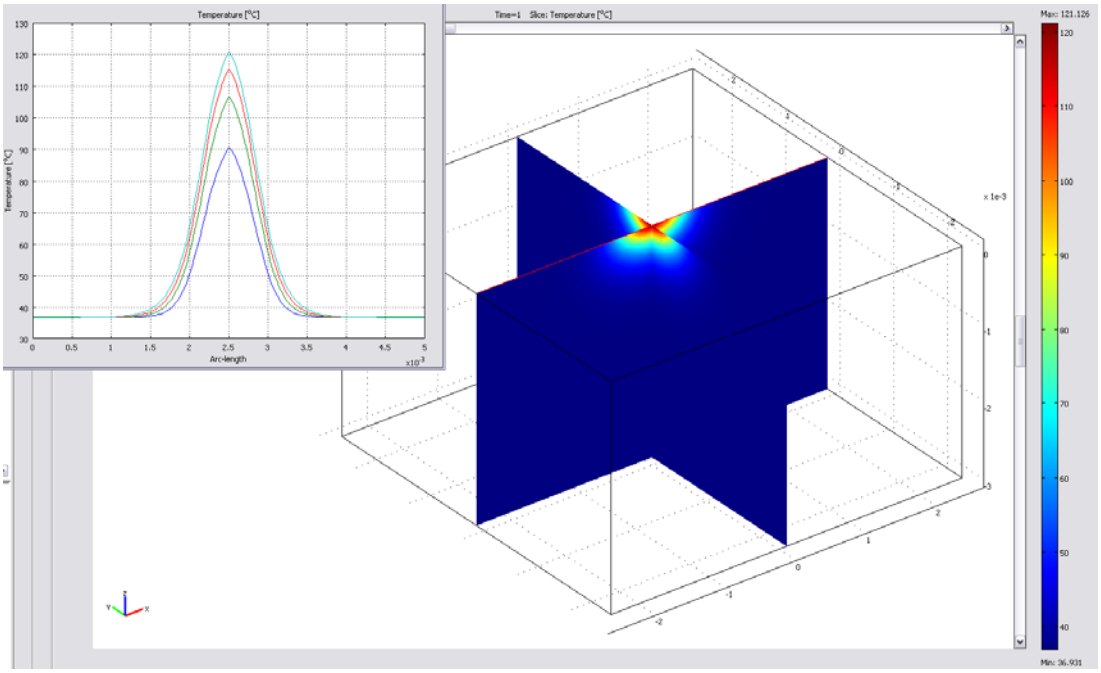

Figure 4.15. CO_2 laser source, temperature distribution and penetration depth.

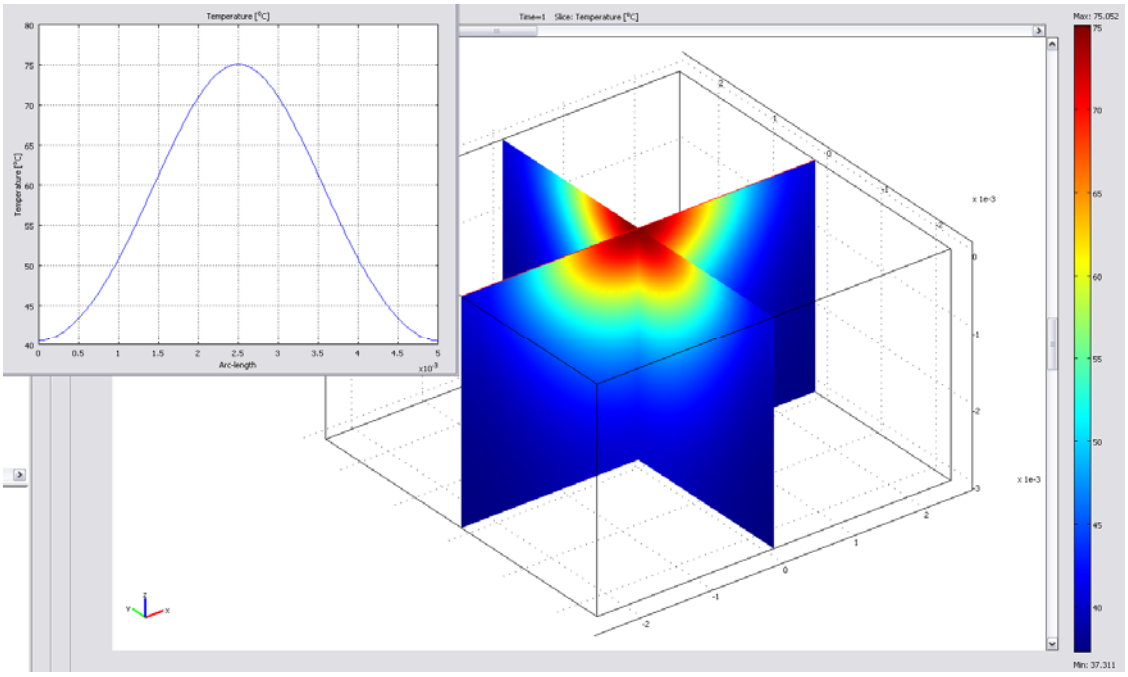

Figure 4.16. Nd:YAG laser source, temperature distribution and penetration depth.

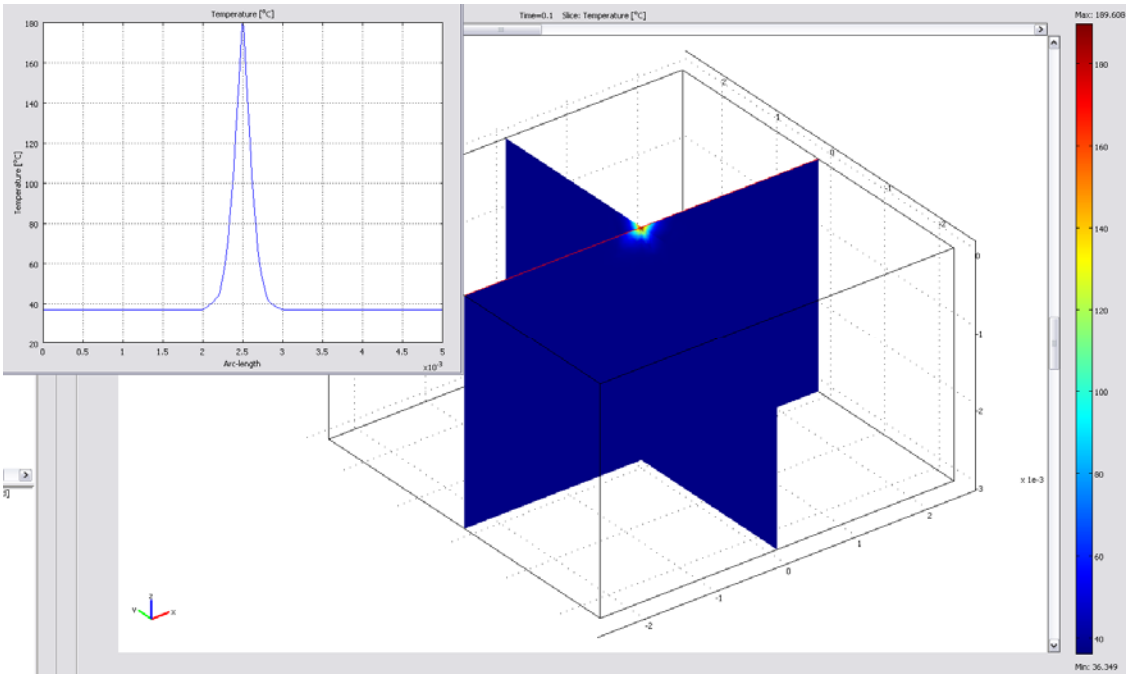

Figure 4.17. ArF excimer laser source, temperature distribution and penetration depth.

4.3.2.2. Multi-Layer Tissue Model. Knowledge of optical properties of skin and subcutaneous tissues is of great importance for interpretation and quantification of diagnostic data, and for prediction of light distribution and absorbed energy for therapeutic and surgical use [58]. The randomly inhomogeneous distribution of blood and various chromophores and pigments in skin produces variations of the average optical properties of the skin layers. This allows subdivision of these layers into sublayers, where the physiological nature, physical and optical properties of their cells and pigments' content are concerned.

The light-tissue interaction is governed by the optical source parameters as well as optical tissue parameters, such the absorption, μ_a, coefficients, which are wavelength-dependent. The absorption coefficient, which can vary over several orders of magnitude, increases towards the visible wavelengths. Typical absorption parameters are in the range of 0.5–5 cm^{-1} at wavelengths $\lambda < 625$ nm. In the red and near-IR regions with $\lambda > 625$ nm, the absorption coefficient varies between 0.01 and 0.5 cm^{-1} [59].

The mathematical modeling developed for obtaining the solution of the Bioheat equation has been applied in order to analyze the dynamics of spatial- temporal temperature distribution $T(x, y, x, t)$ in biological tissues which are exposed to laser beam illumination. The skin is irradiated by a continuous wave Helium-Neon (HeNe) laser source with a wavelength λ=633nm and a Gaussian beam radius r_0. We use an opto-thermal model of the skin obtained from different sources [60]. From the optical point of view, the selected model of the skin tissue is composed of six layers, which are ordered starting from the outside of the skin (the boundary between skin and air) and continue to the inside. Table 4.5 [60] summarizes the optical and thermal parameters of the skin layers, and the geometry of laser–tissue interaction is shown in Figure 4.18 [60]. Figure 4.18 illustrates the multi-layered structure of the skin model (but not to scale as for the layer thicknesses), and it shows interaction of laser and skin tissue in a 3-dimensional structure.

In the simulation examples, the tissue initial temperature was fixed at 36.6°C, and the air temperature at 20°C. The calculation volume of the skin tissue was chosen to be 5mm×5mm×4mm, based on the estimation of the heated volume by the laser used (with radius r_0 = 1 mm). However, the multi-layered structure of skin imposes some limitations

in the definition of the spatial step in the z direction, because of the minimal thickness of the layers, which is 0.06 mm and corresponds to *Epidermis*.

Table 4.5. Optical and thermal parameters for the multilayered model of skin.

LAYER	d (mm)	α (cm^{-1})	ρ (g/cm^3)	c (J/g K)	$k\times10^3$ (W/cm K)	$\omega_b\times10^7$ (cm^3 blood/s g_{tissue})
Epidermis	0.06	25	1	3.77	2.09	0
Upper Dermis	0.56	2.7	1	3.77	3.075	7.51
Blood Plexus	0.1	25	1	3.77	3.075	7.51
Lower Dermis	0.56	2.7	1	3.77	3.075	7.51
Subcutaneous Fat	0.32	0.2	0.85	1.96	2.09	35.07
Muscle	>2	11.2	1.05	3.94	6.42	4.509

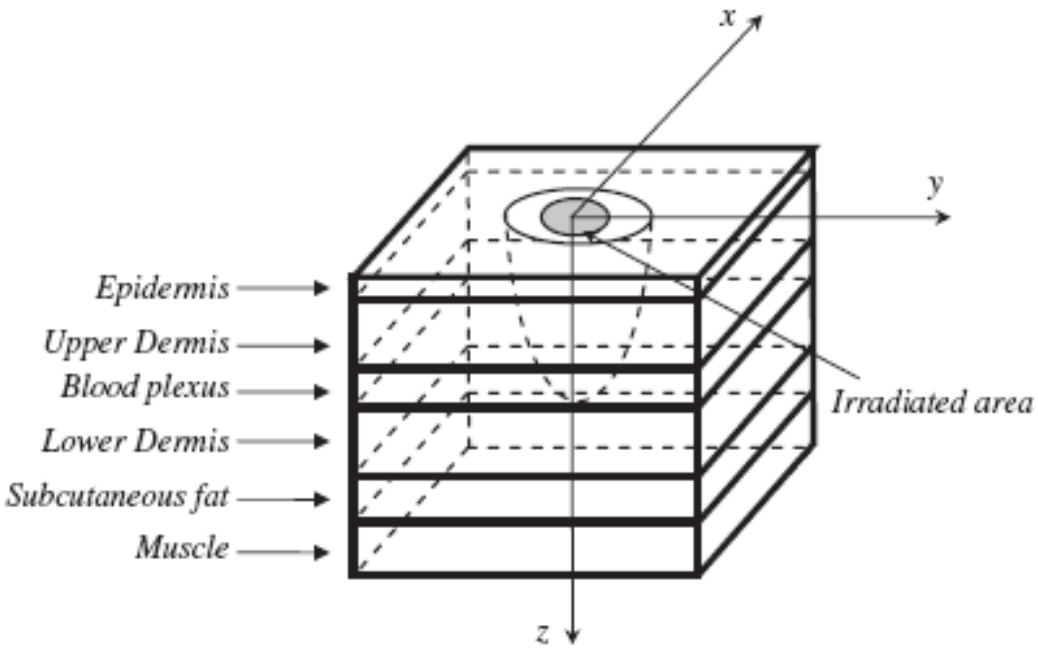

Figure 4.18. The multilayered model of skin and the geometry of laser-tissue interaction.

Simulation results on temperature distribution for the multilayer tissue model at different laser source powers and varying exposure durations are provided in the Figures 4.19 through 4.25. Taking into account the results obtained from the simulations, we can conclude that a predictive analysis of temperature variations is possible by means of the proposed numerical algorithm. Figures 4.19 - 4.25 show the variation of temperature with

depth inside the tissue, as a function of optical power and also as a function of duration of exposure. When these simulation results are examined, the effects of skin layers with different optical and thermal properties, such as absorption coefficient, heat conductivity and so on can be observed. This is why the temperature distribution inside the tissue is usually a non-monotonic function of depth.

All of the results for the simulations of multi-layer model of human skin are summarized in Tables 4.6 and 4.7 and Figures 4.26 and 4.27 so as to clearly understand the variational effects of laser power and duration of exposure on the maximum temperature values. It can be clearly inferred that as duration of exposure to the laser is increased, maximum temperature induced on skin increases. Additionally, as the laser power is increased by keeping the exposure duration constant, maximum temperature due to exposure is increasing linearly.

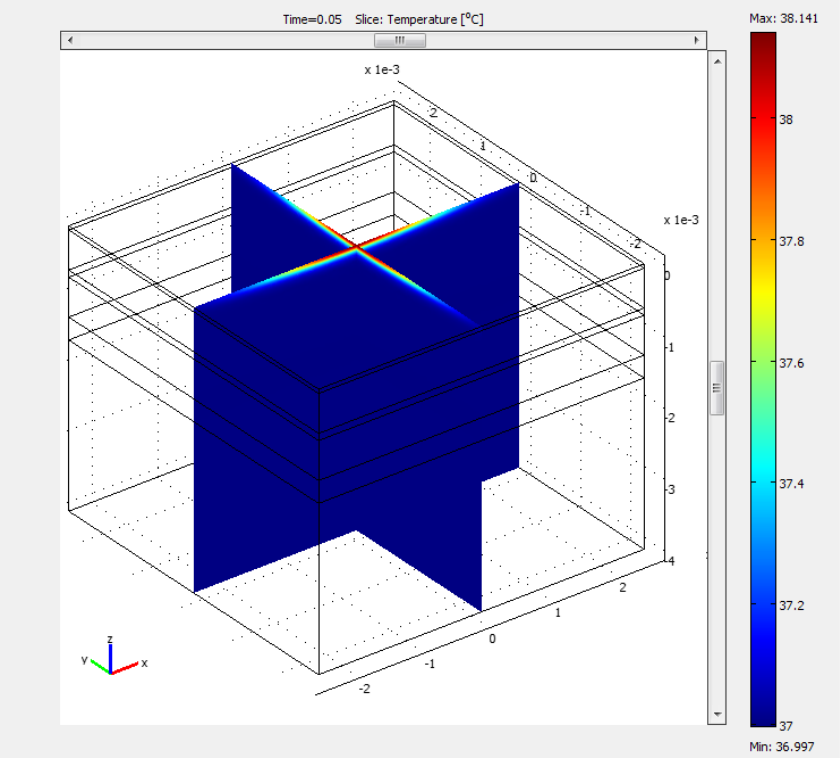

Figure 4.19. Temperature distribution and penetration depth for P=50mW, 50ms duration.

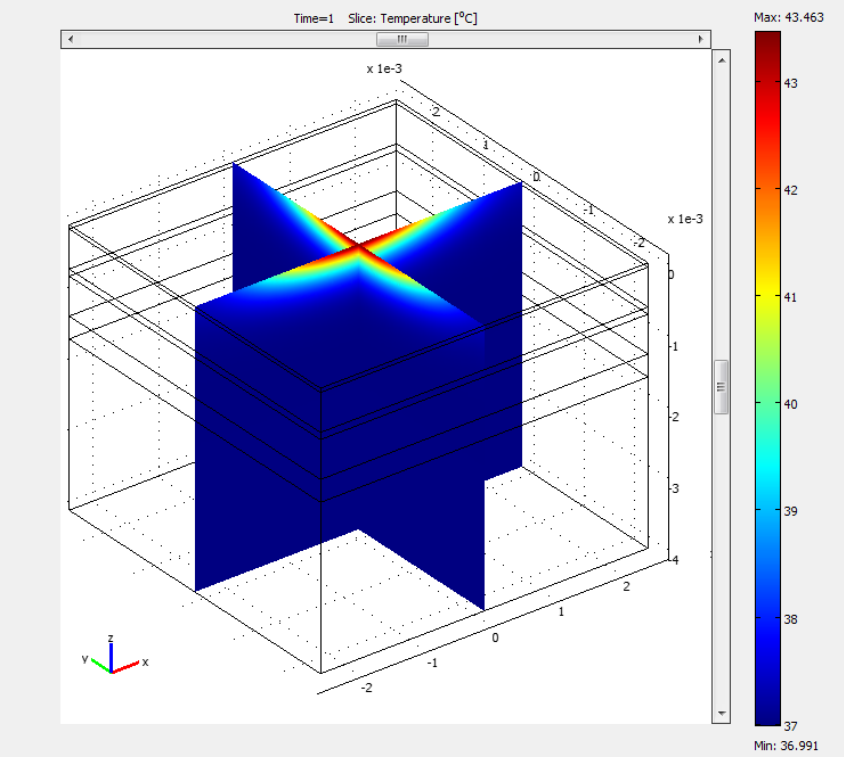

Figure 4.20. Temperature distribution and penetration depth for P=50mW, 1s duration.

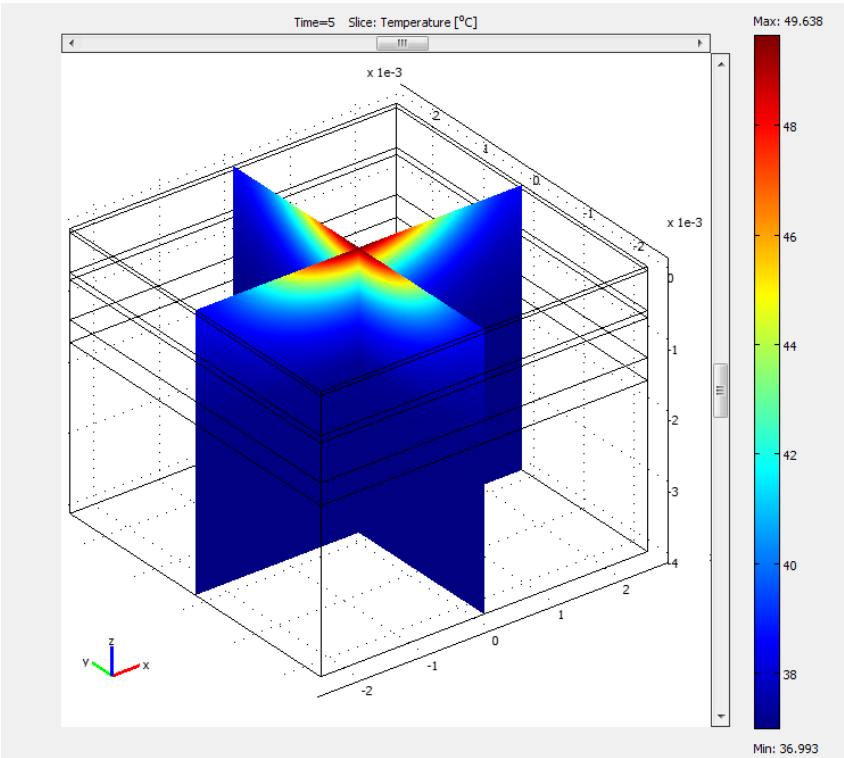

Figure 4.21. Temperature distribution and penetration depth for P=50mW, 5s duration.

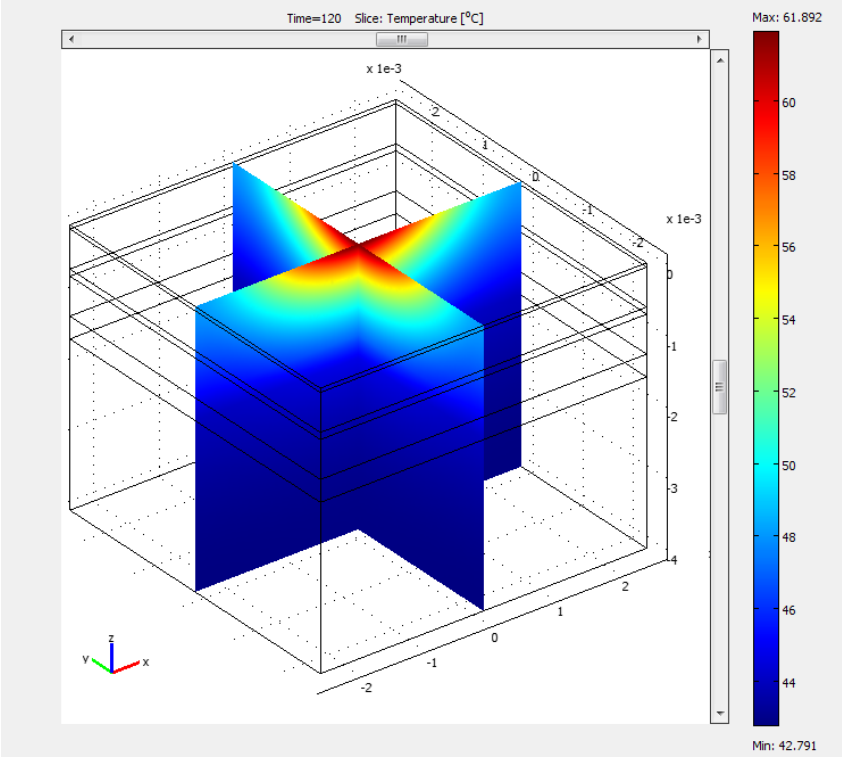

Figure 4.22. Temperature distribution and penetration depth for P=50mW, 120s duration.

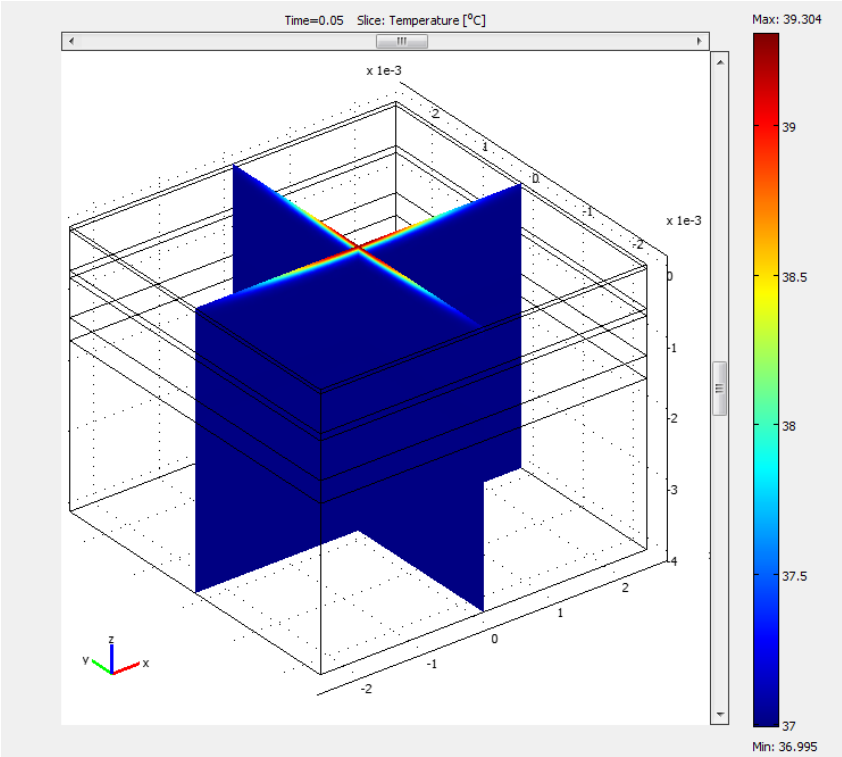

Figure 4.23. Temperature distribution and penetration depth for P=100mW, 50ms duration.

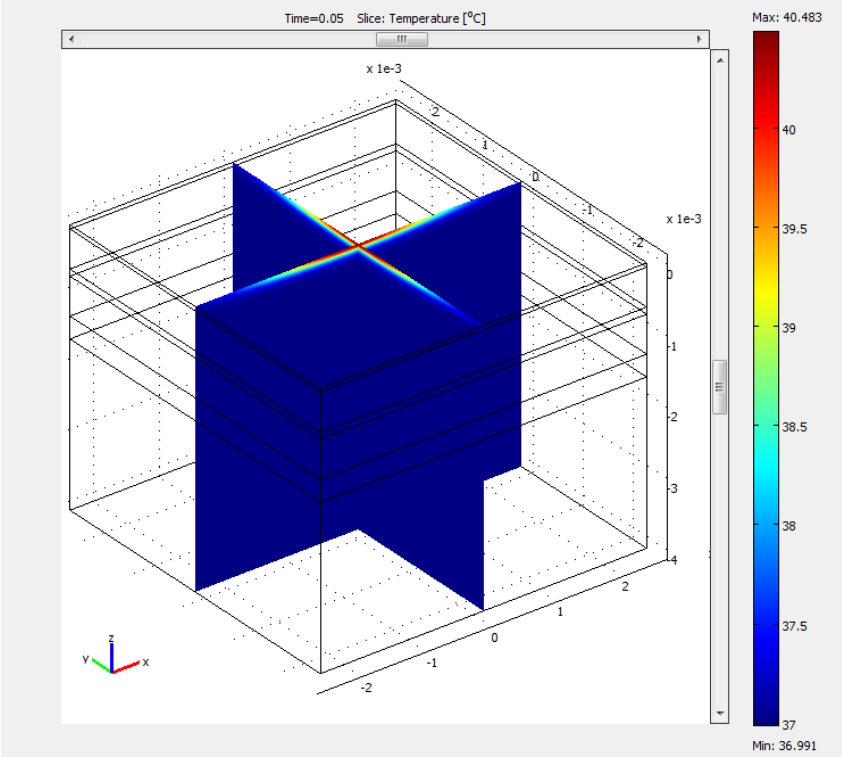

Figure 4.24. Temperature distribution and penetration depth for P=150mW, 50ms duration.

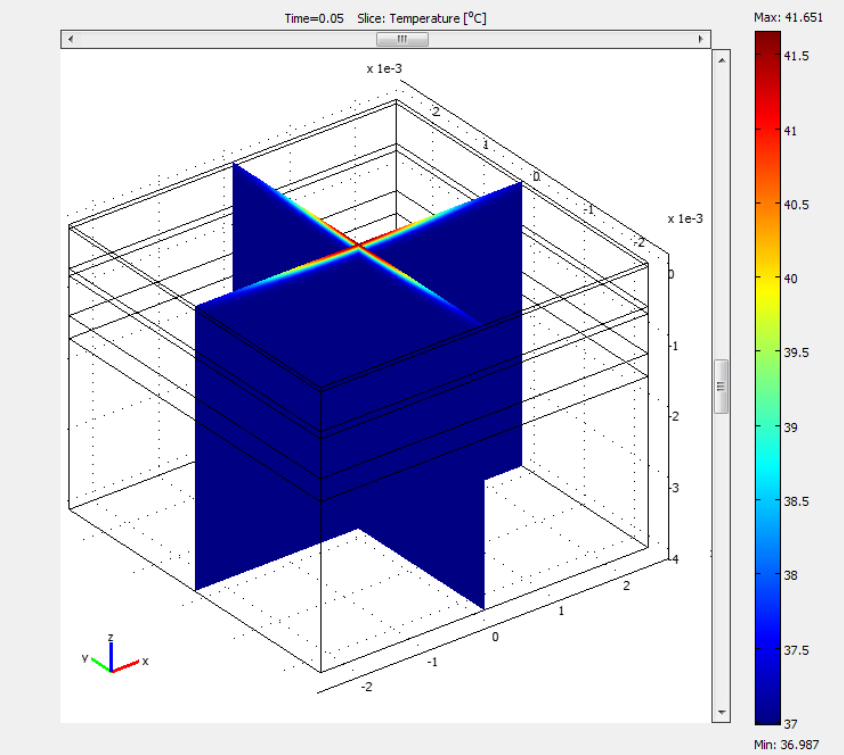

Figure 4.25. Temperature distribution and penetration depth for P=200mW, 50ms duration.

Table 4.6. Maximum Temperature values for varying laser power at exposure duration t=0.05s.

@ Duration of Exposure t = *0.05 s*				
Laser Power (P) (mW)	50	100	150	200
Max. Temperature (T) (°C)	38.141	39.304	40.483	41.651

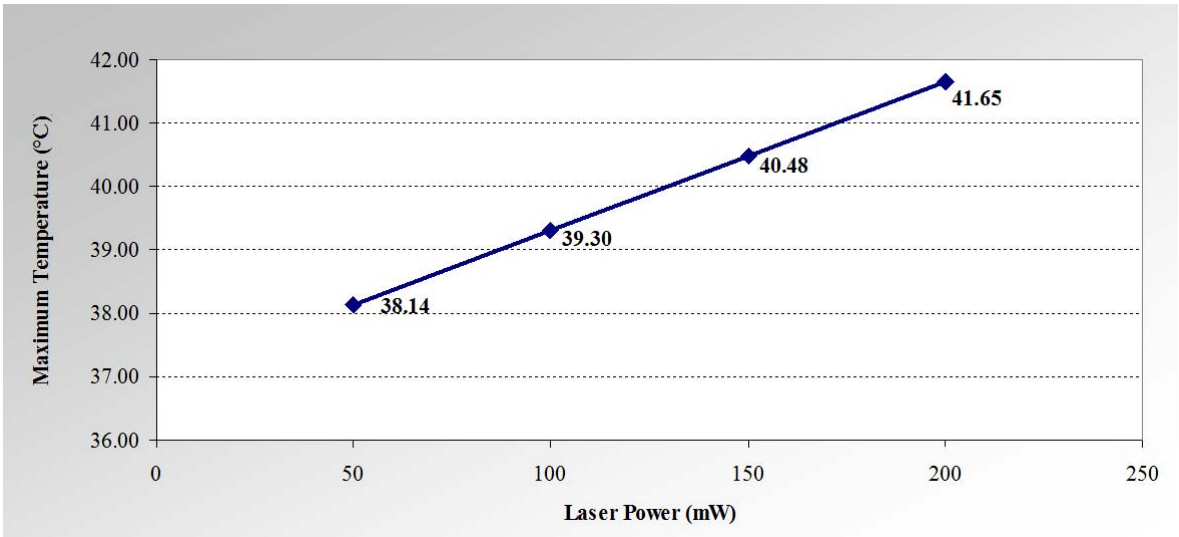

Figure 4.26. Effect of variation of laser power on maximum temperature @ exposure duration t=0.05s.

Table 4.7. Maximum Temperature values for varying exposure durations at laser power P=50mW.

@ Laser Power P = 50 *mW*				
Duration of Exposure (t) (s)	0.05	1	5	120
Max. Temperature (T) (°C)	38.141	43.463	49.638	61.892

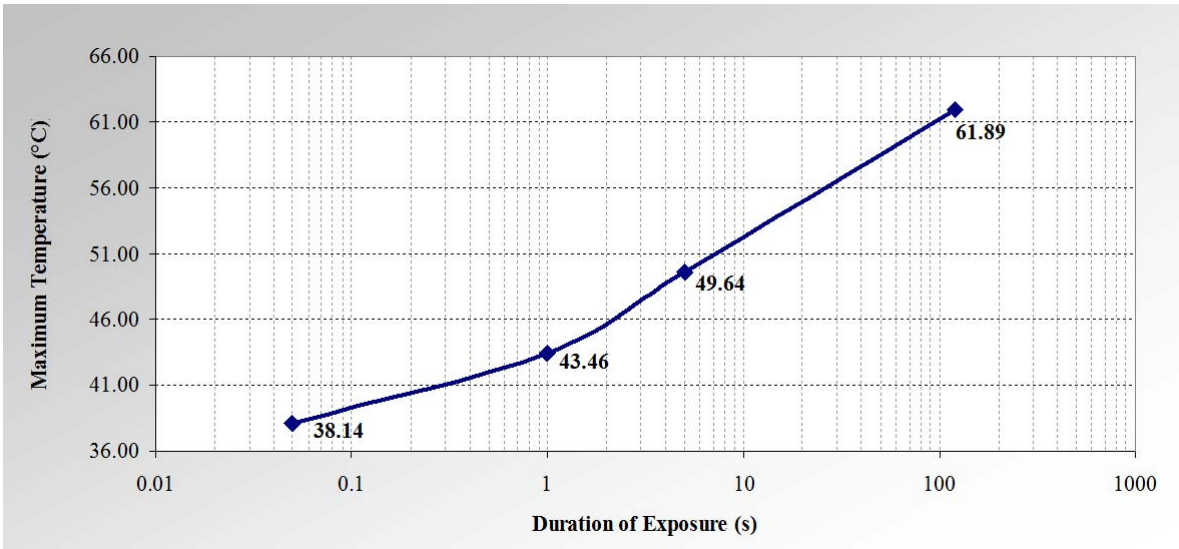

Figure 4.27. Effect of variation of exposure duration on maximum temperature @ laser power P=50mW.

With the help of this study, some important contributions to the literature have been made on the topic of temperature predictions for biological bodies under exposure to light sources. As an initial step, usage of FEM has extended the results of FDTD approach achieving better accuracy for complex geometries with less memory and disk space in shorter solution times. Moreover, simulation results for the single layer model of human skin have provided general and broad understanding of heat flux flow for different types of laser lights at various wavelengths. Not limited to this single layer model, by proposing the multi-layer model of human skin, the reliability of the approach has been enhanced and it provided better understanding for the response of skin to interaction with light sources. Effects of exposure duration, laser power and the wavelength of laser beam are investigated so that appropriate choice of parameters should be selected for medical laser treatment.

5. SIMULATION AND EXPERIMENTAL STUDIES FOR LIGHT SOURCES

5.1. Validation of Light-Tissue Interaction Model and Extended in-Vitro Experiments

The ultimate goal of this study, which is to inspect the photo-thermal effects due to interaction with commonly used light sources with biological tissue, is planned to be reached via first simulating the interaction with a human skin model, then using the findings to verify the model and compare them with the experimental results obtained with a tissue subject to various kinds of light sources. This project, rare in an abundance of many focused on effects of especially laser sources on tissues, can in such a way broaden the horizons in scientific studies that people should be provided insights and made aware of the exposure and its probable hazardous side effects in daily life.

Among the widespread choices, IR lamps with different colors, UV, halogen, incandescent, and LED lamps, as well as CFLs are selected for simulatory and experimental purposes. Usage areas of the lamps, together with their specifications in terms of power and efficiency have dominated the choices for selection.

5.1.1. Simulation Results for Model Verification

Having completed the modeling steps with solving mainly the Bioheat equation in the Finite Element Solver software by creating geometries, putting up the parameters and defining the boundary and sub domain settings, simulations are run with the two selected light sources: Red and Clear IR lights whose relative spectral distributions are well-known from manufacturer data, to visualize the thermal effects with respect to increasing exposure durations. Numerical study outputs are provided in the Figures 5.1 through 5.8.

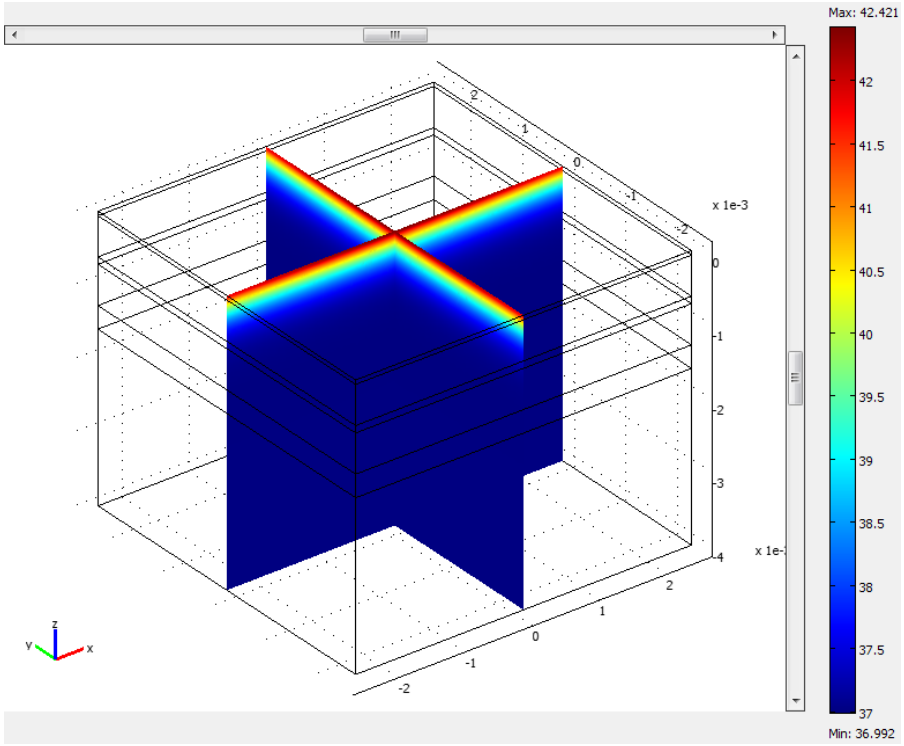

Figure 5.1. Temperature distribution in skin tissue after 1 minute of exposure to IR light with red filter.

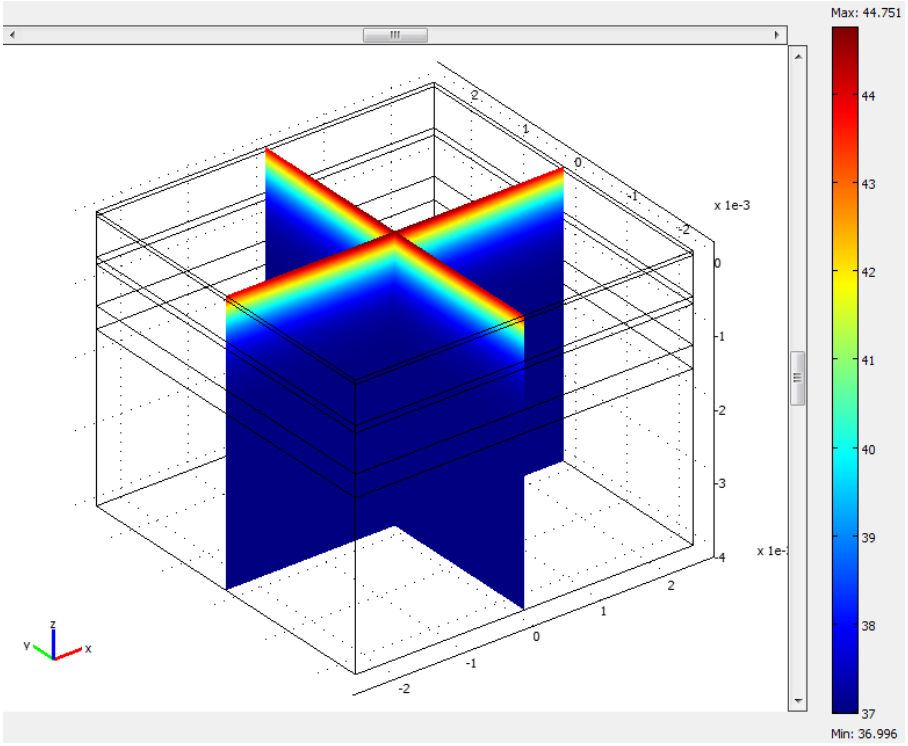

Figure 5.2. Temperature distribution in skin tissue after 2 minutes of exposure to IR light with red filter.

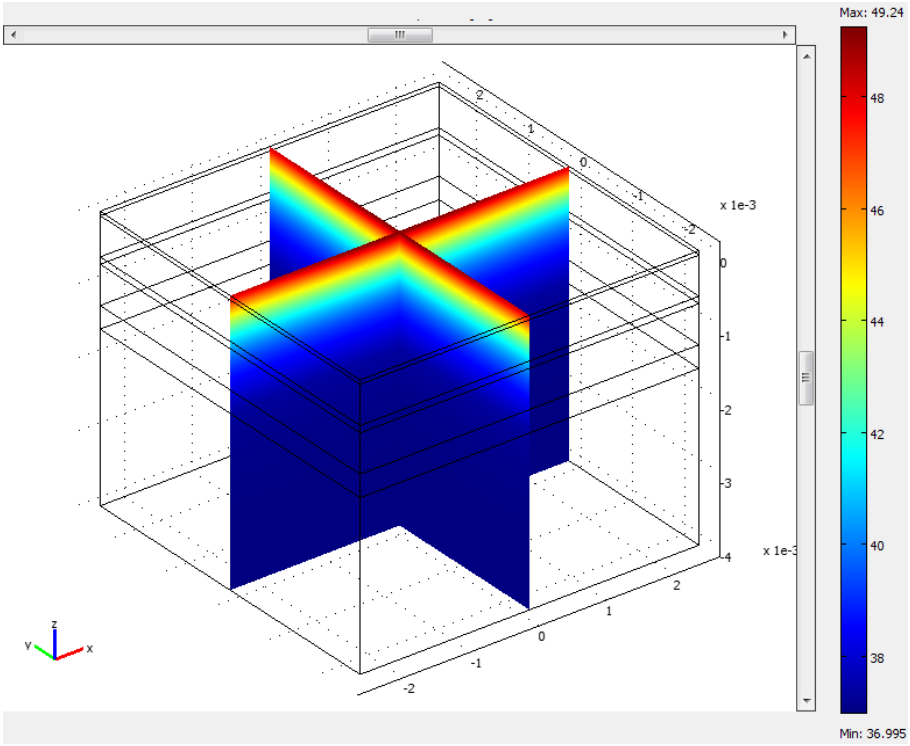

Figure 5.3. Temperature distribution in skin tissue after 5 minutes of exposure to IR light with red filter.

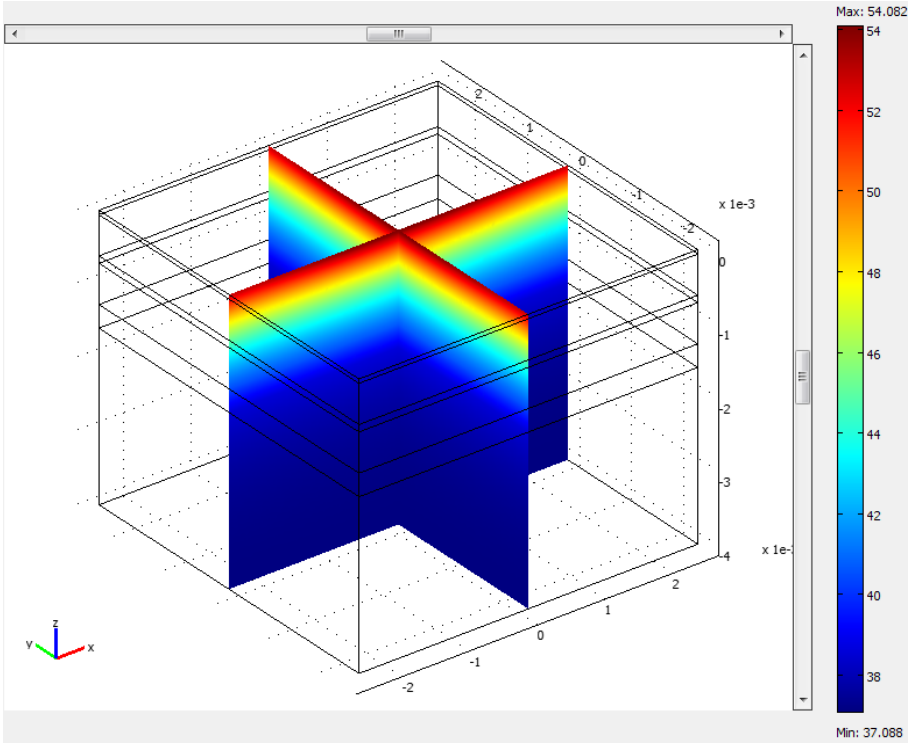

Figure 5.4. Temperature distribution in skin tissue after 10 minutes of exposure to IR light with red filter.

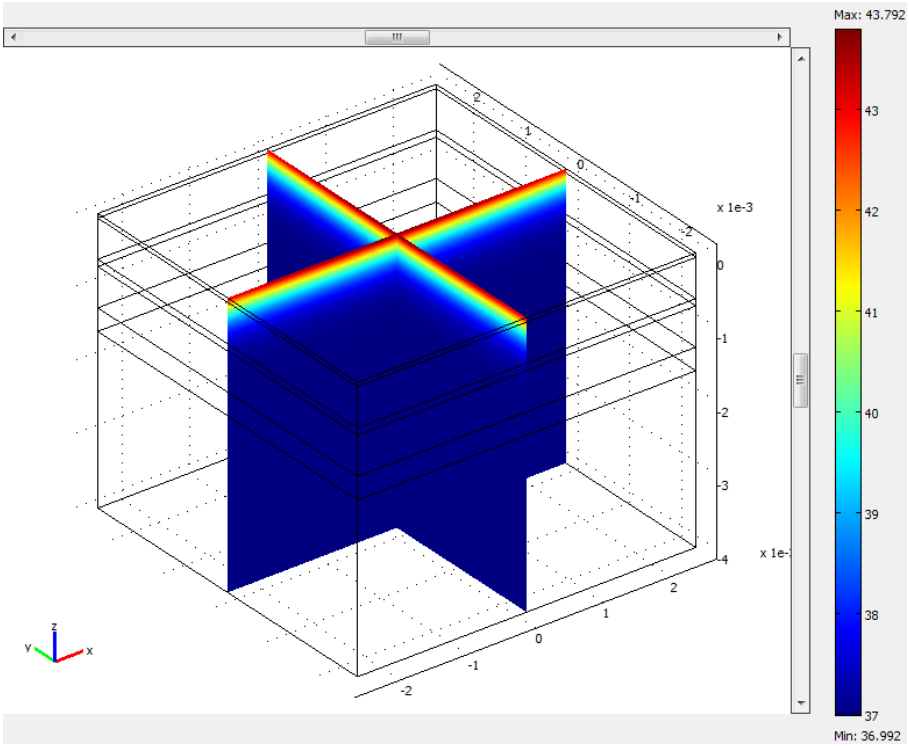

Figure 5.5. Temperature distribution in skin tissue after 1 minute of exposure to clear-type IR light.

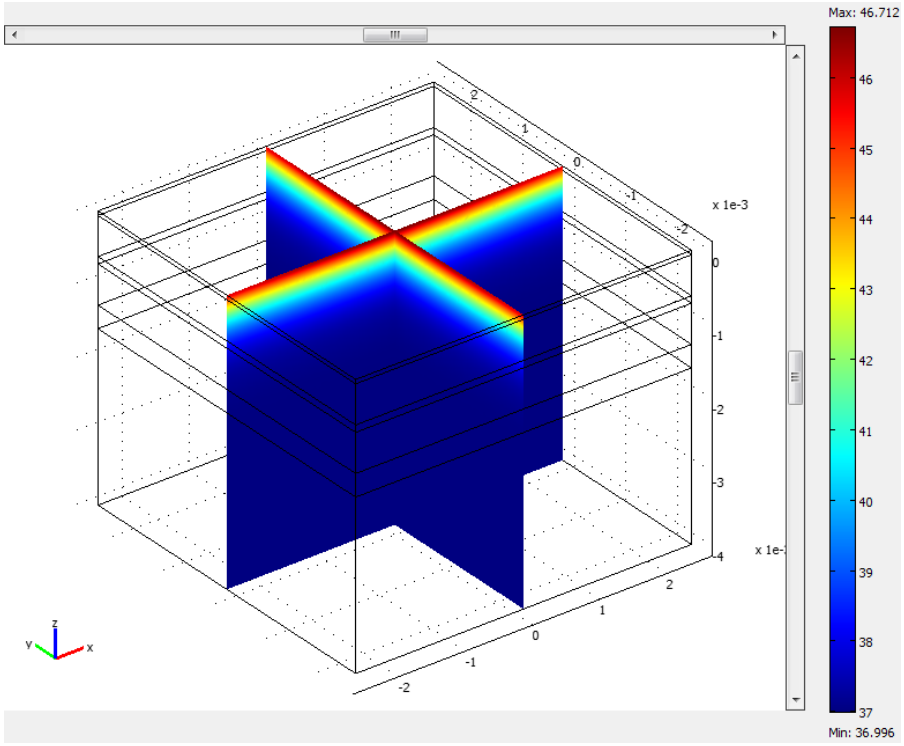

Figure 5.6. Temperature distribution in skin tissue after 2 minutes of exposure to clear-type IR light.

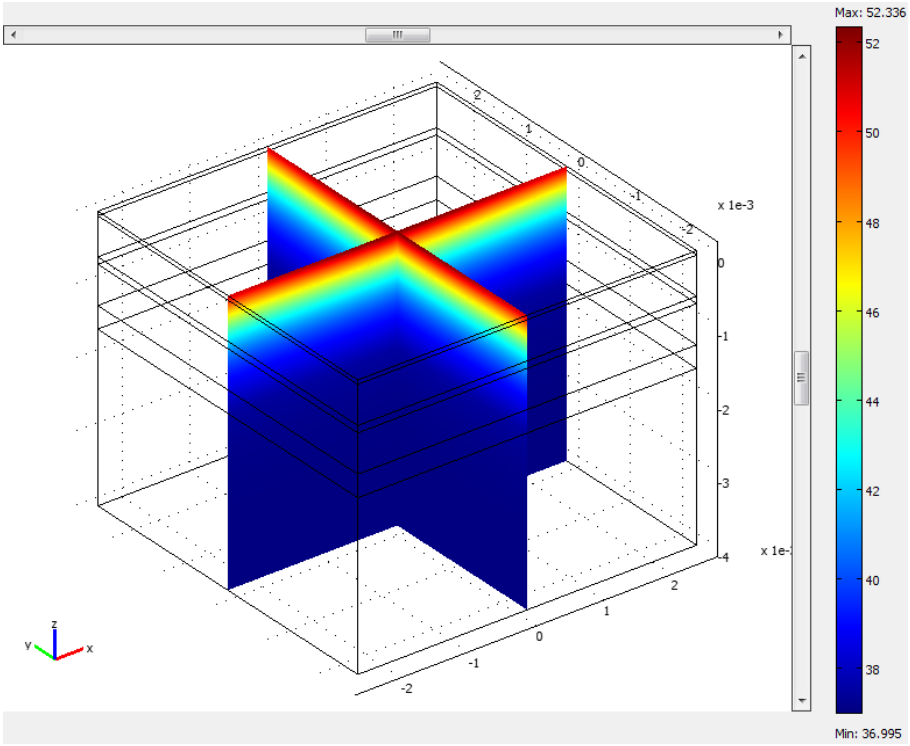

Figure 5.7. Temperature distribution in skin tissue after 5 minutes of exposure to clear-type IR light.

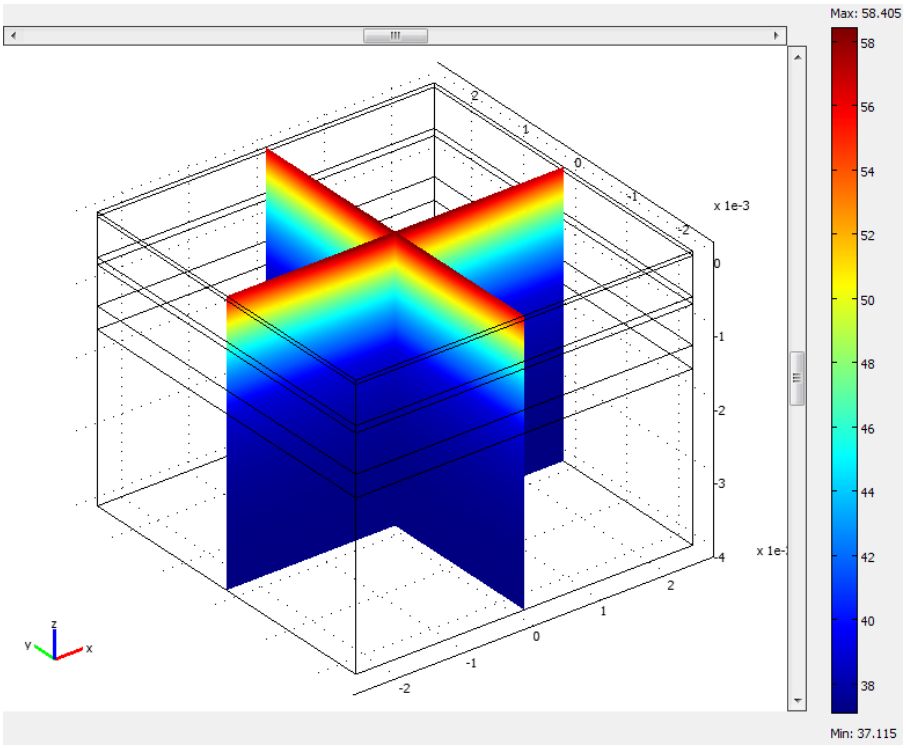

Figure 5.8. Temperature distribution in skin tissue after 10 minutes of exposure to clear-type IR light.

Figure 5.9 and Table 5.1 summarize simulation results of model for two different IR light sources (red and clear) with respect to exposure time.

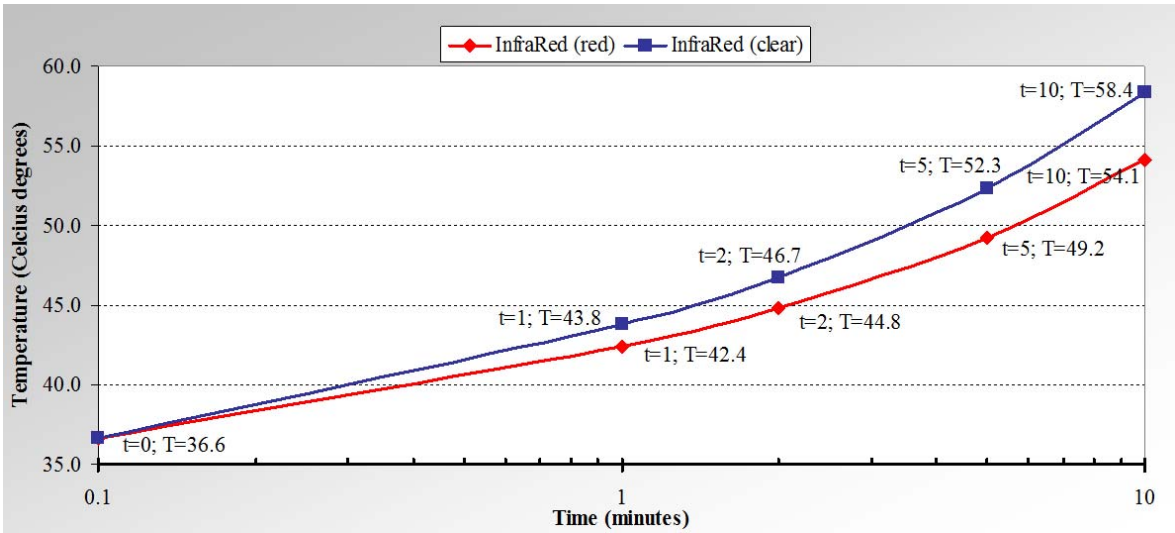

Figure 5.9. Graphical comparison of the simulation results obtained with two light sources at different times.

Table 5.1. Summary of the maximum temperatures obtained via simulations under IR exposure with variable durations.

Temperature Variation (℃) versus Time (min) due to IR exposure to Skin					
Light Source	**t = 0 min**	**t = 1 min**	**t = 2 min**	**t = 5 min**	**t = 10 min**
IR (red)	36.6 °C	42.4 °C	44.8 °C	49.2 °C	54.1 °C
IR (clear)	36.6 °C	43.8 °C	46.7 °C	52.3 °C	58.4 °C

These post processed results clearly show that temperature distribution inside the tissue is generally non-monotonic function of depth, due to varying optothermal parameters of tissue layers, like absorption coefficient, heat conductivity and so on. Temperature increase in tissue is also no-doubt dependent on exposure time and source power. As the exposure duration increases, maximum temperature induced on tissue increases. When it comes to the effects of two different IR light sources, with same spot size but different spectral distributions, namely one clear and other with a red filter, it can be noticed that two light sources have different thermal effects on tissue even though the

lamp rated output powers are the same for each. It is also apparent that as exposure duration gets longer, difference in maximum temperature induced in tissue models increases and gets more significant for the two different types of light sources. Detailed investigation of lamp characteristics from product data sheets reveals that two light sources have different radiant densities. Hence, the obtained results are in line with the expected results in such a way that red filtered lamp should and actually do cause less temperature increase in tissue. Radiant density per watt of lamp output across wavelengths is given in Figure 5.10 [61].

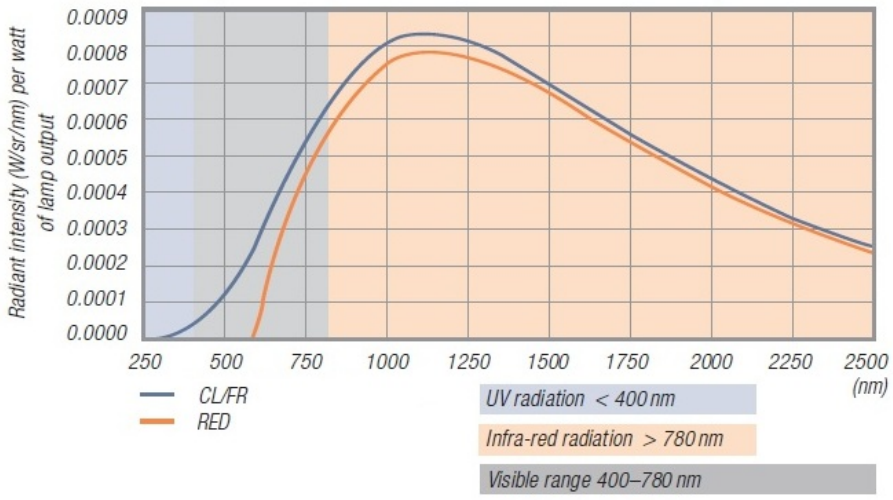

Figure 5.10. Relative Spectral Distribution of IR Lamps.

5.1.2. In-Vitro Experiments

Having obtained simulation results for two IR lights and verified the simulation model and its results by comparing it with theoretical information and expected results, it is now necessary to extend the scope of the paper via experimental study.

Analyzing possible range of the induced thermal effects on biological tissues due to exposure with different light sources requires an extensive effort with numerical methods, since parameters of both tissue and the light sources chosen show quite variations. In this respect, experimental analysis offers more realistic data with comparative advantages to numerical study.

5.1.2.1. Experimental Setup. The experimental setup, graphically shown in Figure 5.11, consists of a light source directed to in vitro biological tissue (namely chicken meat covered with skin), and the thermal interaction between them is monitored via an IR thermal camera with 50mK sensitivity. In order to simulate a living tissue with blood perfusion in effect, in vitro tissue samples are kept in a water bath at 37°C. Distance between tissue and light source, d_1, is set to 30cm and thermal camera is held at a distance d_2 of 50cm for the best visual results, because of the limitation from the focus distance of camera which is 40cm.

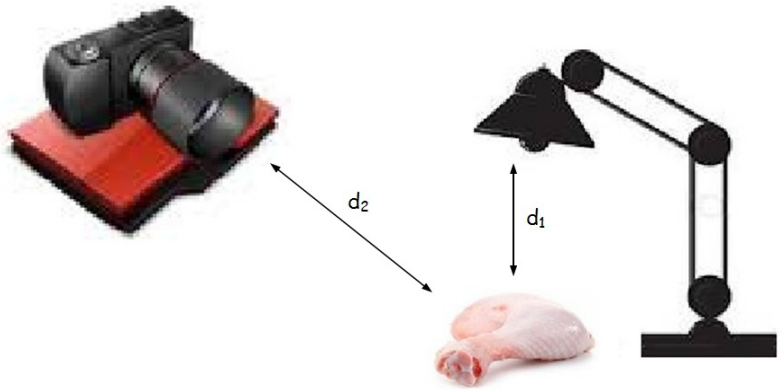

Figure 5.11. Graphical representation of the experimental setup.

First experiments are done with the IR lamps, whose thermal effects are simulated beforehand with Finite Element Solver program. Then distance d_1 is increased to 50cm, where experimental data is obtained for verification of distance variation effect. Next, other lamps, namely UV, Incandescent, LED, CFL and Halogen, are chosen to illustrate the results for various thermally induced tissues. Figure 5.12 illustrates all the light sources used in the experiment.

Figure 5.12. Different daily usage lamps used as the thermal inducing light source. (a) IR with red filter, (b) IR clear, (c) UV, (d) Incandescent, (e) LED, (f) CFL, (g) 100W Halogen, and (h) 205W Halogen lamp.

5.1.2.2. Experimental Results. Experimental data obtained from thermal camera is summarized in the following figures, Figures 5.13 through 5.22.

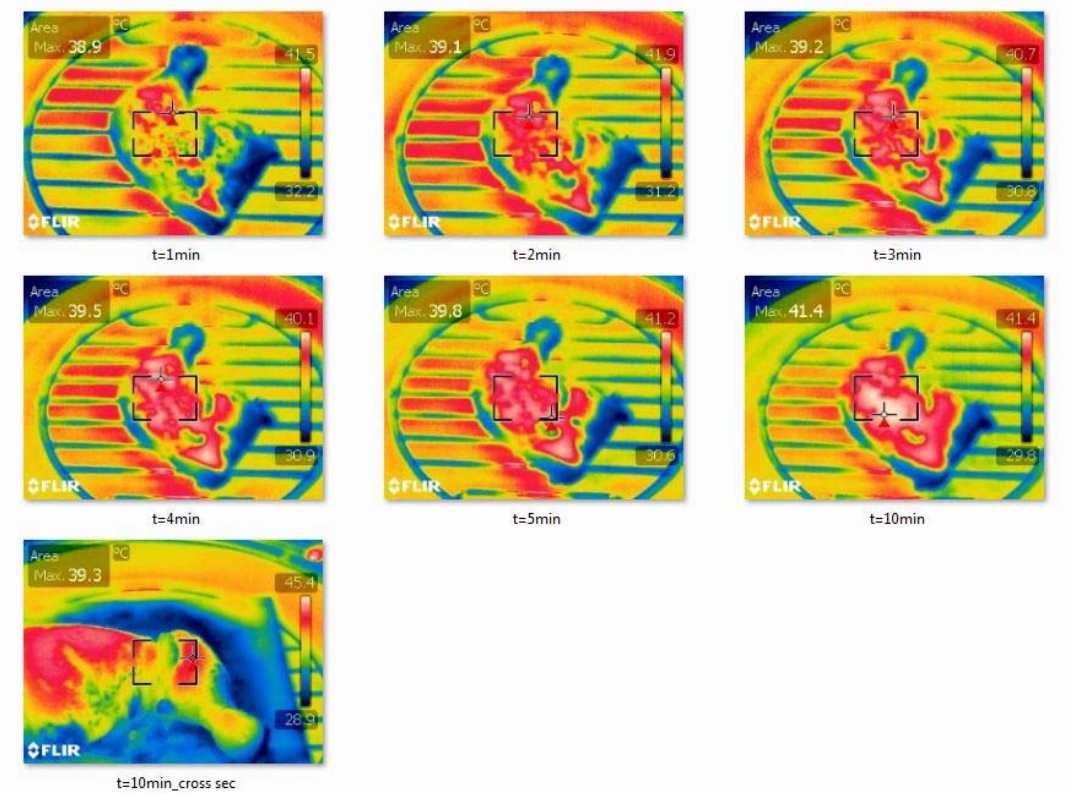

Figure 5.13. Thermal view of tissue exposed to 250W IR lamp with red filter where distance is increased from 30cm to 50cm.

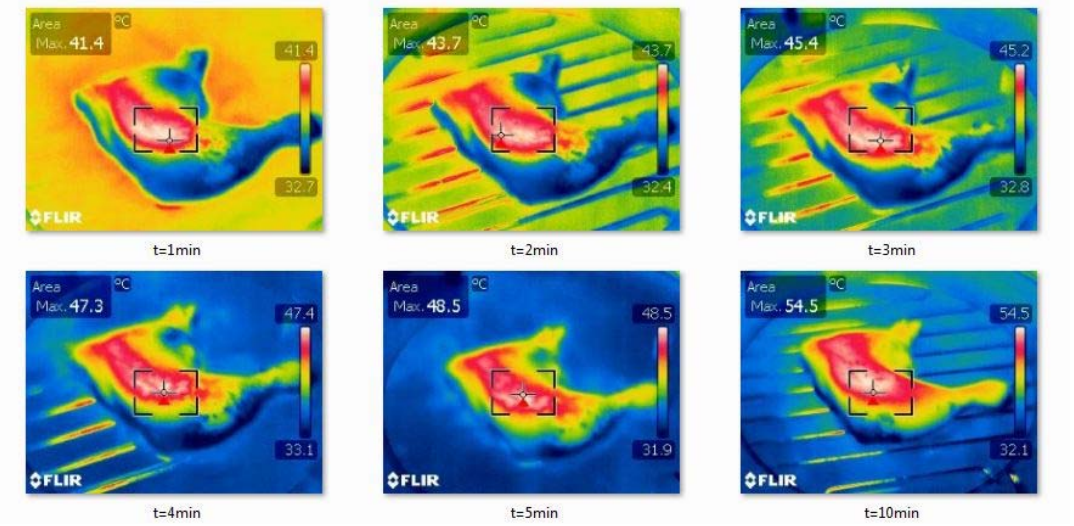

Figure 5.14. Thermal view of tissue exposed to 250W IR lamp with red filter.

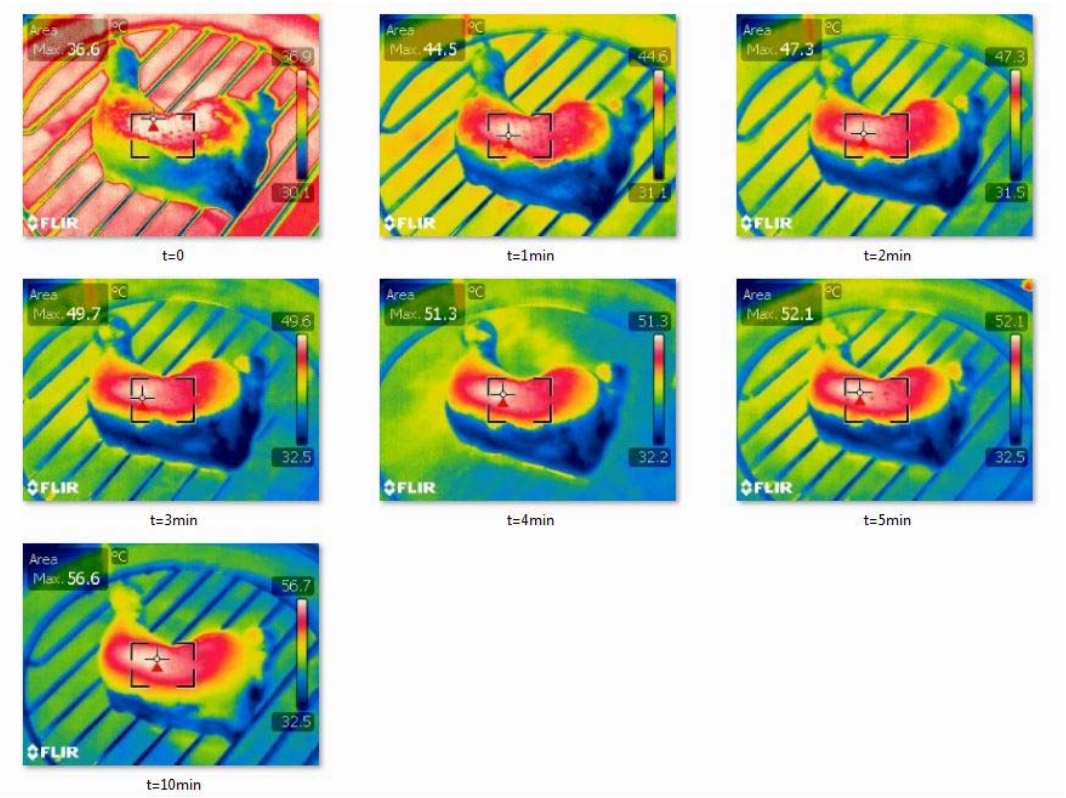

Figure 5.15. Thermal view of tissue exposed to 250W IR lamp clear type.

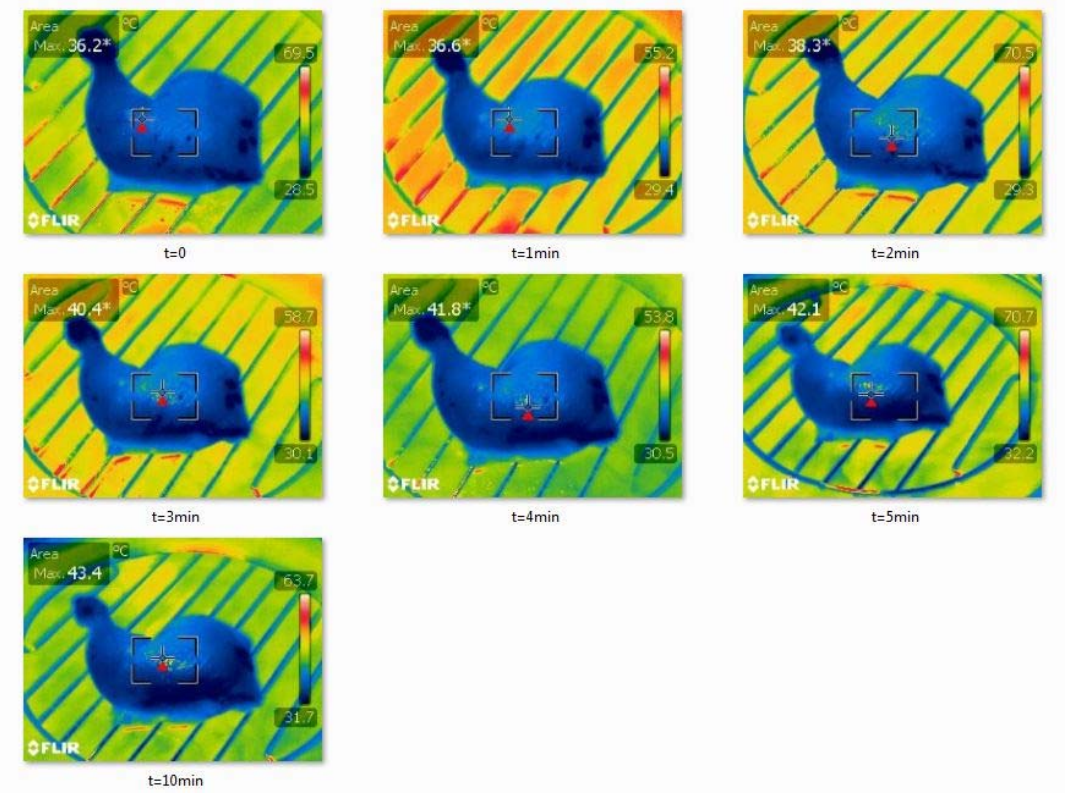

Figure 5.16. Thermal view of tissue exposed to 300W UV lamp.

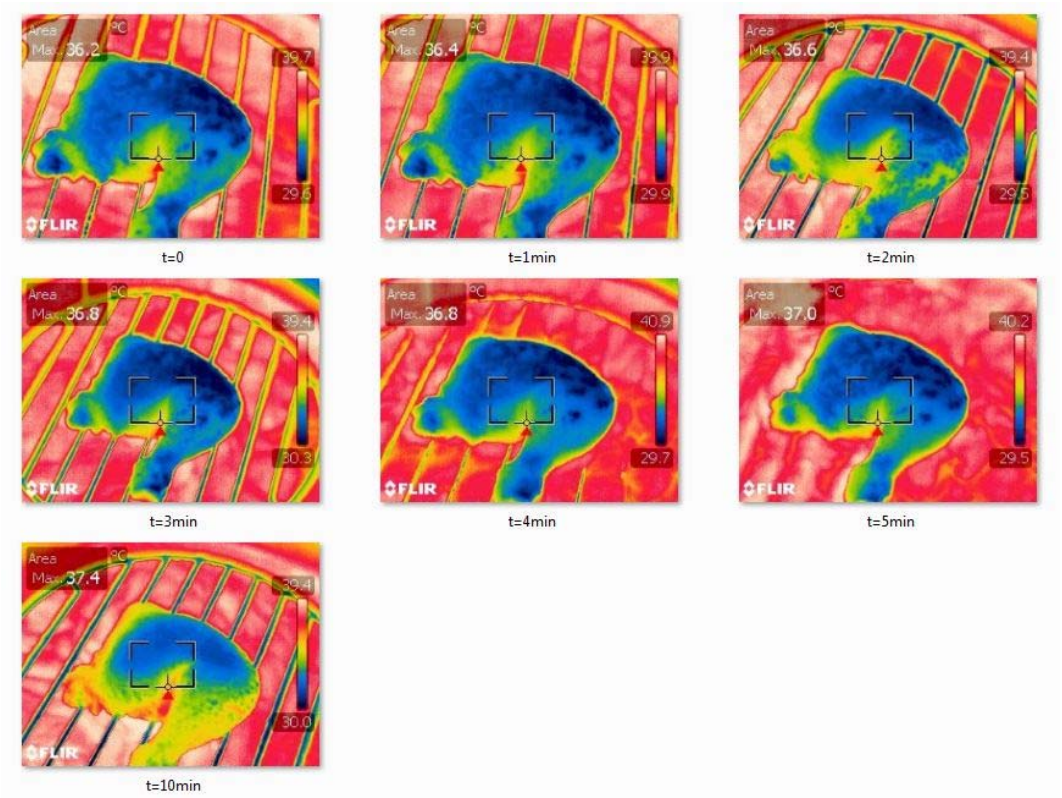

Figure 5.17. Thermal view of tissue exposed to 100W 1340lm Incandescent lamp.

Figure 5.18. Thermal view of tissue exposed to 12W 810lm LED lamp.

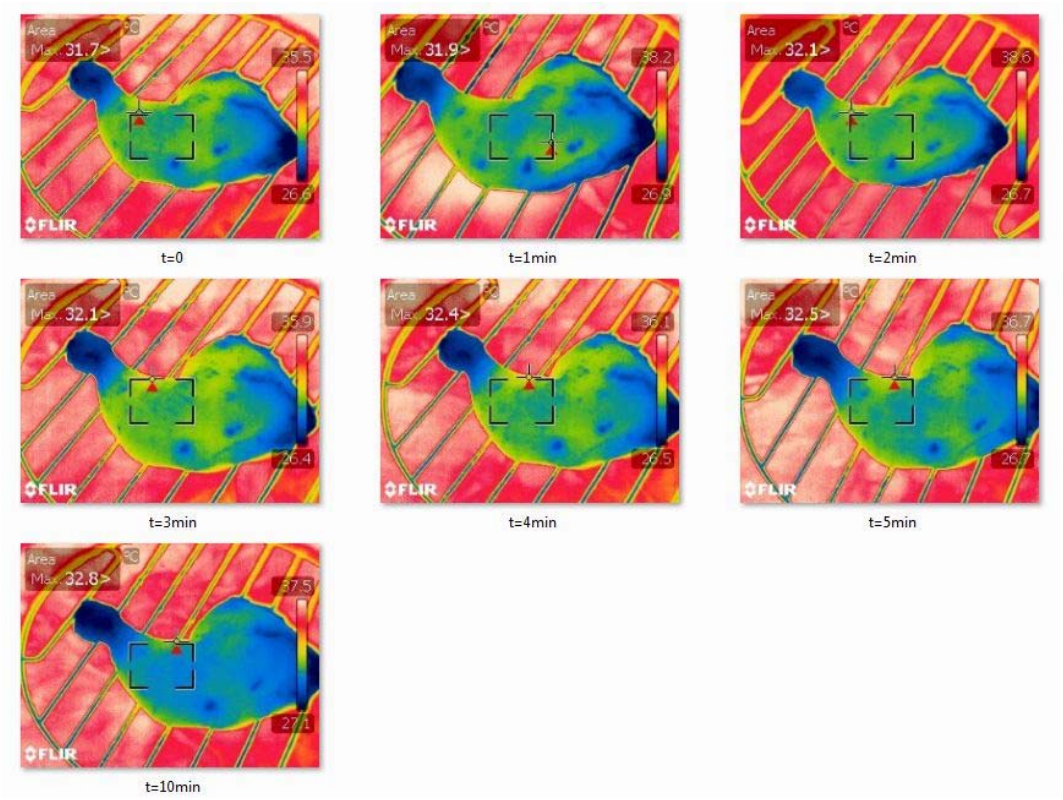

Figure 5.19. Thermal view of tissue exposed to 32W 2100lm CFL.

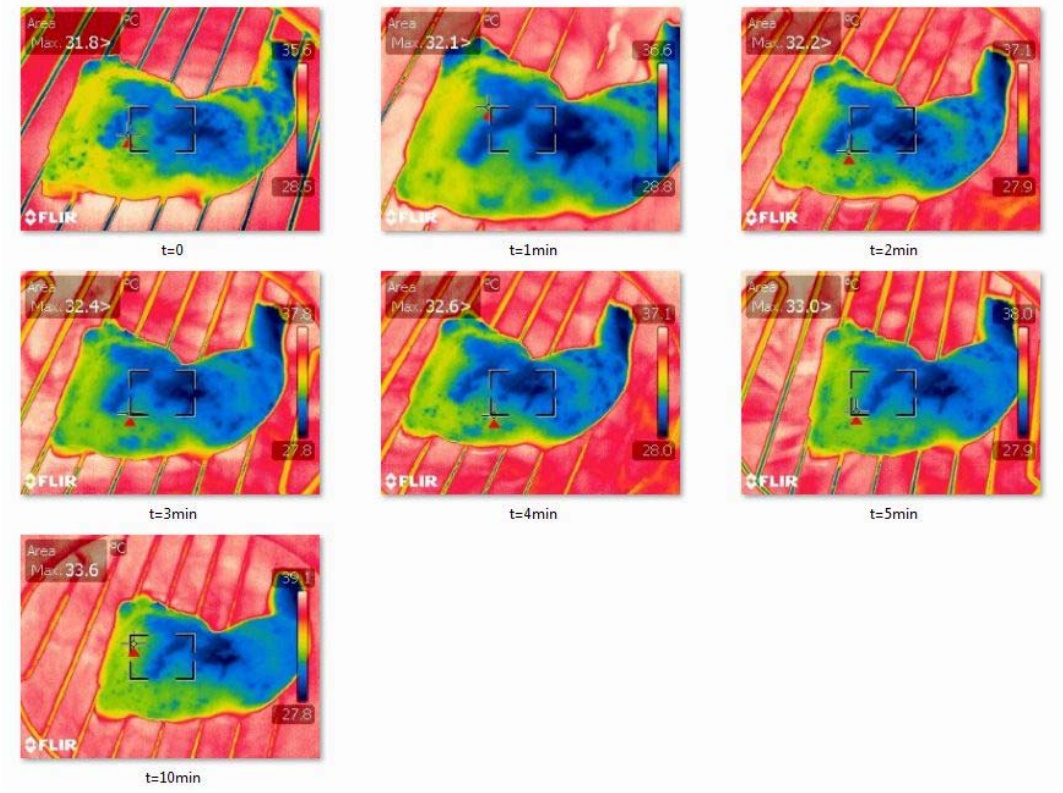

Figure 5.20. Thermal view of tissue exposed to 100W 1800lm Halogen lamp.

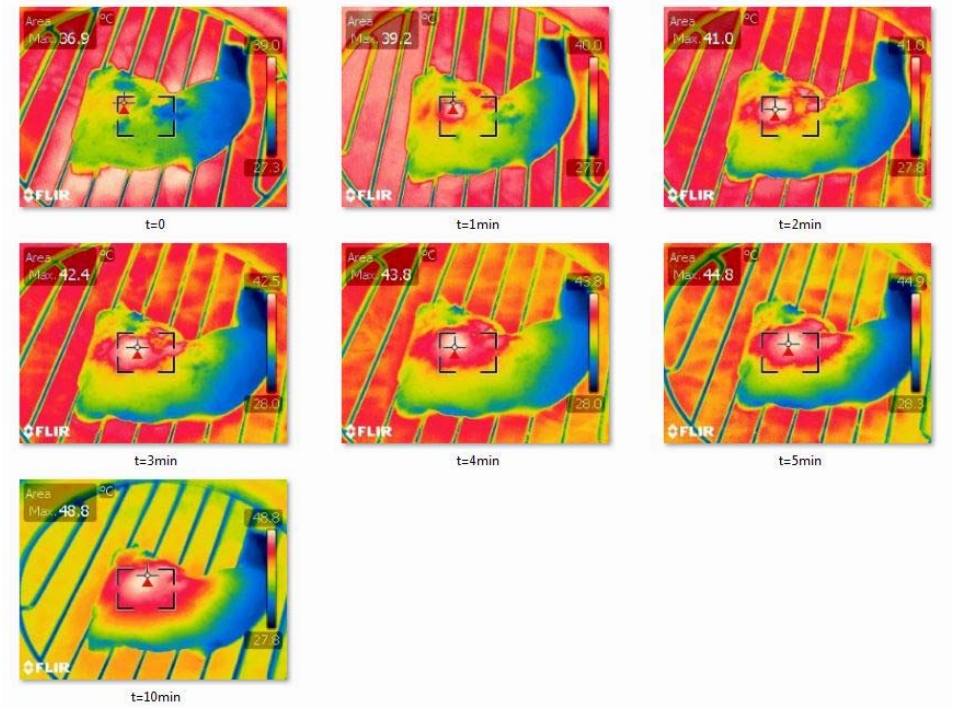

Figure 5.21. Thermal view of tissue exposed to 100W 1800lm Halogen lamp with reflector.

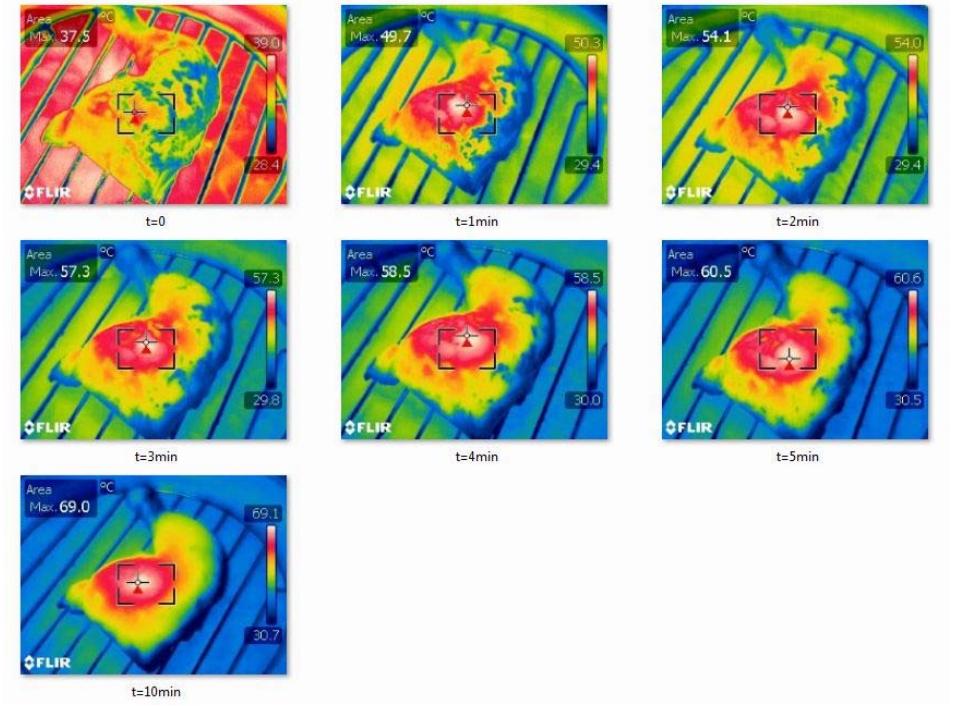

Figure 5.22. Thermal view of tissue exposed to 205W 4200lm Halogen lamp with reflector.

5.1.2.3. Discussion on Experimental Outputs. By means of the preceeding in-vitro experiments, three main objectives have been established. Firstly, simulation outputs are verified by the comparison with experimental results. Then, thermal effects of distance variation and light sources are analyzed.

- *Comparison and verification of Simulation Data with Experiments:* A summary of the maximum temperatures induced on tissue samples for both numerical and experimental solutions are given in Figure 5.23 and Table 5.2. These numerical and experimental studies show comparable results, since the in vitro sample of chicken meat covered with skin tissue has almost similar optothermal properties with our developed simulation model. This comparative study is realized by taking the maximum temperatures induced on tissues, because thermal camera is only able to monitor the surface temperature distribution. In one of the experiments, it has been tried to observe the thermal distribution in cross-sectional view by cutting the tissue, but the operation was hard to manage in a short time, and would not give satisfactory results for the selected tissue sample, please refer to last picture in Figure 5.13.

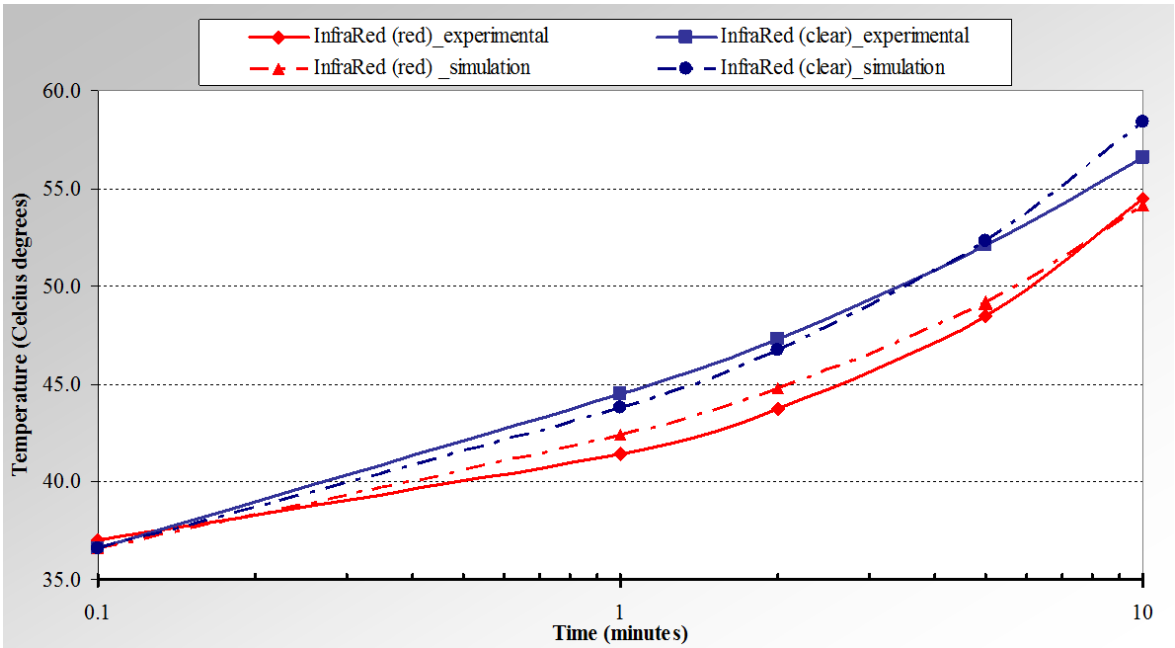

Figure 5.23. Comparison of simulation results with experimental data obtained for IR lamps.

As it can be clearly seen from Figure 5.23 and Table 5.2, obtained results are quite in-line with each other, such that the temperature curves behave in the same way for both experimental and numerically obtained results. From Table 5.2, it can be inferred that there is about 2% difference between the results, which is generally in acceptable limits. Deep analysis of comparative study of the results will reveal possible reasons for this difference in results, for example numerical model contains blood perfusion effect, whereas experimental study is done on in-vitro samples which lack that property. With this comparison between the results, it has also been verified that although specific assumptions and simplifications have been made in modeling step, the simulation results obtained are free of modeling error and compatible with real samples.

Table 5.2. Tabular comparison of experimental and simulation results for IR lamps.

Temperature Variation (℃) versus Time (min) due to IR exposure to Tissue						
	Light Source	**t = 0 min**	**t = 1 min**	**t = 2 min**	**t = 5 min**	**t = 10 min**
Experimental Data	IR (red)	37.0 °C	41.4 °C	43.7 °C	48.5 °C	54.5 °C
	IR (clear)	36.6 °C	44.5 °C	47.3 °C	52.1 °C	56.6 °C
Simulation Results	IR (red)	36.6 °C	42.4 °C	44.8 °C	49.2 °C	54.1 °C
	IR (clear)	36.6 °C	43.8 °C	46.7 °C	52.3 °C	58.4 °C

- *Thermal Effects of Distance Variation:* Having obtained experimental results that are in good agreement with numerical analysis, distance variation will illustrate obvious and easy to expect results on thermal effect of light exposure. For this purpose, distance between tissue and lamp (IR light with red filter) is increased to 50 cm from 30 cm. Figure 5.13 and 5.14 display these comparative results of the two experiments. It should not be so surprising that as exposure distance rises, maximum induced temperature gets low. Hence, it becomes easy to conclude that less photo thermal damage occurs at large exposure distances. In this regard, safety limits can be defined to minimize the hazardous effects of light.
- *Comparison of Thermal Effects of Different Light Sources:* People are exposed to various kinds of light in everyday, so studying the effects of different artificial light sources will demonstrate realistic conclusions for the daily exposure, and these data

can be utilized to draw conclusions on the possible health effects. To reach the goal, several experiments are conducted with different lamps, and thermal behavior of tissue is monitored via thermal camera, as in Figures 5.15 to 5.22. Maximum temperatures induced in tissue samples are summarized in Figure 5.24.

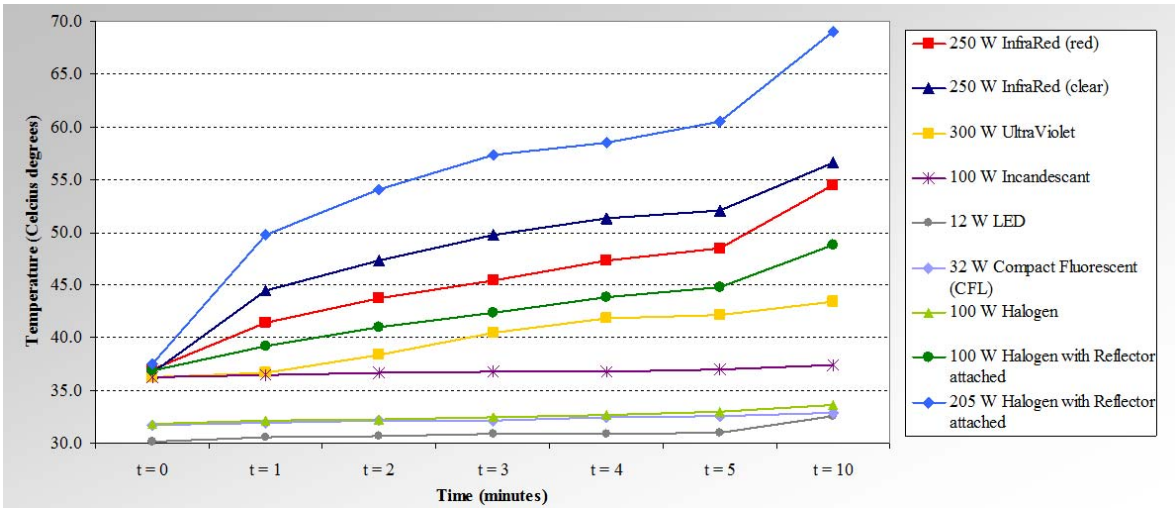

Figure 5.24. Maximum temperatures induced in tissue samples versus time.

From Figure 5.24, experimental results can be used to compare the thermal effects of different light sources. Those with high power outputs, such as IR, Halogen and UV, some of which are designed for usage especially in heating applications, display higher temperature increases during the exposure period. On the other hand, LED and CFLs, today's energy efficient replacements for the most common home-use lamp Incandescent, seem to have little thermal effects on the tissue. Since this minimal effect can be foreseen, some of the experiments are conducted at quite lower tissue initial temperatures of 30°C. Even if the initial tissue temperature is set to a degree which is between air temperature and normal body temperature, these lamps have shown negligible effects on tissue samples in terms of temperature increase. Experiment with the incandescent lamp reveals that there is a minor increase (1°C after 10 minutes of exposure) in skin temperature. The reason can be explained in terms of light efficiency of the lamp compared with other sources at the same output power. Incandescent lamps have relatively low efficiency and as a result of which the surrounding air temperature increases. It has been observed that incandescent light cause the air temperature to increase. When it comes to the question why it has been less effective on increasing the tissue temperature, a reasonable explanation would be the

reflector factor. The experiments conducted with incandescent do not include a reflector surface covering the lamp where light emission is in all directions, not focused on the skin tissue directly.

What is more, from Figure 5.24, it can be inferred that as duration of exposure increased from 1 min, to 5min and 10 minutes, the maximum temperature increase rate gets smaller, that is to say induced maximum temperatures will eventually reach to steady state level as a result of continuous exposure.

Additionally, the aim of choosing two halogen lamps with different power values has been accomplished in such a way that as the output power of the same light source is increased, induced thermal increase on tissue shows a similar trend, where the effect of power can be clearly differentiated.

In the experiments, it has also been observed that some light sources caused temperature increase in the surrounding air, which has also affected the thermal induction in skin tissue. This factor is also expected and taken into account in the study, because in everyday life, occupational exposure media contains surrounding air; hence there is no point in trying to configure an experimental setup which can exclude this effect.

Furthermore, the experiments also provide insight about the effect of reflector surfaces around light bulbs. To illustrate the impact, halogen lamps are chosen to be operated both without reflector -where light emission is in all directions- and with reflector -where directed emission of light to tissue sample is ensured. Figures 5.20 and 5.21 depict the outputs obtained in each case respectively. It can be stated that halogen lamp without a reflector has little thermal increase effect on skin; whereas with the reflector utilized, really high temporal increases can occur on tissue. The results obtained so are in good harmony with the expected behavior since standards about exposure levels also take the light intensity into account.

5.2. Real Time in-Vivo Experimental Study on Human Skin Tissue

The experimental setup, graphically shown in Figure 5.25, consists of a light source directed to live human arm, and the thermal interaction between them is monitored via a thermal camera. Distance between tissue and light source, d_1, is set to 30cm for CFL, LED and Halogen lamps, and thermal camera is held at a distance d_2 of 80cm for the best visual results, because of the limitation from the focus distance of camera which is 40cm.

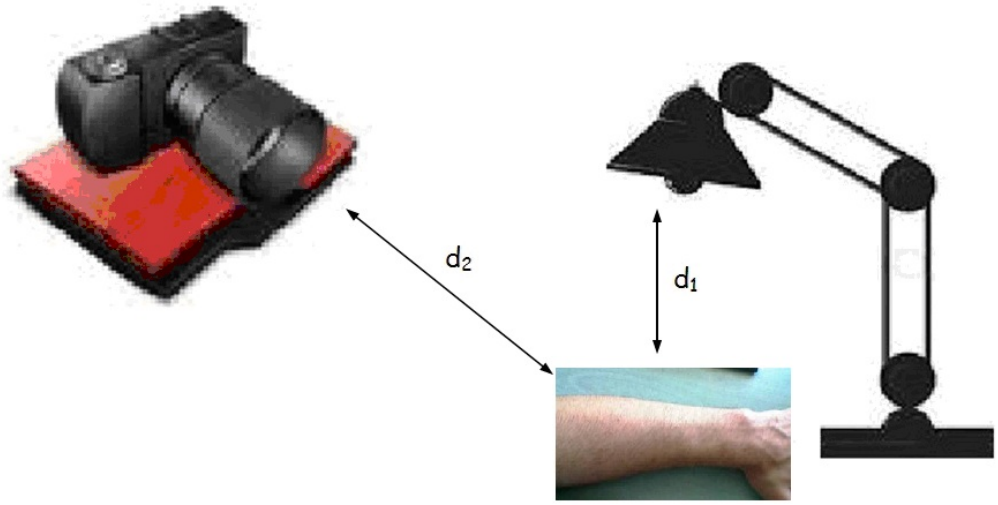

Figure 5.25. Graphical representation of the in-vivo experimental setup.

First experiments, whose results are depicted in Figures 5.26 through 5.29, are done with the CFL, LED and Halogen lamps, which are held at 30cm distance from human arm. These experiments are followed with IR heater studies where the distance of light is increased to 50cm and distance of thermal camera is kept constant. Nevertheless, 50cm distance of IR lamp has a probable harmful effect on skin which causes the subject of the experiment to get burn feeling. Then distance d_1 and d_2 are increased to 100cm and 120cm respectively, since d_1=100cm is officially suggested by the IR heater producer as the minimum safety distance. Next, IR heaters with different power specifications are chosen to illustrate the results for various thermally induced human skin tissues, as shown in Figures 5.31 and 5.31.

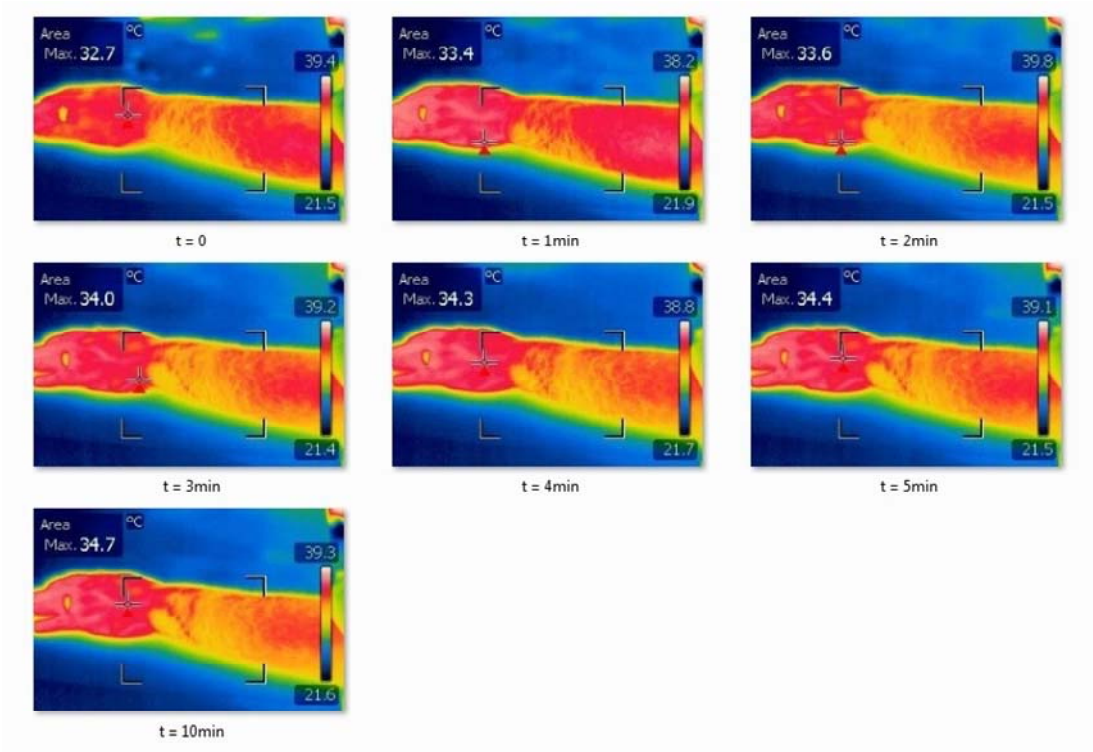

Figure 5.26. Thermal view of human arm exposed to 12W LED lamp at 30cm distance.

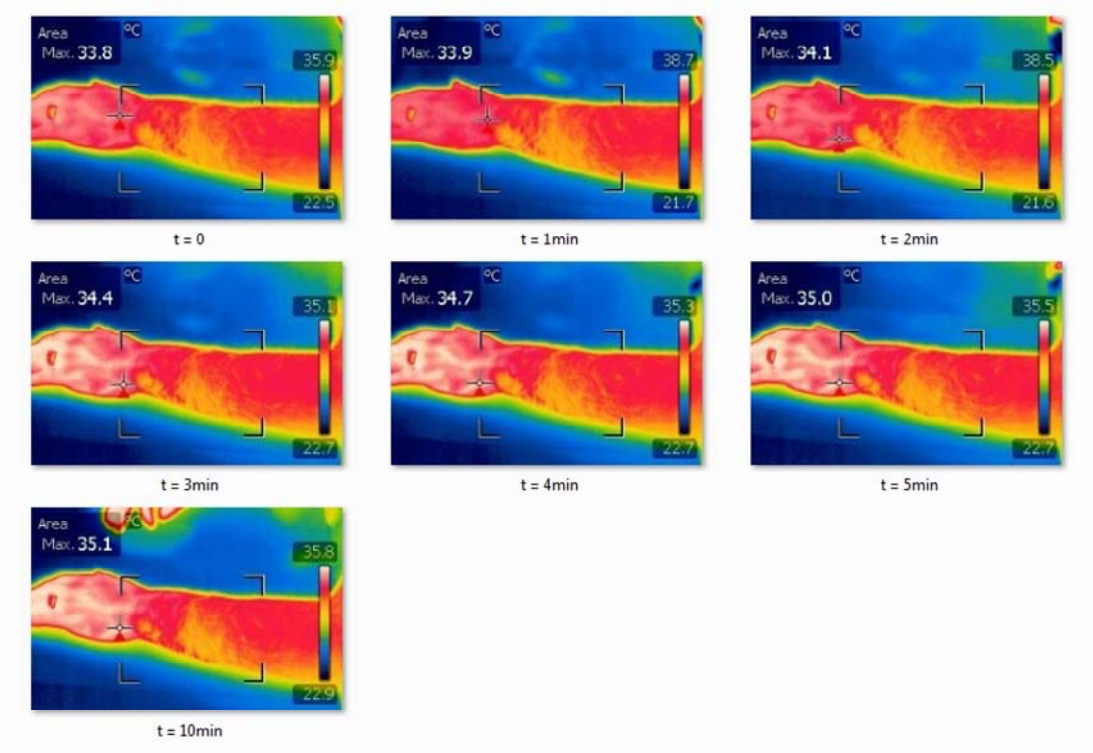

Figure 5.27. Thermal view of human arm exposed to 15W CFL at 30cm distance.

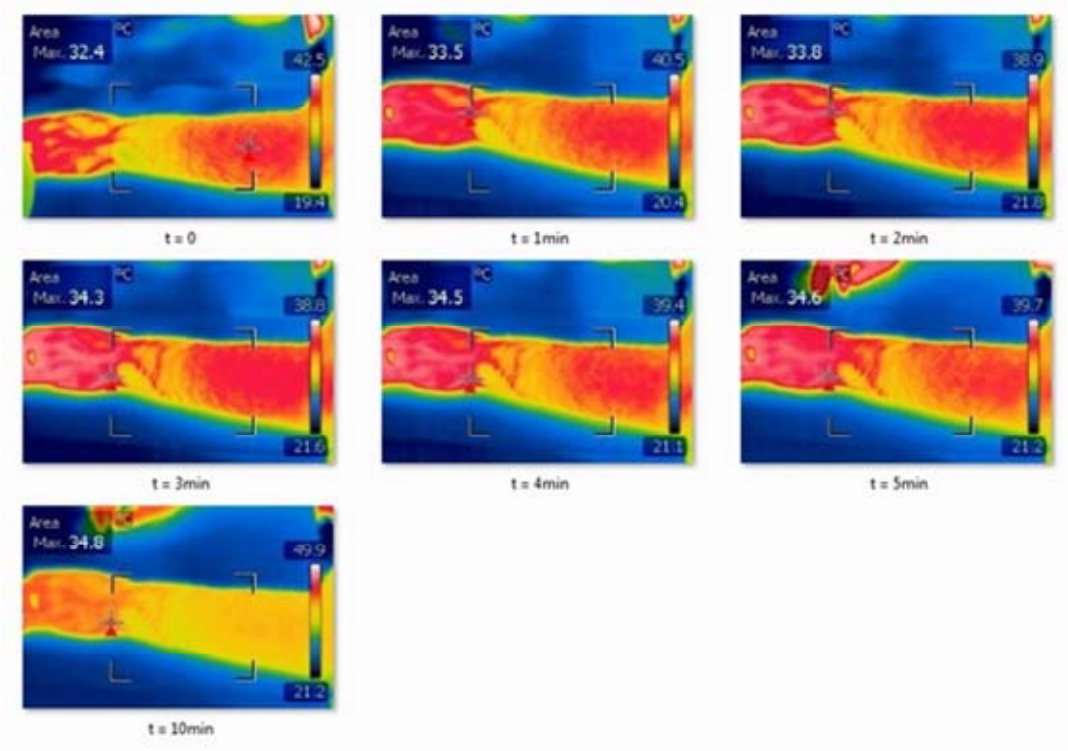

Figure 5.28. Thermal view of human arm exposed to 32W CFL at 30cm distance.

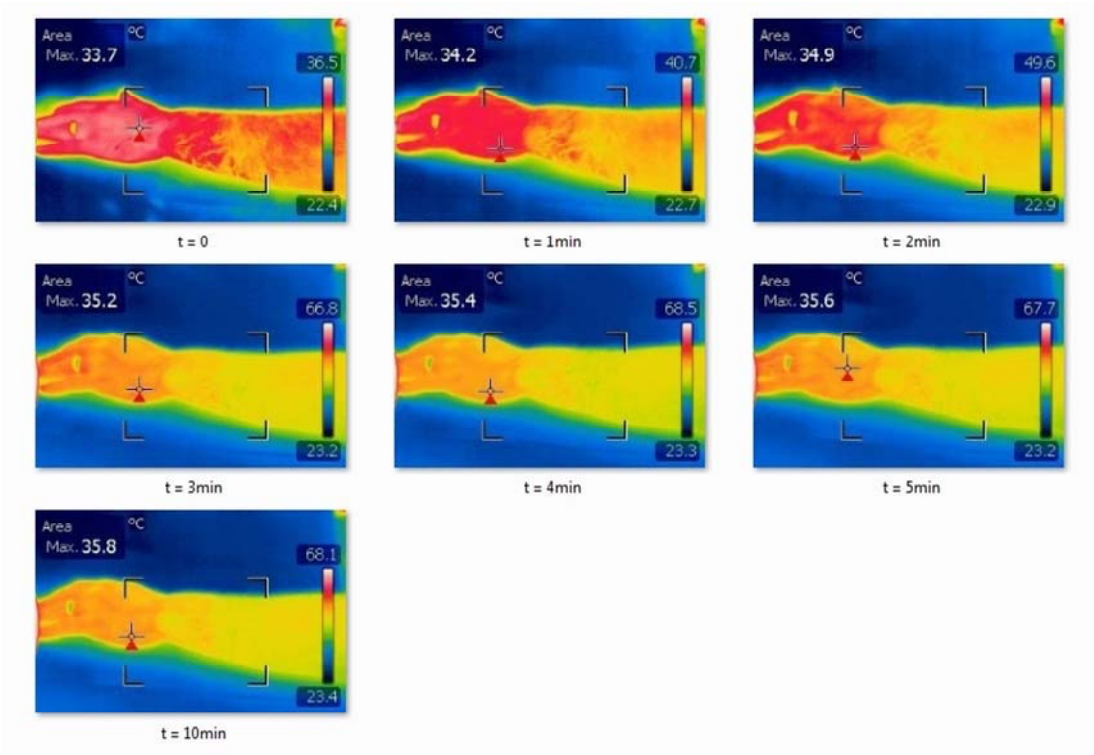

Figure 5.29. Thermal view of human arm exposed to 100W Halogen lamp at 30cm distance.

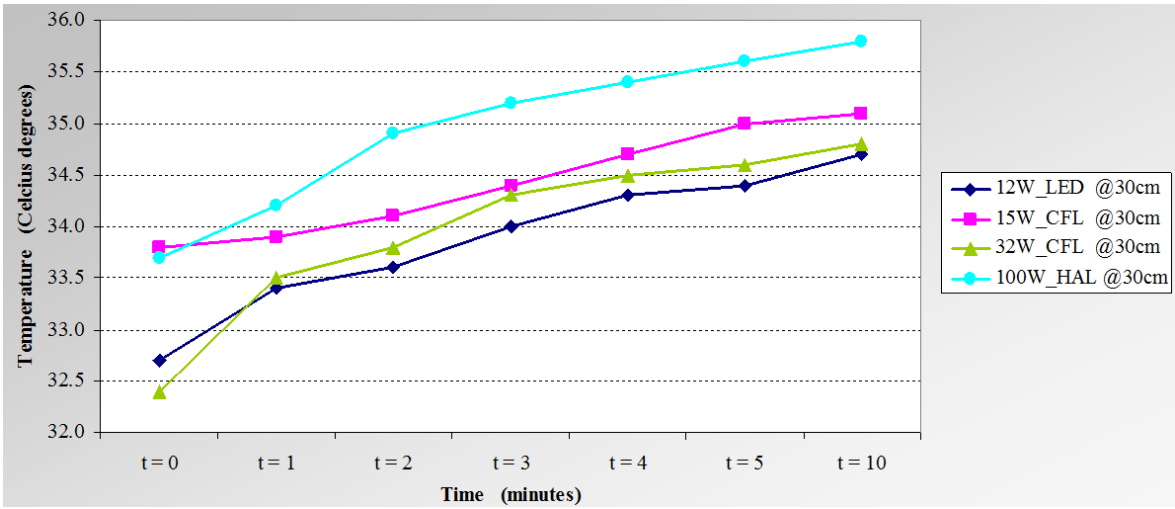

Figure 5.30. Maximum temperatures induced on human skin by various light sources.

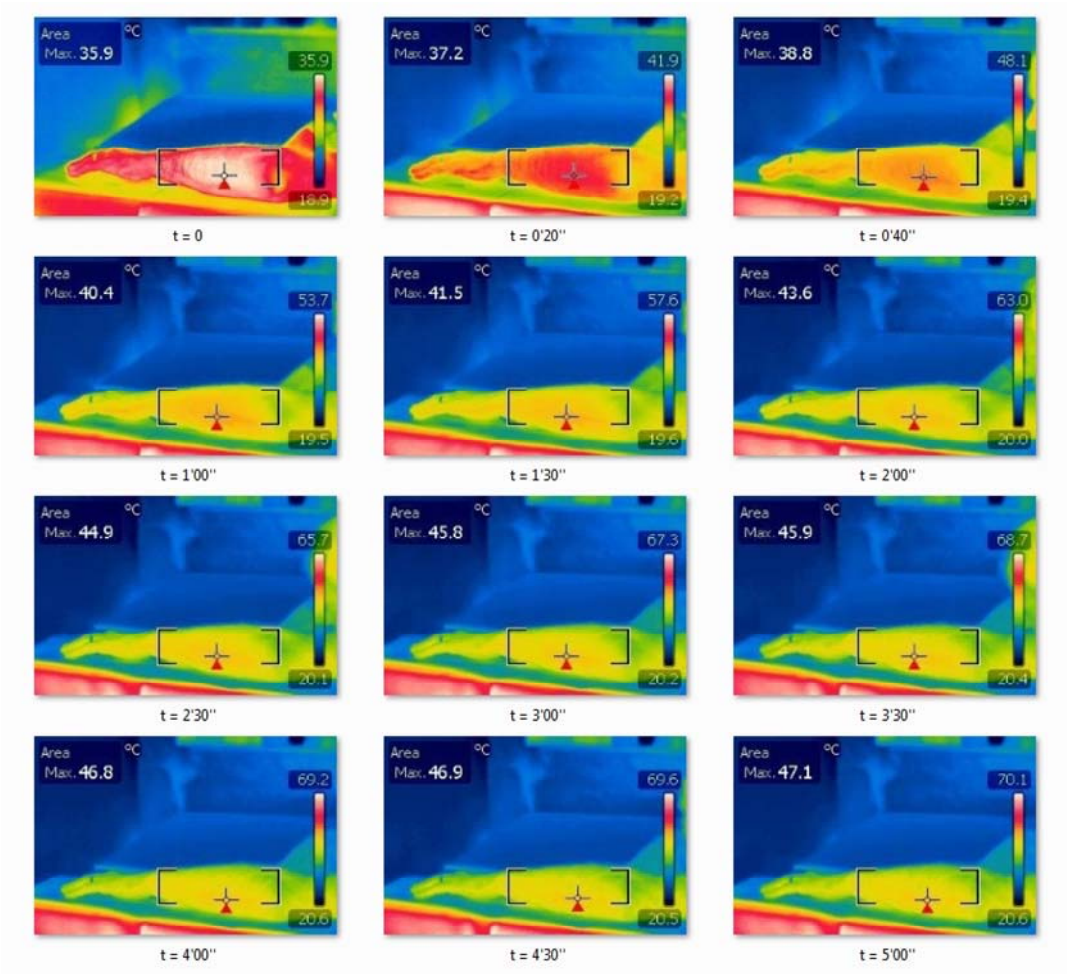

Figure 5.31. Thermal view of human arm exposed to 2500W IR heater at a distance of 100cm.

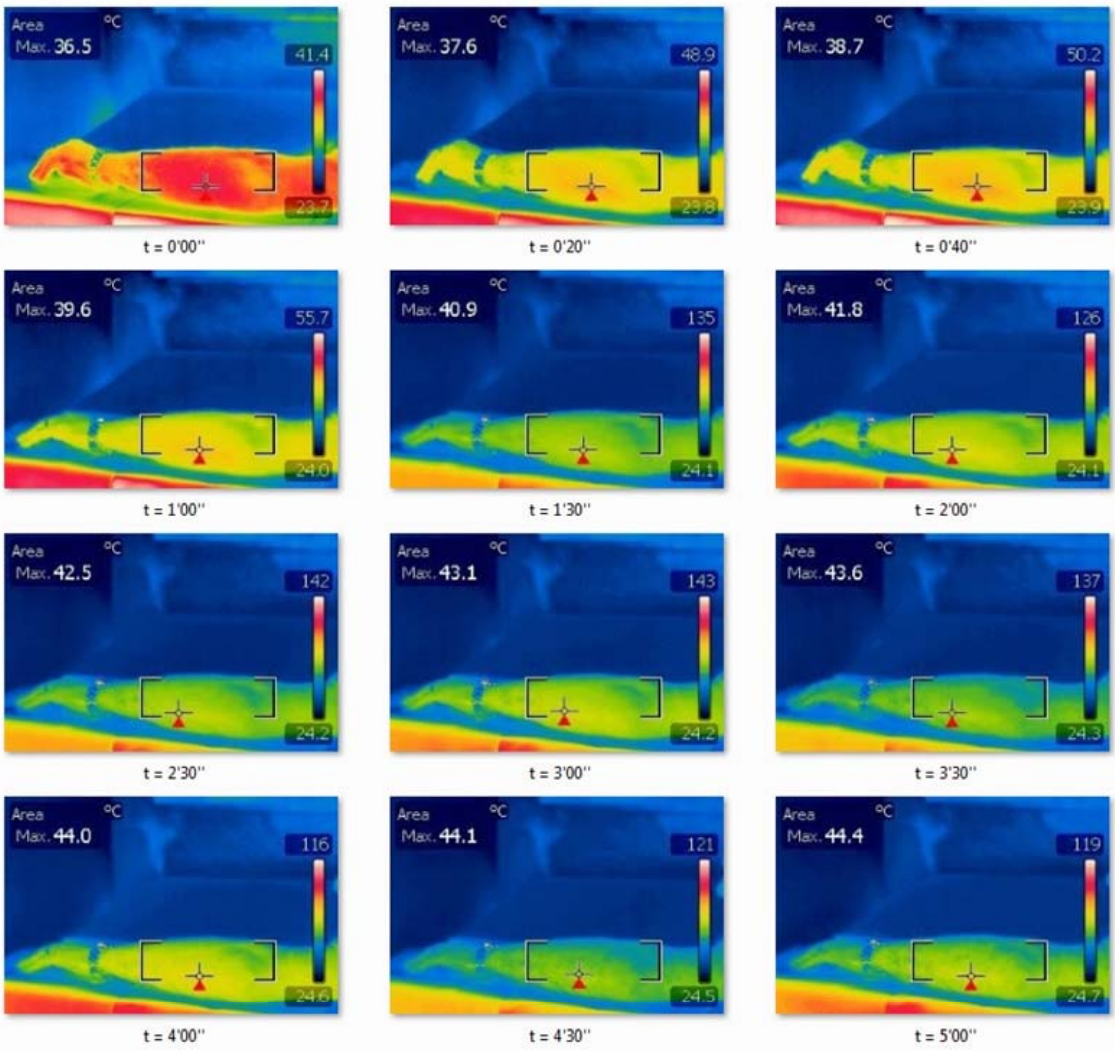

Figure 5.32. Thermal view of human arm exposed to 1750W IR heater at a distance of 100cm.

From Figure 5.30, experimental results can be used to compare the thermal effects of different light sources in ambient temperature of 24°C. Initial skin temperature for the human arm, subject of experiment, is held stable around 33°C and the light sources are positioned at a 30cm distance. Basically, as it can be expected from daily life, even the power specifications of light sources are smaller relatively than heat sources, these light sources also cause temperature increase on skin tissue. The LED lamp whose power is at the minimum level induces a 2°C increase on live skin in a 10 minutes duration.

When it comes to comparing the effects of different Compact Fluorescent Lamps with various power specifications, it is clearly visible that 32W CFL causes higher temperature increase on skin than 15W CFL. On point that needs to be explained is the fact that the reason why 15W CFL ends up with higher skin temperature in 10 minutes than 32W CFL is the higher initial skin temperature for the case of 15W CFL. For the 32W CFL experimental study, initial skin temperature is 1,4°C lower than that of 15W CFL case, and this difference takes about 2 minutes of exposure to be catch up. Looking solely to differential temperatures in both cases, 15W CFL causes 1,3°C whereas 32W CFL causes 2,4°C increase. Hence, the aim of choosing two CFLs with different power values has been accomplished in such a way that as the output power of the same light source is increased, induced thermal increase on tissue shows a similar trend, where the effect of power can be clearly differentiated.

Additionally, 100W Halogen lamp induces about 2,1°C temperature increase on skin tissue whose initial temperature is 33,5°C. Questions may arise here about the difference in experimental results from expectations on the fact that from a constant distance Halogen lamp whose output power is quite high than the CFL should cause relatively higher temperature increase on skin after same duration of exposure. Nevertheless, one should also take the effect of tissue initial temperature into consideration. For this reason, it would be better and more reasonable to compare the effects of Halogen lamp with 15W CFL, since for both experiments initial tissue temperatures can be taken to be the same.

What is more, from Figure 5.30, it can be inferred that as duration of exposure is increased from 1 min, to 5min and 10 minutes, the maximum temperature increase rate gets smaller, that is to say induced maximum temperatures will eventually reach to steady state level as a result of continuous exposure.

In the experiments, it has also been observed that some light sources caused temperature increase in the surrounding air, which has also affected the thermal induction in skin tissue. This factor is also expected and taken into account in the study, because in everyday life occupational exposure media contains surrounding air; hence there is no point in trying to configure an experimental setup which can exclude this effect.

Distance variation will illustrate obvious and expected results on thermal effects of exposure. For this purpose, one experiment is carried out at 50cm distance between tissue and IR heater, whereas others with IR heater are carried out at 100cm distance in accordance with the manufacturer firm's suggestions. The experiment at the 50cm distance cannot be continued for duration more than 1 minute, because the subject of experiment starts to get high skin burns feeling immediately. It is clear from the skin temperature obtained after 1st minute that under such a low exposure distance skin begins to get thermal damage. Consequently, minimum suggested safety distance is the most crucial specification to prevent possible health hazards. Previous experiments are done with different light sources to show the effect of variation under constant exposure distance. Then, the effect of distance is observed with IR heater whose output power is 2500W. Lastly, it is now necessary to examine the effect of power variation of IR heat sources at a constant distance of 100cm, illustrated in Figure 5.33 and Table 5.3. IR heaters cause continuous temperature increase on human tissue whose initial temperature is held around 36°C. It can be inferred from Figure 5.33 that with higher power specifications of an IR heater, induced temperature increase rate is much higher. For instance, after first 3 minutes of exposure, 2500W IR heater causes around 10°C increase while 1750W IR heat source causes only about 6.5°C increase.

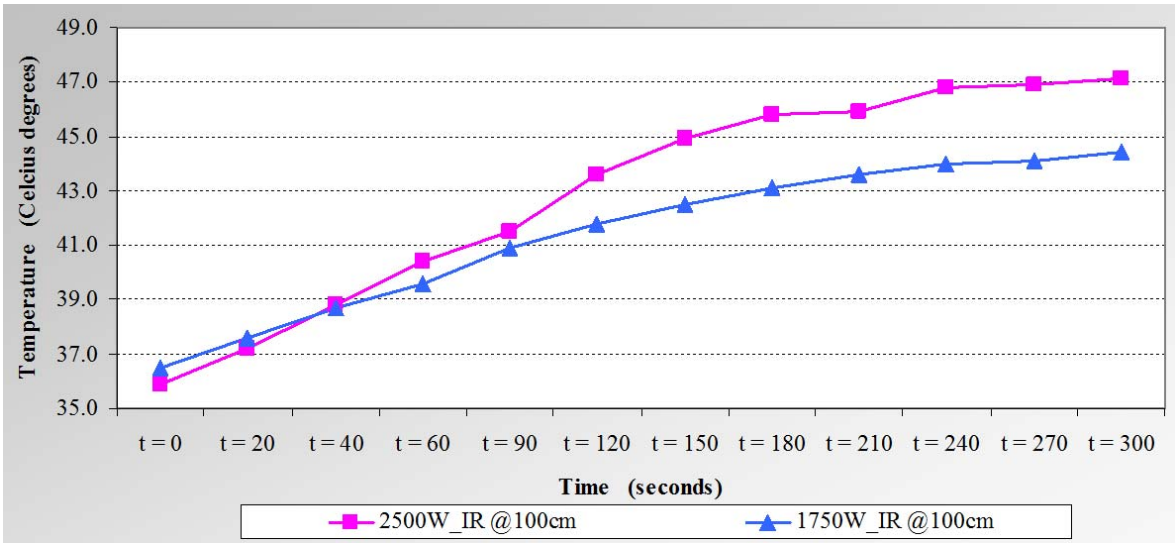

Figure 5.33. Maximum temperatures induced on human skin by various IR Heaters.

Table 5.3. Summary of the maximum temperatures obtained under IR exposure with variable durations.

Temperature Variation (℃) versus Time (min&sec) due to IR Light Exposure on Human Skin												
Time / **Light Source** (@100cm)	**0' 00"**	**0' 20"**	**0' 40"**	**1' 00"**	**1' 30"**	**2' 00"**	**2' 30"**	**3' 00"**	**3' 30"**	**4' 00"**	**4' 30"**	**5' 00"**
2500W IR	35.9°C	37.2°C	38.8°C	40.4°C	41.5°C	43.6°C	44.9°C	45.8°C	45.9°C	46.8°C	46.9°C	47.1°C
1750W IR	36.5°C	37.6°C	38.7°C	39.6°C	40.9°C	41.8°C	42.5°C	43.1°C	43.6°C	44.0°C	44.1°C	44.4°C

6. SUMMARY AND CONCLUSION

The focus on the possible health implications of electromagnetic radiation is more than ever due to its undeniable and elevated significance in scientific and industrial applications. Artificial lighting designs are undergoing a continuous evolution to utilize new technologies in optical radiation. Provided the rapid diffusion of newly developed special purpose light sources especially in medicine, science and consumer applications, there is no doubt that the importance of safety standards and EL on optical radiation continues to be increasing.

Primary biological effects of optical interaction with living tissue are related to heat problems. That is why temperature prediction on biological bodies has attracted great attention. Nevertheless, it is almost impossible to find a study in literature focusing on the thermal effects of commonly-used artificial light sources.

In this thesis, above mentioned concerns have been the primary motives to create and develop a mathematical model for the problem of light-tissue interaction whose solution to be provided by an efficient numerical approach FEM. The computational model is developed to predict the spatial temporal distribution of induced temperature on biological tissue.

Having investigated the temporal distributions with the developed numerical algorithm, the study is then extended with not only in-vitro experiments but also in-vivo human experiments; with the aim of first increasing the reliability of the numerical part of the thesis and secondly providing a foundation for scientific work about the thermal response of human skin under opto thermal radiation.

All of these experiments have yielded comparable and even better results than the numerical algorithm, which utilized FEM in order to solve the dominating partial differential equations with appropriate boundary conditions. These studies have also enabled to draw important conclusions, since the effect of distance variation, output power and the focusing degree of light sources is observed. From a detailed analysis of the

outputs, it can be asserted that at certain times induced temperature on tissue can reach dangerously high levels, which can only be tolerated by human body for only very short durations.

In this thesis, important contributions to literature are achieved on the subject of temperature predictions for biological tissues under exposure to artificial light sources. So as to list some of the enhancements, one can begin with the advantages provided by the implemented numerical model to illustrate thermal response of skin tissue under various light sources with different operational parameters. Furthermore, assessments obtained through the in-vitro and in-vivo experiments act as an important milestone in further scientific research especially on the studies about the possible health implication of light applications.

All in all, this thesis has reached its goal of shedding light on thermal behavior of skin tissue under optical radiation. The scope in future can also be extended to obtain data about the adverse effects of light sources on eye, being one of the most sensitive parts of human body which is definitely under direct and continuous exposure to light.

Although there are some efforts by International Commission on NonIonizing Radiation Protection (ICNIRP), the International Electrotechnical Commission (IEC) and American National Standards Institute (ANSI) to develop regulation about light hazards concentrated not only on skin tissue, but also on eye injury due to radiated energy, there is still lack of scientific studies on heating effects of light sources on human skin and the lack of definition of safety limits for light exposure.

In this regards, the thermal analysis carried out in this work will be useful to get a step forward in the ultimate goal of providing safety EL, so that general public, who are consciously or unconsciously exposed to different light sources in everyday life, can be made aware to take precaution. Not only public exposure, but also the occupational exposure especially to specific-purpose light applications which are widely used in medical treatments is enabled for assessment in terms of adverse health implications, so that enhancements on these medical applications can be obtained and sustained.

REFERENCES

1. Fanjul-Velez, F., N. Ortega-Quijano, J. R. Solana-Quiros, and J. L. Arce-Diego, "Thermal Damage Analysis in Biological Tissues Under Optical Irradiation: Application to the Skin", *International Journal of Thermophysics*, 2009, Vol. 30, No. 4, pp. 1423-1437, 2009.
2. Tuchin, V. V., *Tissue optics : light scattering methods and instruments for medical diagnosis*, 2nd edition, SPIE, Bellingham, WA, USA, 2007.
3. Pennes, H. H., "Analysis of Tissue and Arterial Blood Temperatures in the Resting Human Forearm", *Journal of Applied Physics.,* Vol. 1, pp. 93-122, 1948.
4. ICNIRP*,* "Guidelines on Limits of Exposure to Broad-Band Incoherent Optical Radiation (0.38 to 3μm)", *Health Physics*, Vol. 73, No. 3, 539-554, 1997.
5. Xu, F., T. Wen, T. J. Lu, and K. A. Seffen, "Skin Biothermomechanics for Medical Treatments", *Journal of the Mechanical Behavior of Biomedical Material*s, Vol. 1, pp. 172-187, 2008.
6. Scientific Committee on Emerging and Newly Identified Health Risks (SCENIHR), "Light Sensitivity", 26th Plenary on 23 September 2008, http://ec.europa.eu/health/ph_risk/committees/04_scenihr/docs/scenihr_o_019.pdf, accessed at July 2013.
7. Scientific Committee on Emerging and Newly Identified Health Risks (SCENIHR), "Health Effects of Artificial Light", 17th plenary meeting on 19 March 2012, http://ec.europa.eu/health/scientific_committees/emerging/docs/scenihr_o_035.pdf, accessed July 2013.
8. Sayre, R. M., J. C. Dowdy and M. Poh-Fitzpatrick, "Dermatological Risk of Indoor Ultraviolet Exposure from Contemporary Lighting Sources", *Photochemistry and Photobiology*, Vol. 80, pp. 47-51, 2004.
9. Borton, J.A., and K. A. Daley, "A Comparison of Light Sources for Petrochemical Industry", *IEEE Industry Applications Magazine*, Vol. 3, No. 4, pp 54-62, 1997.
10. Cheng, Y.K., and K.W.E. Cheng, "General Study for using LED to replace traditional lighting devices", *2nd International Conference on Power Eelctronics Systems and Applications*, *ICPESA '06,* 2006.

11. Majithia, C.A., A.V. Desai, and A.K. Panchal, “Harmonic Analysis of some Light Sources used for Domestic Lighting”, *Lighting Research and Technology*, Vol. 43, No. 3, pp. 371-380, 2011.
12. Cole, C., P. D. Forbes, R. E. Davies and F. Urbach, “Effect of Indoor Lighting on Normal Skin”, *Annals of the New York Academy of Sciences,* Vol. 453, pp. 305-316, 1985.
13. ASTM Subcommittee G03.09, *ASTM G173-03 Standard Tables for Reference Solar Spectral Irradaince Direct Normal and Hemispherical on 37° Tilted Surface, Annual Book of ASTM Standards,* Vol. 14.04. ASTM International, West Conshohocken, PA, USA, 2003.
14. Lin, J. C., “Interaction of Electromagnetic Transient Radiation with Biological Materials”, *IEEE Transactions on Electromagnetic*, Vol. EMC-17, No. 2, 1975.
15. L’Etang A., and Z. Huang, “The Effect of Laser Wavelength in the Simulation of Laser Generated Surface Waves in Human Skin Model”, *Proceedings of the 28th IEEE EMBS Annual International Conference*, New York City USA, 2006.
16. United States National Cancer Institute, “Anatomy of the Skin”, http://training.seer.cancer.gov/ss_module14_melanoma/images/illu_skin01.jpg, accesed at July 2013.
17. Xu, F., T. J. Lu, and K. A. Seffen, “Biothermomechanics of Skin Tissues”, *Journal of the Mechanics and Physics of Solids*, Vol. 56, No. 5, pp. 1852-1884, 2008.
18. Ahluwalia, G. S., *Cosmetic Applications Laser and Light-Based Systems*, William Andrew, NewYork, USA, 2009.
19. The Publications Office of the European Union, “Directive 2006/25/EC of the European Parliament and of the Council of 5 April 2006 on the minimum health and safety requirements regarding the exposure of workers to risks arising from physical agents (artificial optical radiation), (19th individual Directive within the meaning of Article 16(1) of Directive 89/391/EEC)”, 27/04/2006, http://eur-lex.europa.eu/LexUriServ/LexUriServ.do?uri=CELEX:32006L0025:EN:HTML, accessed at July 2013.
20. ICNIRP, “Guidelines on Limits of Exposure to Ultraviolet Radiation of Wavelengths Between 180 nm and 400 nm (Incoherent Optical Radiation)”, *Health Physics,* Vol. 87, No. 2, pp. 171-186, 2004.

21. ESNA Photobiology Committee, *Recommended Practice for Photobiological Sufety for Lamps & Lamp Systems-Risk Group Classification & Labeling,* Illuminating Engineering Society of North America, New York, NY, USA, 1996,
22. CIE Technical Committee, *CIE Standard 009/E:2002, Photobiological Safety* of *Lamps and Lamp Systems,* Commision Intemationale de l'Eclairage (CIE) Central Bureau, Vienna, Austria, 2002.
23. ICNIRP, "Guidelines on Limits of Exposure to Laser Radiation of Wavelengths between 180 nm and 1 mm", *Health Physics,* Vol. 71, No. 5, pp. 804-819, 1996.
24. Dua, R., and S. Chakraborty, "A Novel Modeling and Simulation Technique of Photo–thermal Interactions between Lasers and Living Biological Tissues undergoing Multiple Changes in Phase", *Computers in Biology and Medicine,* Vol. 35, No. 5, pp. 447–462, 2005.
25. Martelli, F., S. D. Bianco, A. Ismaelli, and G. Zaccanti, *Light Propagation through Biological Tissue and Other Diffusive Media: Theory, Solutions and Software*, SPI Press, Washington, USA, 2010.
26. Kolios M, A. Worthington, D. Holdsworth, M. Sherar and J. Hunt, "An Investigation of the Flow Dependence of Temperature Gradients near Large Vessels during Steady State and Transient Tissue Heating", *Physics in Medicine and Biology,* Vol. 44, No. 6, pp 1479-97, 1999.
27. Iizuka M. N., I. A. Vitkin, M. C.Kolios, and M. D. Sherar, "The Effects of Dynamic Optical Properties during Interstitial Laser Photocoagulation", Physics in Medicine and Biology*,* Vol. 45, No. 5, pp 1335-1357, 2000.
28. Datta, A., and V. Rakesh, *An Introduction to Modeling of Transport Processes*, Cambridge University Press, Cambridge, UK, 2010.
29. Comsol Multiphysics*, Heat Transfer Module User's Guide,* Comsol AB, *2008.*
30. Mostovnikov, V. A., G. R. Mostovnikova, V. Y. Plavski, L. G. Plavskaja, and R. P. Morozova, "Primary Photophysical Processes which Define the Biological and Therapeutic Effect of Low Intensity Laser Radiation", *5th International Conference on Laser Applications in Life Sciences, SPIE 2370,* 1995.
31. Diffey, B. L., "Human Exposure to Ultraviolet Radiation", *Seminars in Dermatology*, Vol. 9, No. 1, pp 2-10, 1990.

32. Harber, L. C., G. B. Whitman, R. B. Anstrong and V. A. Deleo, "Photosensitivity Diseases Related to Interior Lighting", *Annals of the New York Academy of Sciences,* Vol. 453, pp 317-327, 1985.
33. Beral, V., S. Evans, H. Shaw and G. Milton, "Malignant Melanoma and Exposure to Fluorescent Lighting at Work", *Lancet*, Vol. 2, No. 8293, pp 290-293, 1982.
34. Carlton-Foss, J. A., "Malignant Melanoma and Fluorescent Lighting", *Lancet*, Vol. 2, No. 8302, pp. 818-819, 1982.
35. Diethelm, R., "Skin Cancer from Fluorescent Lamps?", *Schweizerische Medizinische Wochenschrift,* Vol. 100, No. 27, pp. 1159-1160, 1970.
36. Elwood, J. M., "Could Melanoma be Caused by Fluorescent Light? A Review of Relevant Epidemiology", *Recent Results in Cancer Research,* Vol. 102, pp. 127-136, 1986.
37. Griffiths, A. P. and A. Faimey, "Fluorescent Lights, Ultraviolet Lamps, and Cutaneous Melanoma", *British Medical Journal,* Vol. 297, No. 6657, p. 1041, 1988.
38. Maxwell, K. and J. M. Elwood, "Could Melanoma be Caused by Fluorescent Light? A Review of Relevant Physics", *Recent Results in Cancer Research,* Vol. 102, pp. 137-143, 1986.
39. Maxwell, K. J. and J. M. Elwood, "UV Radiation from Fluorescent Lights", *Lancet*, Vol. 322, No. 8349, p. 579, 1983.
40. Swerdlow, A. J., J. S. English, R. M. MacKie, C. J. O'Doherty, J. A. Hunter, J. Clark and D. J. Hole, "Fluorescent Lights, Ultraviolet Lamps, and Risk of Cutaneous Melanoma", *British Medical Journal,* Vol. 297, No. 6657, p. 1172, 1988.
41. Walter, S. D., L. D. Marrett, H. S. Shannon, L. From and C. Hertzman, "The Association of Cutaneous Malignant Melanoma and Fluorescent Light Exposure", *American Journal of Epidemiology,* Vol. 135, No. 7, pp. 749-762, 1992.
42. Khazova , M. and J. B. O'Hagan, "Optical Radiation Emissions from Compact Fluorescent Lamps", *Radiation Protection Dosimetry*, Vol. 131, No. 4, pp. 521-525, 2008.
43. Whillock, M. J., A. F. McKinlay, J. Kemmlert, and P. G. Forsgren, "Ultraviolet Radiation Emission from Miniature (Compact) Fluorescent Lamps", *Lighting Research and Technology,* Vol. 22, No. 2, pp.125-128, 1990.

44. McKinlay, A. and B. Diffey, "A Reference Action Spectrum for Ultraviolet Induced Erythema in Human Skin", *Commision Intemationale de l'Eclairage Journal*, Vol. 6, No. 1, pp. 17-22, 1987.
45. Swerdlow A. J., and M. A. Weinstock, "Do Tanning Lamps Cause Melanoma? An Epidemiologic Assessment", *Journal of the American Academy of Dermatology*, Vol. 38, pp. 89-98, 1998.
46. Spencer J. M., and R.A. Amonette, "Indoor Tanning: Risks, Benefits, and Future Trends", *Journal of the American Academy of Dermatology,* Vol. 33, pp. 288-298, 1995.
47. Fish, J., and T. Belytschko, *A First Course in Finite Elements*, John Wiley, England, 2007.
48. Babuska, I., U. Banerjee, and J. E. Osborn, "Generalized Finite Element Methods: Main Ideas, Results, and Perspective", *International Journal of Computational Methods,* Vol. 1, pp. 67-103, 2004.
49. L. Ahma, M. Ibrani, and E. Hamiti, "Computation of SAR Distribution in a Human Exposed to Mobile Phone Electromagnetic Fields", *PIERS Progress In Electromagnetics Research Symposium Proceedings*, Xi'an-China, pp. 1580-1582, 2010.
50. A. Hirata, and O. Fujiwara, "The Correlation between Mass-averaged SAR and Temperature Elevation in the Human Head Model Exposed to RF Near-Fields from 1 to 6GHz", *Physics in Medicine and Biology,* Vol. 54, pp. 7227-7238, 2009.
51. Bernardi, P., M. Cavagnaro, S. Pisa, and E. Piuzzi, "Specific Absorption Rate and Temperature Increases in the Head of a Cellular-phone User", *IEEE Transactions on Microwave Theory and Techniques,* Vol. 48, No. 7, pp. 1118-1126, 2000.
52. Wang, J., and O. Fujiwara, "FDTD Computation of Temperature Rise in the Human Head for Portable Telephones", *IEEE Transactions on Microwave Theory and Techniques,* Vol. 47, No. 8, pp. 1528-1534, 1999.
53. Bernardi, P., M. Cavagnaro, S. Pisa, and E. Piuzzi, "Power Absorption and Temperature Elevations Induced in the Human Head by a Dual-band Monopole-helix Antenna Phone", *IEEE Transactions on Microwave Theory and Techniques,* Vol. 49, No. 12, pp. 2539-2546, 2001.

54. Rashed, M., I. Faruque, N. Misran, R. Nordin, M. T. Islam, and B. Yatim, "Estimation of Specific Absorption Rate and Temperature Increases in the Human Head due to Portable Telephones", *Scientific Research and Essays*, Vol. 6, pp. 1209-1215, 2011.
55. Yioultsis, T. V., T. I. Kosmanis, E. P. Kosmidou, T. T. Zygiridis, N. V. Kantartzis, T. D. Xenos, and T. D. Tsiboukis, "A Comparative Study of the Biological Effects of Various Mobile Phone and Wireless LAN Antennas", *IEEE Transactions on Magnetics*, Vol. 38, No. 2, pp. 777-780, 2002.
56. Riu, P. J., and K. R. Foster, "Heating of Tissue by Near-Field Exposure to a Dipole: A Model Analysis", *IEEE Transactions on Biomedical Engineering*, Vol. 46, No. 8, pp. 911-917, 1999.
57. Ng, E. Y., H. M. Tan, and E. H. Ooi, "Prediction and Parametric Analysis of Thermal Profiles within Heated Human Skin Using the Boundary Element Method", *Philosophical Transactions of the Royal Society A,* Vol. 368, No. 1912, pp. 655-678, 2010.
58. Cheong, W. F., and S. A. Prahl, and A. J. Welch, "A Review of the Optical Properties of Biological Tissues", *IEEE Journal of Quantum Electronics*, Vol. 26, pp. 2166-2185, 1990.
59. Klose, A. D., and E. W. Larsen, "Light Transport in Biological Tissue Based on the Simplified Spherical Harmonics Equations", *Journal of Computational Physics*, Vol. 220, pp. 441-470, 2006.
60. Fanjul-Velez, F., O. G. Romanov, and J. L. Arce-Diego, "Efficient 3D Numerical Approach for Temperature Prediction in Laser Irradiated Biological Tissues", *Computers in Biology and Medicine*, Vol. 39, pp. 810-817, 2009.
61. OSRAM, "The Versatile Infra-red Lamps from OSRAM", 2010, http://www.osram.com/media/resource/hires/333561/theratherm_siccatherm_infrared-en.pdf, accessed at July 2013.